# SURFACE-WAVE TRANSDUCER MODELING

Thesis for the Degree of Ph. D.

MICHIGAN STATE UNIVERSITY

ALBERT O. SIMEON

1974

This is to certify that the

thesis entitled

SURFACE-WAVE TRANSDUCER
MODELING

presented by

ALBERT O. SIMEON

has been accepted towards fulfillment
of the requirements for

Ph.D. degree in EE

P. David Fisher
Major professor

Date 7/23/74

O-7639

ABSTRACT

SURFACE-WAVE TRANSDUCER MODELING

by Albert O. Simeon

It is the aim of this research to find useful equivalent circuit models which are developed specifically for surface-wave transducers and to show their relation to the already-proven crossed-field model of Smith et al [1].

In order to accomplish this the surface-wave problem is somewhat simplified to obtain a closed form solution. This is done by considering only particle displacements in the sagittal plane. This solution is applied in a new approach to defining dynamic variables and the characteristic impedance for piezoelectric transmission lines: The surface potential is selected as the cross variable. The power flux is calculated from the surface-wave solution and is also related to the cross variable directly. This defines the characteristic admittance of the transmission line.

The response of an alternate phase array of Coquin and Tiersten [2] is extended to frequencies other than the synchronous frequency. This is made possible by considering only the short-circuit current response at first which permits the conformal mapping of the semi-infinite strip and the residual solution of the potential even if the first zeros of its even part are not located halfway between two electrodes.

6598 2

Albert O. Simeon

With the aid of reciprocity the admittance matrix of a basic section is obtained and the corresponding equivalent circuit consisting of a transmission line section and voltage dependent current sources, plus a parallel circuit for the electrical part consisting of a capacitance in parallel with current sources, depending on the cross variable which is the particular solution of the potential problem.

By duality the transmission line part of this circuit is changed and the crossed-field circuit model of Smith et al [1] is obtained. The difference lies in the frequency dependence of the characteristic impedance. However, over any frequency range of practical interest the performance of this circuit resembles theirs very closely so that all the established analysis and design procedures based on the crossed-field model apply here as well.

Applications included are the detection and excitation of surface waves by means of the dependent generator model. The calculation of radiation admittance and the scattering parameters is done with the dual circuit.

The principal contribution of this research is that it relates transducer models directly to surface waves and does not rely on the equivalent bulk-wave behavior implied by other circuit models.

---

[1] Smith, Gerard, Collins, Reeder, and Shaw, "Analysis of Interdigital Surface-Wave Transducers by Use of an Equivalent Circuit Model," IEEE, MTT-17, No. 11, 1969.

[2] G. A. Coquin and H. F. Tiersten, "Analysis of the Excitation and Detection of Piezoelectric Surface Waves in Quartz by Means of Surface Electrodes," The Journal of the Acoustical Society of America, Vol. 41, No. 4, Part 2, 1967.

# SURFACE-WAVE TRANSDUCER MODELING

By

Albert O. Simeon

A THESIS

Submitted to
Michigan State University
in partial fulfillment of the requirements
for the degree of

DOCTOR OF PHILOSOPHY

Department of Electrical Engineering

1974

To my wife

Ilse

## ACKNOWLEDGMENTS

The author wishes to express his sincere appreciation for the active assistance given him by his major professor, Dr. Fisher.

He also acknowledges gratefully the valuable suggestions made by the committee members, Drs. Ho, Hetherington and Nyquist.

Dr. Olin's help with the digital computer was invaluable and so was Mrs. Green's competent typing and organization of the material. Many thanks to both.

TABLE OF CONTENTS

LIST OF FIGURES AND TABLES

| Figure | | Page |
|---|---|---|

| Figure | | Page |
|---|---|---|

| Table | | Page |
|---|---|---|

## CHAPTER 1

## INTRODUCTION

Equivalent circuit models for surface-wave transducers were first developed by Smith et al [10] in 1969, four years after White and Voltmer [17] initially introduced the surface-wave transducer. Such a delay would seem unusual. In the case of transistors, for example, the first modeling was done by Shockley, right after the introduction of the device. The delay in the case of the surface-wave transducer may be explained because fundamental understanding of surface waves is not possible in a one-dimensional representation of the particle motion as it is in semiconductor devices. Particle motion occurs in three dimensions in elliptical trajectories. In addition, there is the complicated electromechanical interaction with the electrodes deposited on the surface.

The particle motion of elastic bulk waves is one-dimensional. Mason [5] had developed earlier equivalent circuit models for bulk-wave transducers. In particular, a model for series excitation and one for crossed-field excitation were developed. Smith et al found that the crossed-field model gives consistently correct results if applied to surface-wave transducers. The justification for this model rests entirely on an analogy between surface waves and bulk waves and, of course, its proven success in applications of design and analysis of various transducer configurations.

It is the aim of this research to find equally useful equivalent circuit models, but which are developed specifically for surface-wave transducers, and to show their relation to the already-proven crossed-field model of Smith et al. It is hoped that this approach to modeling will lead to a better understanding of surface-wave transducers. Concomitantly, predictive models might emerge which will lead researchers to develop improved surface-wave transducers.

In order to accomplish this it will first be necessary to simplify the surface-wave problem somewhat because a general solution in closed form is not possible. This is done in Chapter 2 without losing the characteristic features of the surface-wave particle motion. In Chapter 3 this solution of the surface-wave problem is applied in a new approach to defining dynamic variables and the characteristic impedance for piezoelectric transmission lines. In Chapter 4 it is shown how an equivalent bulk-wave model may be developed from this approach. This, however, is not pursued any further because it is possible to derive surface-wave transducer models without referring back to equivalent bulk-wave behavior. Towards this end, the analysis of surface-wave detection by Coquin and Tiersten [4] is generalized in Chapter 5. With the aid of the results of Chapter 3 and Chapter 5, a reciprocal equivalent circuit model is obtained in Chapter 6. It employs dependent generators, but is rather easy to apply as shown by several examples. By means of various circuit theory techniques, the equivalent circuit is manipulated to resemble the crossed-field model of Smith et al. The similarities and differences are discussed. This form is also used in various applications which tend to support the validity of the model. By comparison with experimental results, it is finally possible to adapt the equivalent circuits developed here to crystal cuts other than the one for which the simplified solution in Chapter 2 was performed.

Throughout this investigation, it is assumed that bulk-wave generation is negligible; that there are no inherent losses in the propagation of surface waves, i.e. internal losses or losses due to mass loading by the air or the metallization on the surface. It is furthermore assumed that the generated waves do not spread, but rather stay in a well confined beam of a width equal to that of the generating electrodes. All these problems have been investigated in the literature [9,18]. Their inclusion would detract from the principal understanding sought here, and as comparison with the experimental results proves, they are only secondary effects.

The results of this research are restated in Chapter 7, where possible future investigations are also suggested from the vantage point of the insights gained here.

# CHAPTER 2

# ELASTIC SURFACE WAVES

## 2.1 Motivation

In this Chapter a simplified treatment of the problem of surface waves on piezoelectric plates will be given for easy reference. A number of articles [1]-[3] have treated the problem without such simplification, but the mathematics cannot be handled then in general symbols. It rather involves the simultaneous solution of two fourth order determinants. The problem is reduced somewhat in complexity if the electromechanical interaction is ignored [4], but this still results in the simultaneous solution of two third order determinants.

In crystals with orthorhombic symmetry, there is no particle motion transverse to the direction of propagation [6]. Here the mathematics becomes tractable. It involves the simultaneous solution of two second order determinants. These can be handled in closed form.

The commonly used materials for piezoelectric surface wave transducers do not have orthorhombic symmetry. However, the coupling to transverse motion is rather small in certain frequently used rotated Y-cuts of quartz [5]-[6].

In the so-called ac cut, which is a rotated Y-cut of 31° about the x-axis, the face shear is decoupled [5]. This results in negligible transverse motion. Coquin and Tiersten [4] bear this out indirectly. For a rotated Y-cut of about 30° to 32° there are only two decay constants. This is typical for a system with motion in the sagittal plane only [6].

For the sake of clarity, generality will be sacrificed. By using the elastic constants of the ac-cut the results correspond very closely to those obtained in a broader treatment [4]-[6].

## 2.2 The Problem Statement

All transverse motion will be neglected and it is assumed that the mechanical electrical interaction is small. Fig. 2.1 shows the reference directions. The wave propagates in the x-direction. The elastic material is confined to the half space $y > 0$. With the present assumptions the linear elastic equations [6] become:

$$T_1 = C_{11}S_1 + C_{12}S_2 \tag{2.1}$$

$$T_2 = C_{12}S_1 + C_{22}S_2 \tag{2.2}$$

$$T_6 = C_{66}S_6 \tag{2.3}$$

where $T_1$ is the tension stress in the x-direction

$T_2$ is the tension stress in the y-direction

$T_6$ is the shear stress about the z-axis.

The $S_i$ are the corresponding strains and the $C_{ij}$ are the elastic stress coefficients. For a rotation of 31.62° (the angle when $C_{56}$ is exactly zero):

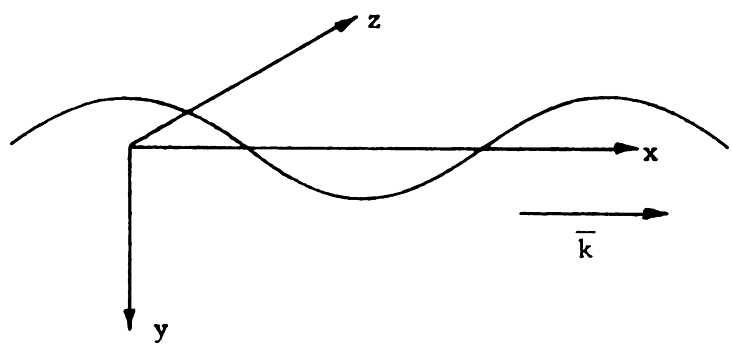


Figure 2.1 - Layout of reference directions for surface waves on semi-infinite piezoelectric slab.

$$C_{11} = 86.74, \quad C_{12} = -7.65$$

$$C_{22} = 127.84, \quad C_{66} = 28.85 \text{ all in } 10^9 \text{ N/m}^2.$$

These values were obtained from Ref. 4, by a method illustrated in Appendix B. It should be realized at this point that without the simplifying assumptions made before one would have instead to deal with the following standard piezoelectric constitutive equations [5]:

$$T_{ij} = C_{ijkl}^{E} S_{kl} - e_{kij} E_k \tag{2.4}$$

$$D_i = e_{ikl} S_{kl} + \varepsilon_{ik}^{S} E_k \quad . \tag{2.5}$$

Clearly Eqs. (2.1)-(2.3) are easier to handle. Let u be a displacement in the x-direction, v a displacement in the y-direction. Their relations to the strains become:

$$S_1 = \frac{\partial u}{\partial x} \tag{2.6}$$

$$S_2 = \frac{\partial v}{\partial y} \tag{2.7}$$

$$S_6 = \frac{\partial v}{\partial x} + \frac{\partial u}{\partial y} \quad . \tag{2.8}$$

The equations of motion are given by

$$\rho \ddot{u} = \frac{\partial T_1}{\partial x} + \frac{\partial T_6}{\partial y} \tag{2.9}$$

and

$$\rho \ddot{v} = \frac{\partial T_6}{\partial x} + \frac{\partial T_2}{\partial y} \ . \tag{2.10}$$

$\rho$ is the density of quartz, $\rho = 2.65 \times 10^3$ kg/m$^3$. As is conventional the particle displacements are next assumed to have the form:

$$u = \mathrm{Re}[U\ e^{-\alpha ky}\ e^{j(\omega t-kx)}] \tag{2.11}$$

and

$$v = \mathrm{Re}[V\ e^{-\alpha ky}\ e^{j(\omega t-kx)}]\ . \tag{2.12}$$

k is the propagation constant of the wave, and

$$k = \frac{\omega}{V_p}\ . \tag{2.13}$$

The quantity $\alpha k$ is the assumed decay constant. Equations (2.11)-(2.12) coupled with Eqs. (2.6)-(2.8) imply that the strains and hence the stresses are also of the same general form given in Eqs. (2.11)-(2.12). For the sake of convenience of notation let the real part operator Re[ ] be implied throughout the following. Then the partial derivatives may be replaced by:

$$\frac{\partial}{\partial x} \longrightarrow -jk \tag{2.14}$$

$$\frac{\partial}{\partial t} \longrightarrow j\omega \tag{2.15}$$

$$\frac{\partial}{\partial y} \longrightarrow -\alpha k\ . \tag{2.16}$$

Equations (2.6)-(2.10) then become:

$$S_1 = -jku, \tag{2.17}$$

$$S_2 = -\alpha kv, \tag{2.18}$$

$$S_6 = -jkv - \alpha ku, \tag{2.19}$$

$$-\rho\omega^2 u = -jkT_1 - \alpha kT_6, \tag{2.20}$$

and

$$-\rho\omega^2 v = -jkT_6 - \alpha kT_2\ . \tag{2.21}$$

When these are combined with Eqs. (2.1)-(2.3) the stresses become:

$$T_1 = -jkC_{11}u - \alpha kC_{12}v, \tag{2.22}$$

$$T_2 = -jkC_{12}u - \alpha kC_{22}v, \tag{2.23}$$

and

$$T_6 = -\alpha kC_{66}u - jkC_{66}v \ . \tag{2.24}$$

With the aid of Eqs. (2.20)-(2.21) and

$$k^2 = \omega^2/V_p^{\ 2} \tag{2.25}$$

the stress relations become the homogeneous equations:

$$(\rho V_p^{\ 2} - C_{11} + \alpha^2 C_{66})u + j\alpha(C_{12} + C_{66})v = 0 \tag{2.26}$$

and

$$j\alpha(C_{12} + C_{66})u + (\rho V_p^{\ 2} - C_{66} + \alpha^2 C_{22})v = 0 \ . \tag{2.27}$$

If $V_p$ were known these could be solved for the two possible $\alpha$'s and the relative amplitudes u and v. This would result in two modes: $\alpha_1, u_1, v_1$ and $\alpha_2, u_2, v_2$.

To proceed the conditions for a free boundary are required: No normal stress can be acting on a surface element:

$$\text{at } y = 0 \quad T_2 = 0 \tag{2.28}$$

$$\text{and} \quad T_6 = 0 \ . \tag{2.29}$$

When both modes are used Eqs. (2.23)-(2.24) become at y = 0:

$$-jkC_{12}[U_1 + U_2] - kC_{22}[\alpha_1 V_1 + \alpha_2 V_2] = 0 \tag{2.30}$$

and

$$-kC_{66}[\alpha_1 U_1 + \alpha_2 U_2] - jkC_{66}[V_1 + V_2] = 0 \ . \tag{2.31}$$

Equation (2.26) gives for each mode the relative amplitudes if $V_p$ were known:

$$\frac{\beta_{U_i}}{\beta_{V_i}} = \frac{U_i}{V_i} = \frac{-j\alpha_i(C_{12} + C_{66})}{\rho V_p^2 - C_{11} + \alpha_i^2 C_{66}} \quad . \tag{2.32}$$

$U_i$ and $V_i$ could be expressed in terms of a mode amplitude $B_i$ as

$$U_i = \beta_{U_i} B_i \tag{2.33}$$

and

$$V_i = \beta_{V_i} B_i \ . \tag{2.34}$$

For convenience the following constants are defined (see [6]):

$$g_{ij} = \frac{C_{ij}}{C_{66}} , \tag{2.35}$$

$$K = g_{12} + 1, \tag{2.36}$$

and

$$q = \frac{\rho V_p^2}{C_{66}} \ . \tag{2.37}$$

Hence,

$$\beta_{U_i} = -j\alpha_i k, \tag{2.38}$$

and

$$\beta_{V_i} = q - g_{11} + \alpha_i^2 \ . \tag{2.39}$$

With this formulation the displacements are

$$u = [\beta_{U_1} B_1 \, e^{-\alpha_1 ky} + \beta_{U_2} B_2 \, e^{-\alpha_2 ky}] \, e^{-jk(x - V_p t)} \tag{2.40}$$

and

$$v = [\beta_{V_1} B_1 \, e^{-\alpha_1 ky} + \beta_{V_2} B_2 \, e^{-\alpha_2 ky}] \, e^{-jk(x - V_p t)} \ . \tag{2.41}$$

Correspondingly, the boundary conditions given in Eqs. (2.30)-(2.31) become

$$(\alpha_1 \beta U_1 + j\beta V_1)B_1 + (\alpha_2 \beta U_2 + j\beta V_2)B_2 = 0 \tag{2.42}$$

and

$$(jg_{12}\beta U_1 + \alpha_1 g_{22}\beta V_1)B_1 + (jg_{12}\beta U_2 + \alpha_2 g_{22}\beta V_2)B_2 = 0. \tag{2.43}$$

These again are two homogeneous equations which must be solved simultaneously with Eqs. (2.26)-(2.27). The determinant of their coefficients is

$$\begin{vmatrix} q - g_{11} + \alpha^2 & j\alpha k \\ j\alpha k & q - 1 + \alpha^2 g_{22} \end{vmatrix} = 0 . \tag{2.44}$$

The unknowns which Eqs. (2.42)-(2.44) must yield first of all are q and the α's. Express Eqs. (2.42)-(2.43) also as a determinant set to zero:

$$\begin{vmatrix} \alpha_1 \beta U_1 + j\beta V_1 & \alpha_2 \beta U_2 + j\beta V_2 \\ jg_{12} \beta U_1 + \alpha_1 g_{22}\beta V_1 & jg_{12}\beta U_2 + \alpha_2 g_{22}\beta V_2 \end{vmatrix} = 0. \tag{2.45}$$

It is shown in Appendix A how the simultaneous solution of Eqs. (2.44)-(2.45) leads to an implicit relation for $q = V_p^2 \rho / C_{66}$:

$$q^3(1 - d) - q^2(1 - e + 2f) + q(2f + f^2) - f^2 = 0, \tag{2.46}$$

$$\text{where} \quad d = \frac{1}{g_{22}} , \; e = \frac{g_{11}}{g_{22}} \; \text{and} \; f = g_{11} - \frac{g_{12}^2}{g_{22}} . \tag{2.47}$$

With the elastic stress coefficients for the rotated Y-cut of 31.62°, Eq. (2.46) becomes:

$$0.7743q^3 - 6.3029q^2 + 14.9258q - 8.9444 = 0, \tag{2.48}$$

which has the following solution:

$$q = 0.9096 \ . \tag{2.49}$$

By definition

$$V_p = \sqrt{\frac{qC_{66}}{\rho}} \ . \tag{2.50}$$

The speed of propagation $V_p$ is therefore

$$V_p = 3147 \text{ m/sec} \ . \tag{2.51}$$

From Eq. (2.44) the $\alpha$'s may be determined:

$$0 = g_{22}\alpha^4 + \alpha^2[q(g_{22} + 1) - 1 - g_{22}g_{11} + K^2] + (q-g_{11})(q-1), \tag{2.52}$$

or

$$0 = 4.4315\alpha^4 - 8.8432\alpha^2 + 0.18957 \ . \tag{2.53}$$

$$\alpha_2 = 0.147 \tag{2.54}$$

$$\alpha_1 = 1.40 \ . \tag{2.55}$$

From Eqs. (2.38)-(2.39) the relative amplitude ratios $\beta$ are obtained:

$$\beta_{U_i} = -j\alpha_i(g_{12} + 1), \tag{2.56}$$

$$\beta_{U_2} = -j0.108, \tag{2.57}$$

$$\beta_{U_1} = -j1.03, \tag{2.58}$$

$$\beta_{V_i} = q - g_{11} + \alpha_i^2, \tag{2.59}$$

$$\beta_{V_2} = -2.08, \tag{2.60}$$

and

$$\beta_{V_1} = -0.123 \ .$$

The ratios of the mode amplitudes $B_i$, as defined by Eqs. (2.33)-(2.34) [or Eqs. (2.40)-(2.41)], may be determined with the aid of Eq. (2.42).

$$\frac{B_2}{B_1} = -\frac{\alpha_1\beta U_1 + j\beta V_1}{\alpha_2\beta U_2 + j\beta V_2} \tag{2.61}$$

$$\frac{B_2}{B_1} = -0.75 \tag{2.62}$$

Equations (2.33)-(2.34) allow the calculation of the surface amplitudes in both directions for each mode. For mode 2 the peak displacement in the vertical direction is

$$V_2 = \beta V_2 \; B_2 \; . \tag{2.63}$$

It is convenient to normalize all others with respect to $V_2$:

$$C_2^{(2)} = \frac{V_2}{V_2} = 1 \tag{2.64}$$

$$C_1^{(2)} = \frac{U_2}{V_2} = \frac{\beta U_2 \; B_2}{\beta V_2 \; B_2} = \frac{\beta U_2}{\beta V_2} = j0.052 \tag{2.65}$$

$$C_1^{(1)} = \frac{U_1}{V_2} = \frac{\beta U_1 \; B_1}{\beta V_2 \; B_2} = -j0.66 \tag{2.66}$$

$$C_2^{(1)} = \frac{V_1}{V_2} = \frac{\beta V_1 \; B_1}{\beta V_2 \; B_2} = -0.079 \; . \tag{2.67}$$

The superscript of these normalized surface amplitudes refers to the mode. The subscript 1 to the x-direction, 2 to the v-direction.

The values obtained here on the basis of a two-dimensional formulation correspond very closely to the numerical analvsis of the AT cut (a 35.25° rotated Y-cut) in [6]. There, however, a third mode is present because of shear about the x-axis which represents particle motion in the transverse direction (z-axis) with a rather small amplitude.

The j's in Eqs. (2.64)-(2.65) stand for phase shifts of 90° with respect to the vertical particle displacements of mode 2. This should be expressed in the time domain in Eqs. (2.40)-(2.41) as follows:

$$u(x,y,t) = |C_1^{(1)}|\, e^{-\alpha_1 ky} \cos(\omega t - kx - \tfrac{\pi}{2}) + |C_1^{(2)}|\, e^{-\alpha_2 ky} \cos(\omega t - kx + \tfrac{\pi}{2}) \tag{2.68}$$

is the horizontal displacement, and

$$v(x,y,t) = |C_2^{(1)}|\, e^{-\alpha_1 ky} \cos(\omega t - kx - \pi) + |C_2^{(2)}|\, e^{-\alpha_2 ky} \cos(\omega t - kx) \tag{2.69}$$

is the vertical particle displacement.

$k = \omega/V_p$ is the propagation constant.

$\omega$ is the radian frequency.

$V_p$, $\alpha_i$ and $|C_i^{(j)}|$ are:

$$V_p = 3147 \text{ m/sec} \tag{2.70}$$

$$\alpha_1 = 1.40 \tag{2.71}$$

$$\alpha_2 = 0.147 \tag{2.72}$$

$$|C_1^{(1)}| = 0.66, \ |C_1^{(2)}| = 0.052, \ |C_2^{(1)}| = 0.079,$$

$$|C_2^{(2)}| = 1 \ . \tag{2.73}$$

In Fig. 2.2 v(0,0,t) is plotted against u(0,0,t), separatelv for each mode and combined. This represents the trajectory of a particle at the surface. Typical dimensions are of the order of a few Angstroms. Fig. 2.3 shows $v(0,4/k\alpha_1,t)$ vs. $u(0,4/k\alpha_1,t)$. In this plot mode 1 has decayed to 1.8% of its surface value. Mode 2 is practically unaffected.

$$u(0,4/k\alpha_1,t) = 0.66 \times e^{-4} \cos(\omega t - \tfrac{\pi}{2}) + 0.052 \ e^{-4 \times \alpha_2/\alpha_1}$$

$$\times \cos(\omega t + \tfrac{\pi}{2}) \tag{2.74}$$

and

$$v(0,4/k\alpha_1,t) = 0.079 \ e^{-4} \cos(\omega t - \pi) + 1.0 \ e^{-4 \times \alpha_2/\alpha_1}$$

$$\times \cos(\omega t + 0) \ . \tag{2.75}$$

With the $\alpha$-values $\alpha_1 = 1.40$ and $\alpha_2 = 0.147$ this becomes:

$$u = 0.022 \cos(\omega t + \tfrac{\pi}{2}) \tag{2.76}$$

and

$$v = 0.66 \cos(\omega t + 0) \ . \tag{2.77}$$

The motion is almost entirely that of a shear wave, but it has taken on a very slight clockwise rotation, as mode 2. This is calculated at 0.4 times the decay distance of mode 2. On the basis

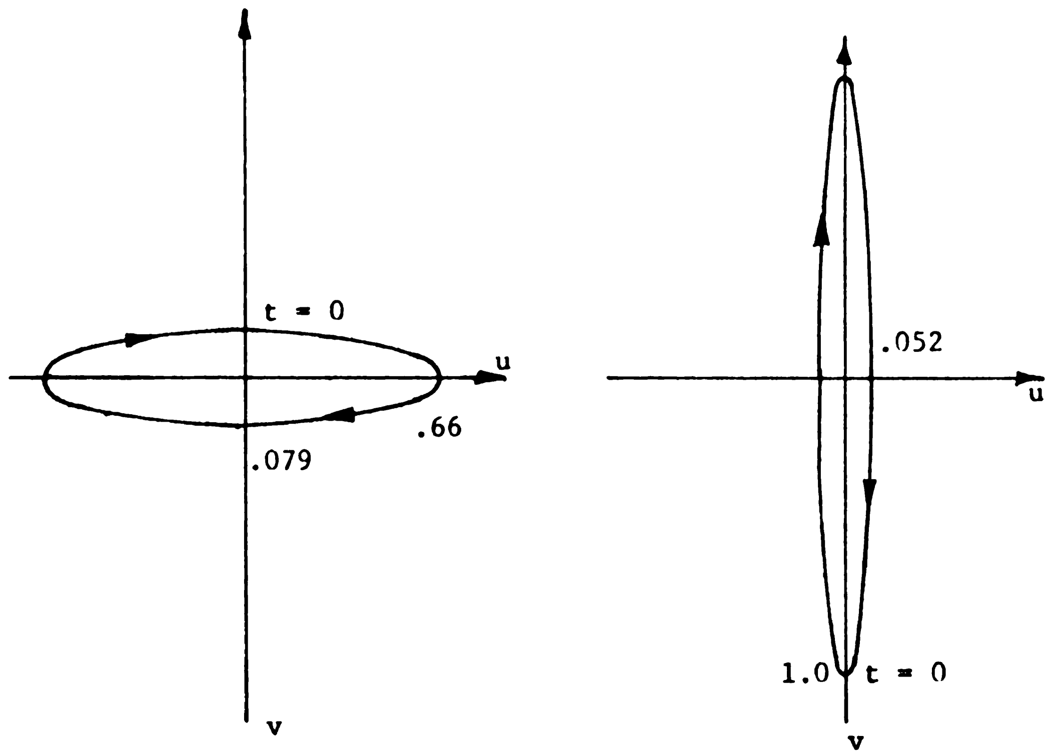


$u^{(1)}(0,0,t) = 0.66\cos(\omega t - \pi/2)$ $\quad$ $u^{(2)}(0,0,t) = 0.052\cos(\omega t + \pi/2)$

$v^{(1)}(0,0,t) = 0.079\cos(\omega t - \pi)$ $\quad$ $v^{(2)}(0,0,t) = 1.0\cos(\omega t + 0)$

(a)

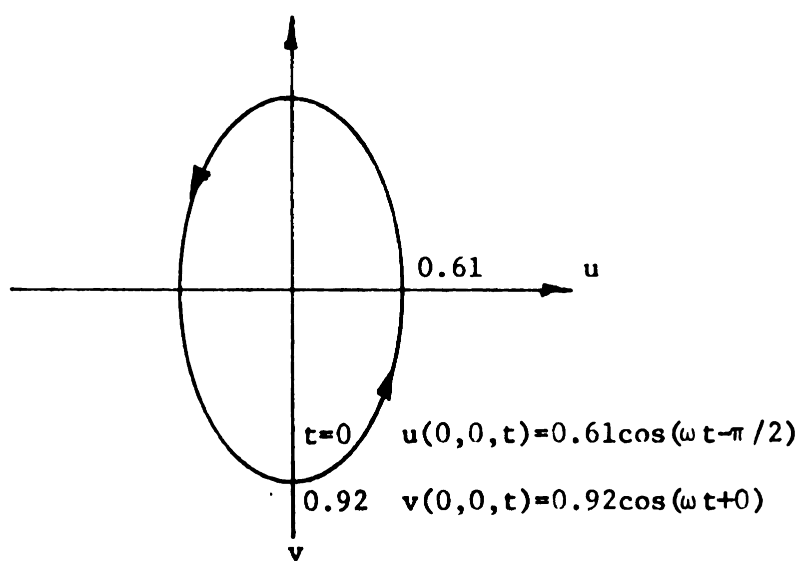


(b)

Figure 2.2 - (a) Relative particle displacement at the surface decomposed into individual modes. (b) Combined particle trajectory at the surface.

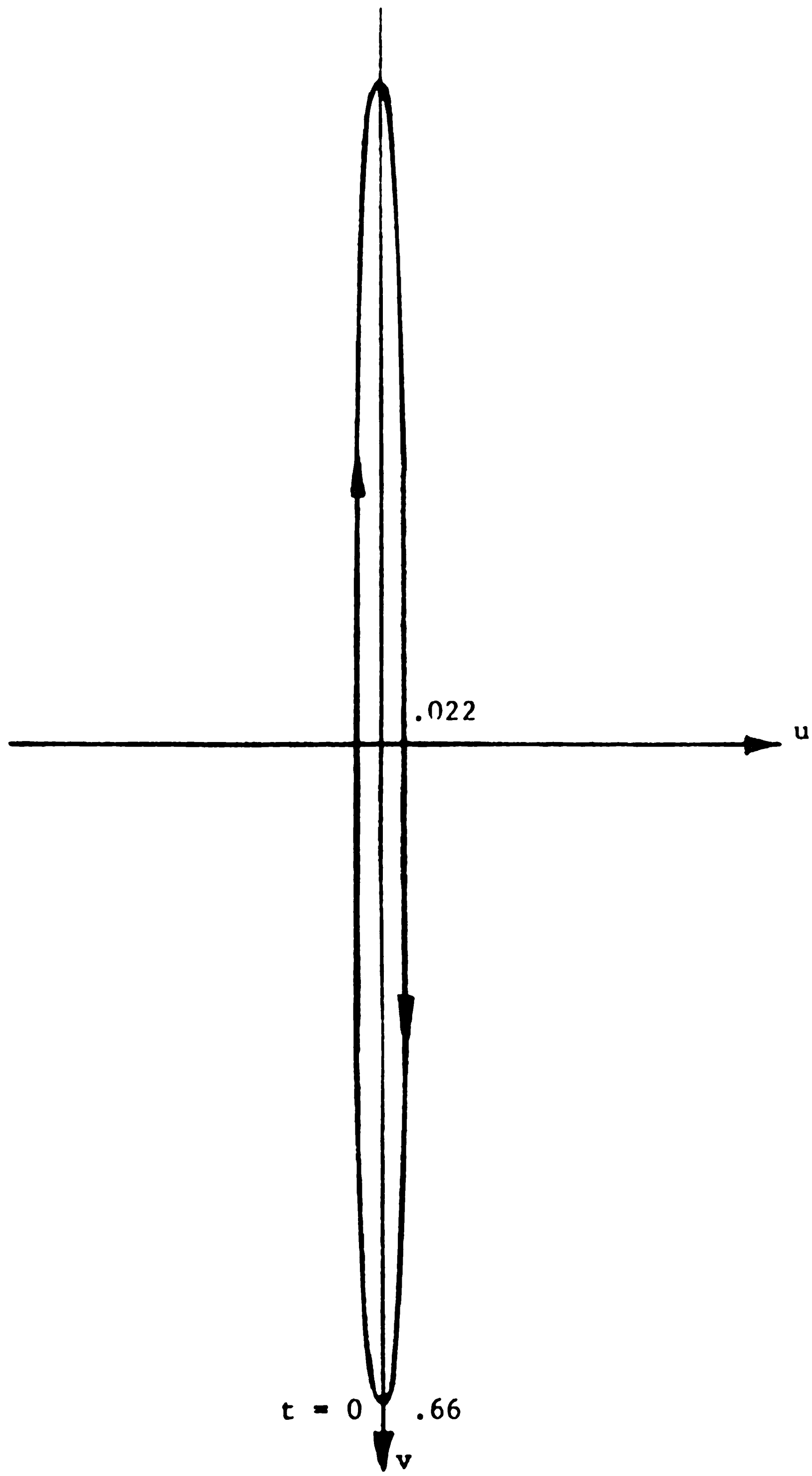


Figure 2.3 - Combined particle trajectory at four decay constants of mode 1.

of this it can be safely said that the dominant behavior of a surface wave is that of a vertical shear wave.

CHAPTER 3

PIEZOELECTRIC TRANSMISSION LINES

## 3.1 Equivalent Circuits for Transmission Line Sections in General

Equivalent circuits for surface wave transducers [7], as well as "crossed-field" bulk-wave transducers [5] degenerate into sections of piezoelectric transmission lines when the electric terminals are shorted (see Fig. 3.1).

It is the intent of the following treatment to show how such a transmission line equivalent circuit is obtained. It is necessary that in all cases a pair of complimentary variables must be found. With their aid the characteristic impedance is defined.

Consider the section of lossless transmission line shown in Fig. 3.2. Without loss in generality the cross variable may be denoted by V and the through variable by I. It is well known that in Laplace transform notation for a delay $t_o$ the terminal quantities are related by the following transmission matrix [8]

$$\left\|\begin{matrix} V_1 \\ I_1 \end{matrix}\right\| = \left\|\begin{matrix} \cosh(st_o) & Z_o\sinh(st_o) \\ Y_o\sinh(st_o) & \cosh(st_o) \end{matrix}\right\| \left\|\begin{matrix} V_2 \\ I_2 \end{matrix}\right\| . \qquad (3.1)$$

For convenience this is derived in Appendix C.

These "ABCD-parameters" are readily converted into "z-parameters" (Appendix C):

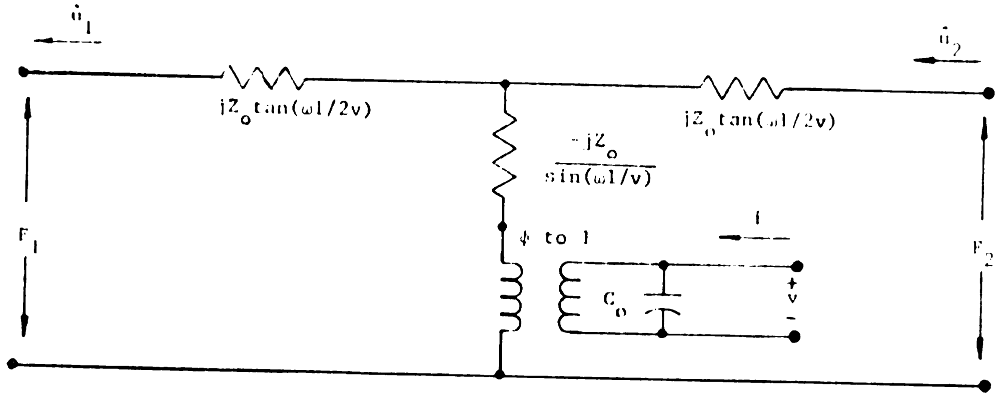


(a)

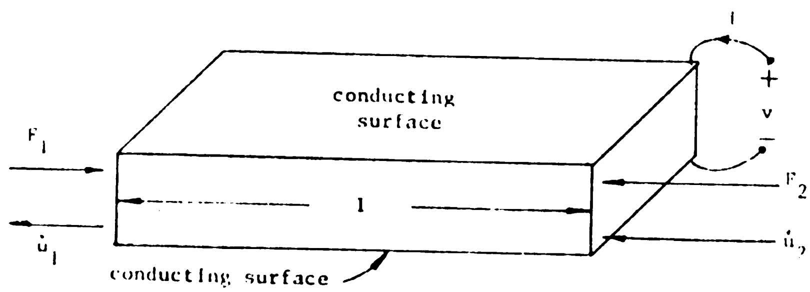


(b)

Figure 3.1 - (a) The equivalent circuit of a longitudinal bulk-wave transducer.
(b) Its actual layout.

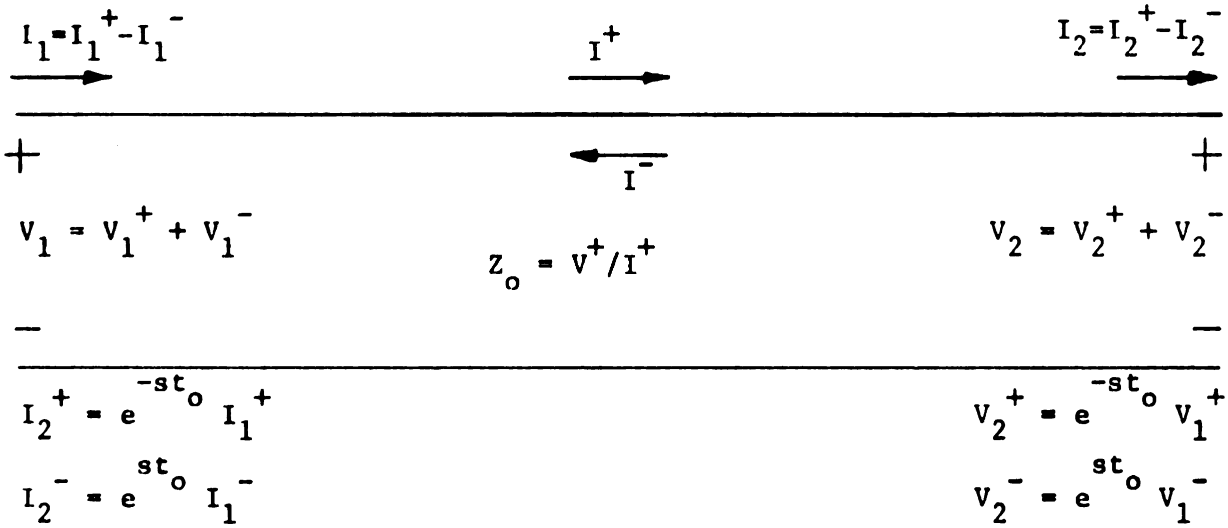


Figure 3.2 - A transmission line section with delay $t_o$.

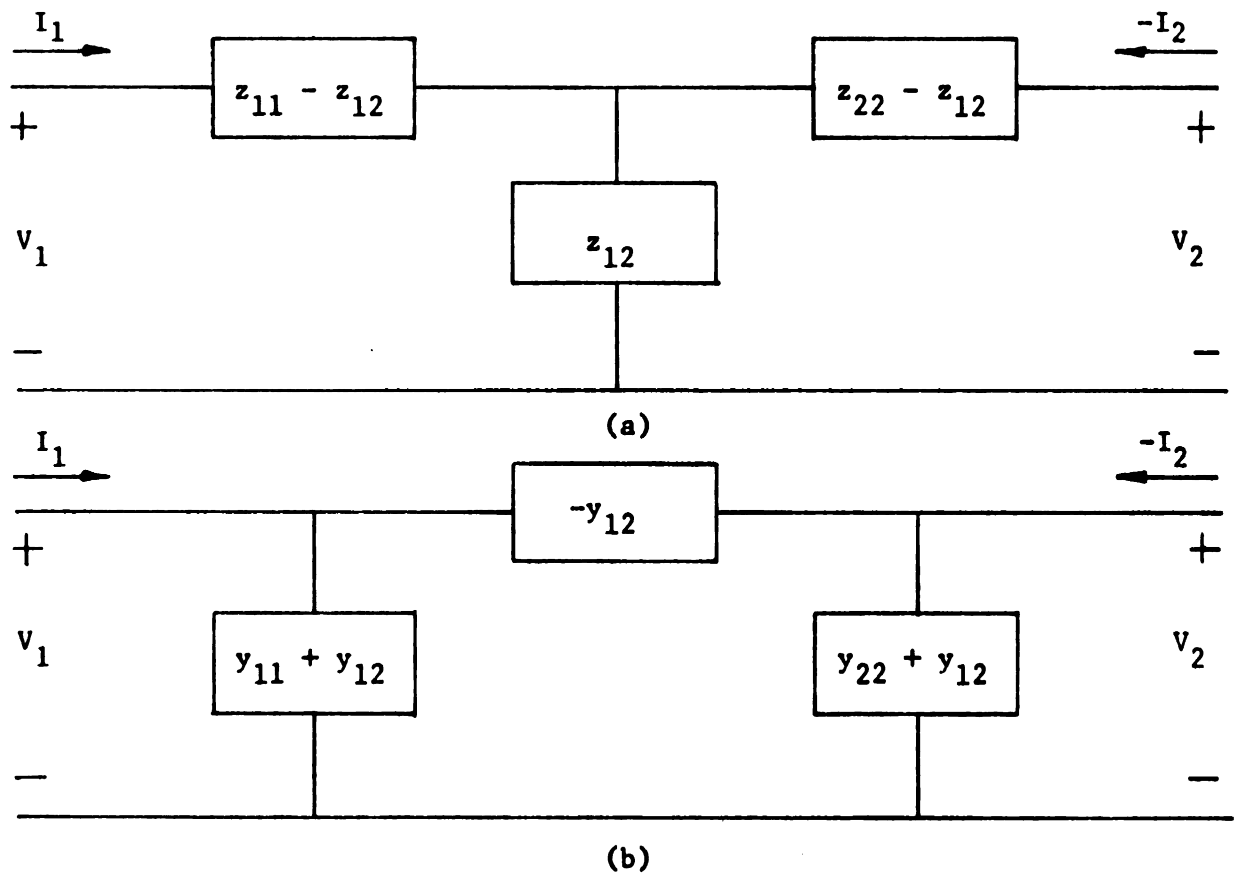


Figure 3.3 - Equivalent circuits for a passive linear bilateral two-port. (a) The T-model. (b) The $\pi$-model.

$$\begin{Vmatrix} V_1 \\ \\ V_2 \end{Vmatrix} = \begin{Vmatrix} \dfrac{Z_o}{\tanh(st_o)} & \dfrac{Z_o}{\sinh(st_o)} \\ \\ \dfrac{Z_o}{\sinh(st_o)} & \dfrac{Z_o}{\tanh(st_o)} \end{Vmatrix} \begin{Vmatrix} I_1 \\ \\ -I_2 \end{Vmatrix} \tag{3.2}$$

or "y-parameters" (Appendix C):

$$\begin{Vmatrix} I_1 \\ \\ -I_2 \end{Vmatrix} = \begin{Vmatrix} \dfrac{Y_o}{\tanh(st_o)} & \dfrac{-Y_o}{\sinh(st_o)} \\ \\ \dfrac{-Y_o}{\sinh(st_o)} & \dfrac{Y_o}{\tanh(st_o)} \end{Vmatrix} \begin{Vmatrix} V_1 \\ \\ V_2 \end{Vmatrix} . \tag{3.3}$$

Laplace transforms and phasor transforms are related by the simple expediency of setting s equal to $j\omega$. The delay $t_o$ translates then into a phase shift

$$\theta = \omega t_o . \tag{3.4}$$

Equations (3.2)-(3.3) then become:

$$\begin{Vmatrix} V_1 \\ \\ V_2 \end{Vmatrix} = \begin{Vmatrix} \dfrac{Z_o}{j\tan\theta} & \dfrac{Z_o}{j\sin\theta} \\ \\ \dfrac{Z_o}{j\sin\theta} & \dfrac{Z_o}{j\tan\theta} \end{Vmatrix} \begin{Vmatrix} I_1 \\ \\ -I_2 \end{Vmatrix} \tag{3.5}$$

$$\begin{Vmatrix} I_1 \\ \\ -I_2 \end{Vmatrix} = \begin{Vmatrix} \dfrac{Y_o}{j\tan\theta} & \dfrac{-Y_o}{j\sin\theta} \\ \\ \dfrac{-Y_o}{j\sin\theta} & \dfrac{Y_o}{j\tan\theta} \end{Vmatrix} \begin{Vmatrix} V_1 \\ \\ V_2 \end{Vmatrix} . \tag{3.6}$$

Figure 3.3 shows the T- and $\pi$-model for a bilateral linear network. $z_{11}-z_{12}$ become here

$$z_{11} - z_{12} = \frac{Z_o}{j} \left[\frac{\cos\theta}{\sin\theta} - \frac{1}{\sin\theta}\right] = \frac{Z_o}{j} \left[\frac{\cos(2\,\frac{\theta}{2}) - 1}{\sin(2\,\frac{\theta}{2})}\right] , \tag{3.7}$$

or

$$z_{11} - z_{12} = \frac{Z_o}{j} \left[\frac{-2\sin^2(\frac{\theta}{2})}{2\sin(\frac{\theta}{2})\cos(\frac{\theta}{2})}\right] = j\, Z_o \tan(\frac{\theta}{2}) = z_{22} - z_{12} \,. \tag{3.8}$$

Similarly $y_{11} + y_{12}$ become

$$y_{11} + y_{12} = y_{22} + y_{12} = j\, Y_o \tan(\frac{\theta}{2}) \,. \tag{3.9}$$

The resultant equivalent circuits are then shown in Fig. 3.4. It is seen that Fig. 3.3a is indeed the Mason circuit with $v = 0$ and a delay $t = l/v$, $\theta = \omega l/v$.

It should be pointed out here that although the Mason circuit was developed specifically for bulk waves, it has been used successfully for the equivalent circuit description of surface wave transducers. The appropriateness of this model is discussed in Chapter 4. The present development has shown that important aspects of the Mason circuit are found in all lossless transmission lines.

## 3.2 Selection of Dynamic Variables

Surface waves, as described in the preceding Chapter, exhibit time delay independent of frequency and propagate, as formulated in Eqs. (2.68)-(2.69), unattenuated in the x-direction. These are requirements for lossless transmission line behavior, but in order to complete an equivalence satisfactory dynamic variables must be determined. In the Mason model, Fig. 3.1, the dynamic variables are force and particle velocity. In an electric trans-

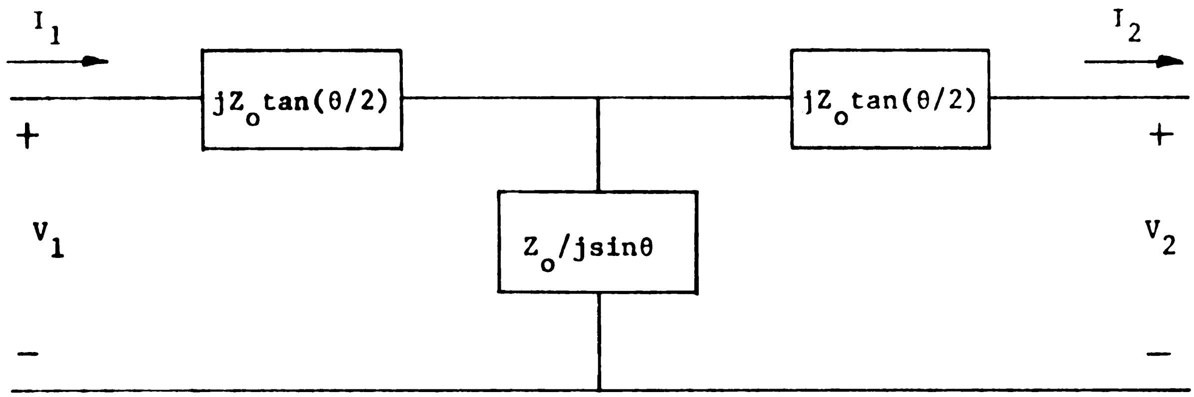


(a)

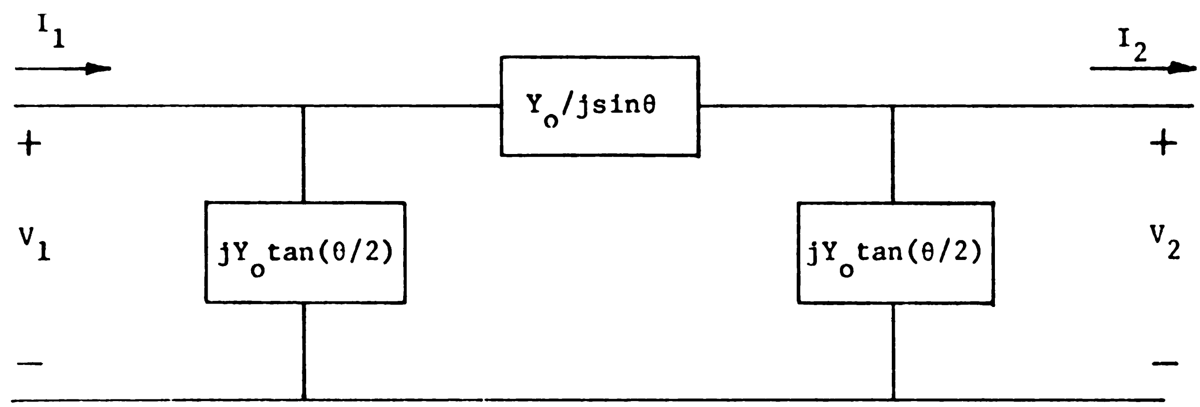


(b)

Figure 3.4 - Equivalent circuits for a lossless transmission line section which introduces a phase shift $\theta = \omega t_o$.

mission line they are voltage and current. The common feature is that the time average power flux of a wave travelling in the x-direction is

$$P_x = \frac{1}{2} \mathrm{Re}[V^+ I^{+*}] \ . \tag{3.10}$$

$V^+$ and $I^+$ are the cross-variable and through-variable respectively for a wave travelling in the positive x-direction. Since

$$V^+ = I^+ Z_o \tag{3.11}$$

$$P_x = \frac{1}{2} |I^+|^2 \mathrm{Re}[Z_o] \tag{3.12}$$

or conversely, since $\mathrm{Re}[Y_o^*] = \mathrm{Re}[Y_o]$:

$$P_x = \frac{1}{2} |V^+|^2 \mathrm{Re}[Y_o] \ . \tag{3.13}$$

V and I should be taken generally as cross- and through-variables rather than as voltage and current in particular.

In the case of surface waves, the power flux requirement is satisfied as follows: Conveniently one of the two variables is selected first. This could be done in various ways. One could select, for example, the vertical velocity of mode 2 as the through-variable. As another example, the piezoelectrically generated surface potential could be chosen as the cross-variable. Both of these will be considered later on. Whatever the choice, Eqs. (3.12)-(3.13) will then determine uniquely $\mathrm{Re}[Z_o]$ or $\mathrm{Re}[Y_o]$, since it is shown in Coquin and Tiersten [4] that $P_x$ follows from the determination of the decay constants $\alpha_j$ and the amplitudes $C_i^{(j)}$ which have been determined in the last Chapter.

The second dynamic variable is not uniquely determined. If $I^+$ were defined and $Re[Z_o]$ was found subsequently by

$$Re[Z_o] = 2P_x/|I^+|^2 \tag{3.14}$$

then $V^+(= Z_o I^+)$ still requires $Im[Z_o]$. It turns out that this does not really present a serious problem if Eq. (3.10) is generalized to the complex power flux:

$$\overline{P}_x = \frac{1}{2} V^+ I^{+*} \tag{3.15}$$

and similarly Eqs. (3.12)-(3.14) would become:

$$\overline{P}_x = \frac{1}{2} |I^+|^2 Z_o \tag{3.16}$$

$$\overline{P}_x = \frac{1}{2} |V^+|^2 Y_o^* \tag{3.17}$$

from which follows

$$Z_o = \frac{2\overline{P}_x}{|I^+|^2} \quad \text{or} \quad Y_o = \frac{2\overline{P}_x^*}{|V^+|^2} \quad . \tag{3.18}$$

The complex power flux is obtained from Coquin and Tiersten [4] very simply by leaving out the Re[ ] operator.

## 3.3 Complex Power Flux

For all rotated Y-cuts the power flux vector and the propagation direction are co-linear [4]. This is not generally the case [9], but such cuts are not used in practical applications. Components of principle interest are [4]:

$$P_i = -\frac{1}{2} \int_0^\infty Re(T_{ij}\dot{u}_j^*)dx_2 \tag{3.19}$$

This is done with the understanding that the wave front is 1m wide. For a width W and propagation in the $x_1$-direction Eq. (3.19) is modified to become the relation for the required complex power, i.e.

$$\bar{P}_1 = -\frac{W}{2}\int_0^\infty T_{1j}\dot{u}_j^* \, dx_2 \, . \tag{3.20}$$

The tensor subscripts must be interpreted according to Table B.8 in Appendix B. Then for Eq. (3.20):

$$\bar{P}_x = -\frac{W}{2}\int_0^\infty dy[T_1\dot{u}^* + T_6\dot{v}^* + T_5 \times 0], \tag{3.21}$$

where $x_1 = x$, $x_2 = y$, $u_1 = u$, $u_2 = v$ and $u_3 = 0$ in accordance with the treatment of Chapter 2.

The quantities u and v must be taken here as the complex amplitudes of Eqs. (2.68)-(2.69) multiplied by $e^{j(\omega t-kx)}$, from which $\dot{u}^*$ and $\dot{v}^*$ follow:

$$u(x,y,t) = [C_1^{(1)}\, e^{-\alpha_1 ky} + C_1^{(2)}\, e^{-\alpha_2 ky}]\, e^{j(\omega t-kx)} \tag{3.22}$$

and

$$v(x,y,t) = [C_2^{(1)}\, e^{-\alpha_1 ky} + C_2^{(2)}\, e^{-\alpha_2 ky}]\, e^{j(\omega t-kx)}, \tag{3.23}$$

which imply

$$\dot{u}^* = -j\omega[C_1^{(1)*}\, e^{-\alpha_1 ky} + C_1^{(2)*}\, e^{-\alpha_2 ky}]\, e^{-j(\omega t-kx)} \tag{3.24}$$

and

$$\dot{v}^* = -j\omega[C_2^{(1)*}\, e^{-\alpha_1 ky} + C_2^{(2)*}\, e^{-\alpha_2 ky}]\, e^{-j(\omega t-kx)}. \tag{3.25}$$

$T_1$ and $T_6$ are obtained from Eqs. (2.1) and (2.6), and $S_1$, $S_2$ and $S_6$ from Eqs. (2.6)-(2.8). Then,

$$T_1 = C_{11}\, S_1 + C_{12}\, S_2 = C_{11} \frac{\partial u}{\partial x} + C_{12} \frac{\partial v}{\partial y} , \tag{3.26}$$

and

$$T_6 = C_{66}\, S_6 = C_{66} \frac{\partial v}{\partial x} + C_{66} \frac{\partial u}{\partial y} . \tag{3.27}$$

Also,

$$\frac{\partial u}{\partial x} = -jku, \tag{3.28}$$

$$\frac{\partial u}{\partial y} = [-\alpha_1 k C_1^{(1)}\, e^{-\alpha_1 ky} - \alpha_2 k C_1^{(2)}\, e^{-\alpha_2 ky}]\, e^{j(\omega t - kx)}, \tag{3.29}$$

$$\frac{\partial v}{\partial x} = -jkv, \tag{3.30}$$

and

$$\frac{\partial v}{\partial y} = [-\alpha_1 k C_2^{(1)}\, e^{-\alpha_1 ky} - \alpha_2 k C_2^{(2)}\, e^{-\alpha_2 ky}]\, e^{j(\omega t - kx)} . \tag{3.31}$$

These relations are worked out in Appendix D. It is found there that in terms of $C_2^{(2)}$, the peak amplitude of the dominant mode, $\overline{P}_x$ is real and has a value of

$$P_x = \frac{1}{2}\, \omega W [C_2^{(2)}]^2 \times 90 \times 10^9 . \tag{3.32}$$

It is also seen that, had only the vertical motion of the dominant mode been considered, the value for the power flux would have differed from Eq. (3.32) by only 9%. This suggests that a vertical shear wave of suitable depth is a good approximation for the surface wave. This is born out by the fact that Eq. (2.50) gives a speed of propagation of

$$V_p = \sqrt{\frac{0.9096 \times C_{66}}{\rho}} \qquad (3.33)$$

which differs from that of a vertical shear wave

$$V_p = \sqrt{\frac{C_{66}}{\rho}} \qquad (3.34)$$

by only 4.6%.

## 3.4 The Forced Electrostatic Problem

Any piezoelectrical interaction has been neglected so far. In quartz this is quite justified because the interaction is weak, and the expression for the power flux developed in the preceding section is quite accurate. To obtain the potential the solution obtained in Chapter 2 is now used as a forcing function in Eq. (2.5)

$$D_i = e_{ikl}\, S_{kl} + \varepsilon_{ik}^{\ \ s}\, E_k \,. \qquad (3.35)$$

Since the divergence of $\overline{D}$ is zero in the crystal (no free charges) it will be convenient to perform this operation on Eq. (3.35) with the result:

$$D_{i,i} = e_{ikl}\, S_{kl,i} + \varepsilon_{ik}^{\ \ s}\, E_{k,i} = 0 \,. \qquad (3.36)$$

The subscripts behind the commas donote a partial derivative. It can be said, furthermore, that $\overline{E}$ is $-\nabla\phi$ as in an electrostatic problem since typical dimensions are much smaller here than one wavelength in free space. It follows that

$$e_{ikl}\, S_{kl,i}\ \varepsilon_{ik}^{s}\ \phi_{,ki} = 0\ . \tag{3.37}$$

In all rotated Y-cuts in quartz the dielectric constant matrix $\varepsilon_{ij}^{s}$ is given by [4]:

$$\varepsilon_{ij}^{s} = \begin{Vmatrix} \varepsilon_{11} & 0 & 0 \\ 0 & \varepsilon_{22} & \varepsilon_{23} \\ 0 & \varepsilon_{23} & \varepsilon_{33} \end{Vmatrix} . \tag{3.38}$$

Since no variations in the z-direction are assumed Eq. (3.37) becomes:

$$\varepsilon_{11} \frac{\partial^2 \phi}{\partial x^2} + \varepsilon_{22} \frac{\partial^2 \phi}{\partial y^2} = e_{1kl} \frac{\partial}{\partial x} S_{kl} + e_{2kl} \frac{\partial}{\partial y} S_{kl} \quad . \tag{3.39}$$

In terms of engineering notation the tensor subscripts must be once more interpreted according to Table A.8 in Appendix A:

$$\begin{aligned} \varepsilon_{11} \frac{\partial^2 \phi}{\partial x^2} + \varepsilon_{22} \frac{\partial^2 \phi}{\partial y^2} = {} & e_{11} \frac{\partial S_1}{\partial x} + e_{12} \frac{\partial S_2}{\partial x} + e_{13} \frac{\partial S_3}{\partial x} + e_{14} \frac{\partial S_4}{\partial x} \\ & + e_{15} \frac{\partial S_5}{\partial x} + e_{16} \frac{\partial S_6}{\partial x} + e_{21} \frac{\partial S_1}{\partial y} + e_{22} \frac{\partial S_2}{\partial y} + e_{23} \frac{\partial S_3}{\partial y} \\ & + e_{24} \frac{\partial S_4}{\partial y} + e_{25} \frac{\partial S_5}{\partial y} + e_{26} \frac{\partial S_6}{\partial y} \quad . \end{aligned}$$

The matrix for the piezoelectric constants is also largely empty for rotated Y-cuts:

$$e_{ip} = \left\| \begin{matrix} e_{11} & e_{12} & e_{13} & e_{14} & 0 & 0 \\ 0 & 0 & 0 & 0 & e_{25} & e_{26} \\ 0 & 0 & 0 & 0 & e_{35} & e_{36} \end{matrix} \right\| . \qquad (3.40)$$

Furthermore, according to the treatment of Chapter 2, only $S_1$, $S_2$ and $S_6$ are not zero; which results in the inhomogeneous differential equation:

$$\varepsilon_{11} \frac{\partial^2 \phi(x,y,t)}{\partial x^2} + \varepsilon_{22} \frac{\partial^2 \phi(x,y,t)}{\partial y^2} = e_{11} \frac{\partial S_1}{\partial x} + e_{12} \frac{\partial S_2}{\partial x}$$

$$+ e_{26} \frac{\partial S_6}{\partial y} . \qquad (3.41)$$

The strains relate through Eqs. (2.6)-(2.8) to the solutions of the simplified surface-wave problem in complex notation Eqs. (3.22)-(3.23). The general solution is found in [4]; for this particular case it will be simpler than there. For convenience it is worked out in Appendix E. Of particular interest is the potential at the surface.

$$\phi^+ = \phi_s \, e^{j(\omega t - kx)} = \phi(x,0,t) \qquad (3.42)$$

It follows from the solution in Appendix E (Eq. E.8) that $\phi_s$ is:

$$\phi_s = \frac{(re_{11} + \alpha_1 e_{26})C_1^{(1)} + j(e_{26} - r\alpha_1 e_{12})C_2^{(1)}}{(1 + r\alpha_1)\sqrt{\varepsilon_{11}\varepsilon_{22}}}$$

$$+ \frac{(re_{11} + \alpha_2 e_{26})C_1^{(2)} + j(e_{26} - r\alpha_2 e_{12})C_2^{(2)}}{(1 + r\alpha_2)\sqrt{\varepsilon_{11}\varepsilon_{22}}} ,$$

$$r = \sqrt{\frac{\varepsilon_{22}}{\varepsilon_{11}}} . \qquad (3.43)$$

## 3.5 Transmission Line Models Based on Surface Potential

Two initial choices for dynamic variables are made in connection with $\phi^+$. First, it will be taken as the cross-variable. This will lead to a $\pi$-circuit as shown in Fig. 3.4b. The next choice is not quite as direct, but it leads ultimately to equivalent circuits for surface wave transducers which are very similar to the Mason circuit for bulk waves (see Fig. 3.1a):

$$I^+ = j\omega\sqrt{\varepsilon_{11}\varepsilon_{22}}\, W\phi^+ \tag{3.44}$$

and

$$I^- = -j\omega\sqrt{\varepsilon_{11}\varepsilon_{22}}\, W\phi^- \,, \tag{3.45}$$

where I(x) is the through-variable as defined in Fig. 3.2

$$I(x) = I^+(x) - I^-(x) \tag{3.46}$$

and

$$\phi^- = \Phi_s\, e^{j(\omega t+kx)} \tag{3.47}$$

represents a generalization of the treatment where only waves in the (+)x-direction are considered. For either approach, it will first be necessary to evaluate $\Phi_s$ in Eq. (3.43) in terms of $C_2^{(2)}$ so that the characteristic impedance or admittance may be determined according to Eq. (3.18).

By means of the tensor transformation [4]

$$e_{ijk}' = \alpha_{ir}\, \alpha_{js}\, \alpha_{kl}\, e_{rst} \tag{3.48}$$

the required piezoelectric constants for the AC cut are obtained:

$$e_{11}' = 0.171 \text{ C/m}^2$$

$$e_{12}' = -0.1615 \text{ C/m}^2$$

$$e_{26}' = 0.106 \text{ C/m}^2 \quad .$$

$\varepsilon_{11} = 39.21 \times 10^{-12}$ F/m is not affected by the rotation about the x-axis, but $\varepsilon_{22}$ suffers a slight change, i.e.

$$\varepsilon_{22}' = \alpha_{2r}\,\alpha_{2s}\,\varepsilon_{rs} \tag{3.49}$$

or

$$\varepsilon_{22}' = \cos^2\theta\,\varepsilon_{22} + 2\cos\theta\sin\theta\,\varepsilon_{23} + \sin^2\theta\,\varepsilon_{33} \tag{3.50}$$

or

$$\varepsilon_{22}' = 39.71 \times 10^{-12} \text{ F/m} \; . \tag{3.51}$$

The potential at the surface becomes

$$\phi_s = \frac{(0.17+1.4\text{x}0.106)(-j0.66) - j(0.106+1.4\text{x}0.163)(0.079)}{(1 + 1.0063 \times 1.4) \times 39.46 \times 10^{-12}} C_2^{(2)}$$

$$+ \frac{(0.17+0.147\text{x}0.106)(j0.052)+j(0.106+0.147\text{x}0.163)}{(1 + 1.0063 \times 0.147) \times 39.46 \times 10^{-12}} C_2^{(2)}. \tag{3.52}$$

This reduces to

$$\phi_s = -j2.225 \times 10^{+9}\, C_2^{(2)} - j0.277 \times 10^{+9}\, C_2^{(2)} + j0.215 \times 10^{+9}\, C_2^{(2)} + j2.867 \times 10^{+9}\, C_2^{(2)} \; . \tag{3.53}$$

Hence,

$$\phi_s = j5.8 \times 10^8 \; C_2^{(2)} \; (58 \text{ mV for } C_2^{(2)} = 10^{-10}\text{m}) . \qquad (3.54)$$

The numbers were left in the same order in which they appear in Eq. (3.43). It is seen that the slowly decaying "shear" mode still furnishes the main contribution to this particular property of the surface wave, but it is strongly opposed by the electric interaction of the "longitudinal" mode which exists closer to the surface.

$\phi$ is now selected as the cross variable

$$\phi(x) = \phi^+(x) + \phi^-(x) . \qquad (3.55)$$

The characteristic admittance according to Eq. (3.18) is then

$$Y_o = 2P_x/|\phi_s|^2 . \qquad (3.56)$$

From Eqs. (3.32) and (3.54) follows the value for $Y_o$.

$$Y_o = \omega W[C_2^{(2)}]^2 \times 90 \times 10^9/[5.8 \times 10^8 \; C_2^{(2)}]^2 \qquad (3.57)$$

$$Y_o = \omega W \times 2.68 \times 10^{-7} \mho \qquad (3.58)$$

Typical values for W are 3mm and for $\omega$ $10^9$ rad/sec. Then $Y_o = 0.8\mho$ and the corresponding through variable would be $I^+ = Y_o \phi^+$ where $I^+ = 0.8 \times 58 \times 10^{-3} \sim 50$ ma for a wave in the x-direction. The line potential was based in Eq. (3.54) on a peak vertical displacement of 1Å at the surface. It should be noted in Eq. (3.58) that the line admittance increases with frequency. This result defines now for any section of line the equivalent circuit shown in Fig. 3.4b, or if $Z_o = 1/Y_o$ is used, the circuit in Fig. 3.4a.

Alternately a through-variable may be defined first as in Eq. (3.44). $Z_o$ follows from Eq. (3.18):

$$Z_o = 2P_x/\omega^2\varepsilon_{11}\varepsilon_{22}\, W^2|\phi_s|^2 \tag{3.59}$$

with the values obtained in Eqs. (3.54) and (3.32) this becomes:

$$Z_o = \frac{\omega W \times 90 \times 10^9 \times 10^{24}}{\omega^2 W^2 \times 39.21 \times 39.71 \times 5.8^2 \times 10^{16}}\ \Omega \tag{3.60}$$

$$Z_o = \frac{1.72 \times 10^{14}}{\omega W}\ \Omega\ . \tag{3.61}$$

$Z_o$ decreases with frequency. For a wave to the right, of peak amplitude $C_2^{(2)}$ of 1A, $I^+ = j\omega\sqrt{\varepsilon_1\varepsilon_2}\, W\phi^+$ has a peak value of 6.87μA for $\omega = 10^9$/sec and $W = 3 \times 10^{-3}$ m. The corresponding cross-variable is then

$$V^+ = Z_o\, I^+\ . \tag{3.62}$$

$Z_o$ at $\omega = 10^9$/sec, $W = 3 \times 10^{-3}$ m is 57.3 MΩ. $V^+$ has then a peak amplitude of 394 volts. With the aid of Eq. (3.61) the equivalent circuit shown in Fig. 3.4a is now defined for any given length of transmission line.

## 3.6 The Vertical Shear Wave Approximation

It was pointed out earlier that the speed of propagation of a vertical shear wave differs from that of the surface wave by only 4.6%. Furthermore the major contribution to the power flux (Eq. 3.32) comes from the last term in Eq. (D.3), Appendix D:

$$P_x \approx \frac{c_{66}\, W\omega}{4\alpha_2}\, |C_2^{(2)}|^2 \; . \tag{3.63}$$

The error here was only 8.8%. This contribution is the same as the power flux of a vertical shear wave of effective thickness h, where h can be found from an expression corresponding to Eq. (3.20).

$$\overline{P}_x = -\frac{W}{2}\, [T_6\, \dot{v}^*]\, h \tag{3.64}$$

For $\dot{v}^*$ the value of the surface wave at y = 0 is taken, but for mode 2 only (Eq. 3.25):

$$\dot{v}^* = -j\omega\, C_2^{(2)*}\, e^{-j(\omega t-kx)} \; . \tag{3.65}$$

$T_6$ follows from Eq. (3.27), consistent with the present approximation.

$$T_6 = c_{66}\, S_6 = c_{66}\, \frac{\partial v}{\partial x} = -jk\, c_{66}\, v, \tag{3.66}$$

which becomes through Eq. (3.23):

$$v(x,0,t) \approx C_2^{(2)}\, e^{j(\omega t-kx)} \tag{3.67}$$

$$T_6 = -jk\, c_{66}\, C_2^{(2)}\, e^{j(\omega t-kx)} \; . \tag{3.68}$$

The power flux, as defined in Eq. (3.64), is then

$$\overline{P}_x = -\frac{W}{2}\, [-jk\, c_{66}\, C_2^{(2)}\, C_2^{(2)*}\, (-j\omega)]\, h, \tag{3.69}$$

where

$$\frac{2\pi}{\lambda} = k = \omega/V_p \; , \text{ and } \frac{V_p}{\omega} = \frac{1}{k} = \frac{\lambda}{2\pi} \; . \tag{3.70}$$

Hence,

$$\overline{P}_x = \frac{W\omega^2}{2V_p}\, c_{66}\, |C_2^{(2)}|^2\, h \; . \tag{3.71}$$

This is to equal Eq. (3.63):

$$\frac{c_{66}\, W\omega}{4\alpha_2} = \frac{c_{66}\, W\omega^2}{2V_p} h \;. \tag{3.72}$$

It follows that the effective thickness h of the equivalent shear wave should be:

$$h = \frac{V_p}{2\omega\alpha_2} = \frac{10700}{\omega} \text{ m} \;. \tag{3.73}$$

It decreases with frequency. In terms of a wave length the effective thickness is

$$h = \frac{\lambda}{4\pi\alpha_2} = 0.54\lambda \;. \tag{3.74}$$

In the Mason model (see Fig. 3.1a) particle velocity is taken to be the through-variable. There longitudinal waves were considered. In that case the natural choice for reference directions would be such that the forward and reverse waves would subtract as shown in Fig. 3.2. For a shear wave the particle velocity is in the transverse direction. The displacement at the surface given by Eq. (3.23) is, using the "mode 2" approximation:

$$v^+ = C_2^{(2)}\, e^{j(\omega t - kx)} \;. \tag{3.75}$$

The reverse wave would have displacement:

$$v^- = C_2^{(2)}\, e^{j(\omega t + kx)} \;. \tag{3.76}$$

By Eq. (3.66) the shear stress is

$$T_6 = c_{66} \frac{\partial v}{\partial x} \;. \tag{3.77}$$

This results in

$$T_6^{\ +} = -jk\ C_2^{\ (2)}\ e^{j(\omega t-kx)}\ C_{66} \tag{3.78}$$

and

$$T_6^{\ -} = jk\ C_2^{\ (2)}\ e^{j(\omega t+kx)}\ C_{66}\ . \tag{3.79}$$

The velocities add and the stresses subtract. One could take various choices now. Here, arbitrarily, the cross-variable will be defined as

$$V = -T_6 Wh = -T_6^{\ +}Wh - T_6^{\ -}Wh = V^+ + V^- \tag{3.80}$$

and the through-variable has to be taken then as

$$I = I^+ - I^-\ , \tag{3.81}$$

where $I^+$ and $I^-$ must be in accordance with Eq. (3.64)

$$I^+ = j\omega C_2^{\ (2)}\ e^{j(\omega t-kx)} = \dot{v}^+ \tag{3.82}$$

and

$$I^- = -j\omega C_2^{\ (2)}\ e^{j(\omega t+kx)} = -\dot{v}^-\ . \tag{3.83}$$

The quantity $(WhT_6)$ is the counter force acting externally on the section. For this reason, the power flux expression contains a minus sign. Accordingly $V^+$ equals $-T_6Wh$. The characteristic impedance is now

$$Z_o = \frac{V^+}{I^+} = \frac{-T_6 Wh}{\dot{v}^+} = \frac{jkC_{66}\ C_2^{\ (2)}\ Wh}{j\omega\ C_2^{\ (2)}} = \frac{kC_{66}Wh}{\omega}\ . \tag{3.84}$$

By Eq. (3.74): $h = \lambda/4\pi\alpha_2$, $k = 2\pi/\lambda$ and hence $Z_o$ becomes

$$Z_o = \frac{C_{66}\ W}{2\alpha_2\ \omega} \quad . \tag{3.85}$$

This last expression (Eq. (3.85)) resembles Eq. (3.61) where the surface potential was used. There, also, the numerator is proportional to $C_{66}$ if the dominant term for the power flux is considered (Eq. D.3, Appendix D):

$$P_x = \frac{C_{66}\ W\omega}{2} \cdot \frac{|C_2^{(2)}|^2}{2\alpha_2} \quad . \tag{3.86}$$

By Eq. (3.59) $Z_o$ is

$$Z_o = 2P_x/\omega^2\varepsilon_{11}\varepsilon_{22}\ W^2\ |\Phi_s|^2 \ . \tag{3.87}$$

According to Eqs. (3.53) and (3.43) the largest contribution to $\Phi_s$ is:

$$\frac{j\ e_{26}\ C_2^{(2)}}{\sqrt{\varepsilon_{11}\varepsilon_{22}}} \quad . \tag{3.88}$$

Because of cancellations $\Phi_s$ is less:

$$\Phi_s \simeq 0.215 \times \frac{j\ e_{26}\ C_2^{(2)}}{\sqrt{\varepsilon_{11}\varepsilon_{22}}} \quad . \tag{3.89}$$

The characteristic impedance in Eq. (3.61) is then in general symbols approximately:

$$Z_o \simeq \frac{C_{66}\ W\omega}{2\alpha_2} \cdot \frac{1}{\omega^2\varepsilon_1\varepsilon_2\ W^2} \cdot \frac{\varepsilon_{11}\varepsilon_{22}}{0.215^2\ e_{26}^2} \tag{3.90}$$

$$Z_o \simeq \frac{C_{66}\ W}{2\alpha_2\ \omega} \times \left(\frac{22}{W^2 e_{26}^2}\right) \ . \tag{3.91}$$

Comparison of Eqs. (3.91) and (3.85) shows the relation between the purely mechanical representation of a piezoelectric transmission line section and the representation through the surface potential. It should be noted that both expressions are proportional to $C_{66}$ and, therefore, to $V_p^2$. This differs from the treatment by Smith et al [7], [10], [11]. There $Z_o$ is proportional to $V_p$. That result follows directly from Eq. (3.84):

$$Z_o = \frac{kC_{66}Wh}{\omega} = \frac{C_{66}Wh}{V_p} , \qquad (3.92)$$

$$C_{66} = V_p^2 \rho \qquad (3.93)$$

is next replaced to yield

$$Z_o = \rho V_p Wh . \qquad (3.94)$$

This is Mason's expression for $Z_o$ which would apply here if h were to be taken as a constant. But $h = \lambda/4\pi\alpha_2$ results in the correct expression Eq. (3.85) used here.

## 3.7 Modification of $Z_o$ Through Consideration of the Piezoelectric Interaction

In this section it will be established that for the vertical shear wave $C_{66}$ must be modified when the electric field is not disregarded. This treatment is taken from Berlincourt et al [12]. The piezoelectric constitutive Eqs. (2.4)-(2.5) are for this special case:

$$T_6 = c^E_{66} S_6 - e_{26} E_2 \qquad (3.95)$$

$$D_2 = e_{26} S_6 + \varepsilon_2 E_2 . \qquad (3.96)$$

But the region is charge-free so that the divergence of D is zero. In this case then

$$\frac{\partial D_2}{\partial x} = 0 = e_{26}\,\frac{\partial S_6}{\partial x} + \varepsilon_2\,\frac{\partial E_2}{\partial x} \qquad (3.97)$$

may be combined with Eq. (3.95) to eliminate $E_2$. Then

$$\frac{\partial T_6}{\partial x} = C^E_{66}\,\frac{\partial S_6}{\partial x} - e_{26}\,\frac{\partial E_2}{\partial x}\ . \qquad (3.98)$$

But $\frac{\partial T_6}{\partial x}$ is the net force per unit volume acting in the y-direction:

$$\frac{\partial T_6}{\partial x} = \rho\frac{\partial^2 v}{\partial t^2}\quad , \qquad (3.99)$$

$S_6$ is here $S_6 = \frac{\partial v}{\partial x}$ so that Eq. (3.98) becomes:

$$\rho\,\frac{\partial^2 v}{\partial t^2} = C^E_{66}\,\frac{\partial^2 v}{\partial x^2} - e_{26}\,\frac{\partial E_2}{\partial x}\ . \qquad (3.100)$$

Let the speed of propagation for an independent E-field be $V_p{}^E = \sqrt{\frac{C_{66}}{\rho}}$ . Then Eq. (3.100) may be regarded as an inhomogeneous wave equation with $(e_{26}/C^E_{66})\,\frac{\partial E_2}{\partial x}$ as the source term:

$$\frac{\partial^2 v}{\partial x^2} - \frac{1}{(V^E_p)^2}\,\frac{\partial^2 v}{\partial t^2} = \frac{e_{26}}{C^E_{66}}\,\frac{\partial E_2}{\partial x}\quad . \qquad (3.101)$$

If $E_2$ is forced externally then $V_p{}^E$ is indeed the speed of propagation. Through Eq. (3.97) $\frac{\partial E_2}{\partial x}$ and $\frac{\partial^2 v}{\partial x^2}$ are interdependent:

$$\frac{\partial E_2}{\partial x} = -\,\frac{e_{26}}{\varepsilon_2}\,\frac{\partial^2 v}{\partial x^2}\ . \qquad (3.102)$$

Equation (3.100) then becomes

$$\rho \frac{\partial^2 v}{\partial t^2} = C_{66}^E \left[1 + \frac{e_{26}^2}{\varepsilon_2 C_{66}^E}\right] \frac{\partial^2 v}{\partial x^2} , \qquad (3.103)$$

which defines $C_{66}^D$ as

$$C_{66}^D = C_{66}^E \left[1 + \frac{e_{26}^2}{\varepsilon_2 C_{66}^E}\right] . \qquad (3.104)$$

The corresponding speed of propagation

$$V_p^D = \sqrt{\frac{C_{66}^D}{\rho}} \qquad (3.105)$$

is then higher, i.e.

$$V_p^D = V_p^E \sqrt{1 + \frac{e_{26}^2}{\varepsilon_2 C_{66}^E}} . \qquad (3.106)$$

For the values used before $(e_{26}^2/C_{66}\varepsilon) \approx 0.01$. This means from Eq. (3.104) that $Z_o$ should be taken 1% higher in Eq. (3.61) and in Eq. (3.85). The velocity Eq. (3.106) would increase by only 1/2%.

Smith et al [11] state that the changes in impedance and velocity are the same:

$$\frac{Z_o}{Z_m} = \frac{V_o}{V_m} \approx 1 + \frac{1}{2} k_c^2 . \qquad (3.107)$$

The quantity $k_c$ is the electromechanical coupling coefficient. In the present case this would be

$$k_c = \frac{e_{26}}{\sqrt{\varepsilon_2 C_{66}}} . \qquad (3.108)$$

Equation (3.106) agrees with Eq. (3.107). However, the change in impedance should be proportional to $1 + k_c^2$. This follows directly from Eq. (3.104) and Eq. (3.85). Smith et al [11], on the other hand, base their conclusion (Eq. (3.107)) on the expression for $Z_o$ given in Eq. (3.94) where $Z_o$ seems to be proportional to $V_p$. The correct statement is

$$Z_o = Z_m(1 + k_c^2) \ . \tag{3.109}$$

The quantities $Z_m$ and $Z_o$ are the uncorrected and corrected impedance values.

## 3.8 Summary

A method has been described by which an equivalent circuit may be obtained for a section of piezoelectric surface wave transmission line. The expression for the characteristic impedance followed from the value of the power flux and a suitably chosen dynamic variable. By means of the vertical shear wave approximation, it was finally shown how, in retrospect, the initially omitted electric interaction may be accounted for to produce slightly higher values for the characteristic impedance and the speed of propagation.

## CHAPTER 4

## THE MODIFIED MASON MODEL

### 4.1 Description of a Surface Wave Transducer and its Simplified Physical Model

The typical layout of a surface wave transducer is shown in Fig. 4.1. Alternate electrodes are interconnected. When the transducer is used for excitation of surface waves, the array is connected to an electric signal source. Conversely, the surface potential difference can be detected by the array when a surface wave travels through it.

The electric field distribution between adjacent electrodes is rather complicated. It will be dealt with in subsequent chapters. In the current literature it is assumed that only the field component in the y-direction contributes significantly to the surface potential [7], [13]. Mason's bulk wave transducer model [5] with crossed-field excitation (Fig. 3.1) is there employed for an interspace and half of its two nearest neighbors. According to the results of Chapter 2, the surface wave behavior is in several respects similar to that of a vertical shear wave. The equivalent thickness was developed in Chapter 3, Eq. (3.74):

$$h = \lambda/4\pi\alpha_2 = 10700/\omega \ . \tag{4.1}$$

The surface potential Eq. (3.43) also obtained its major contribution from the vertical displacement producing an E-field in the

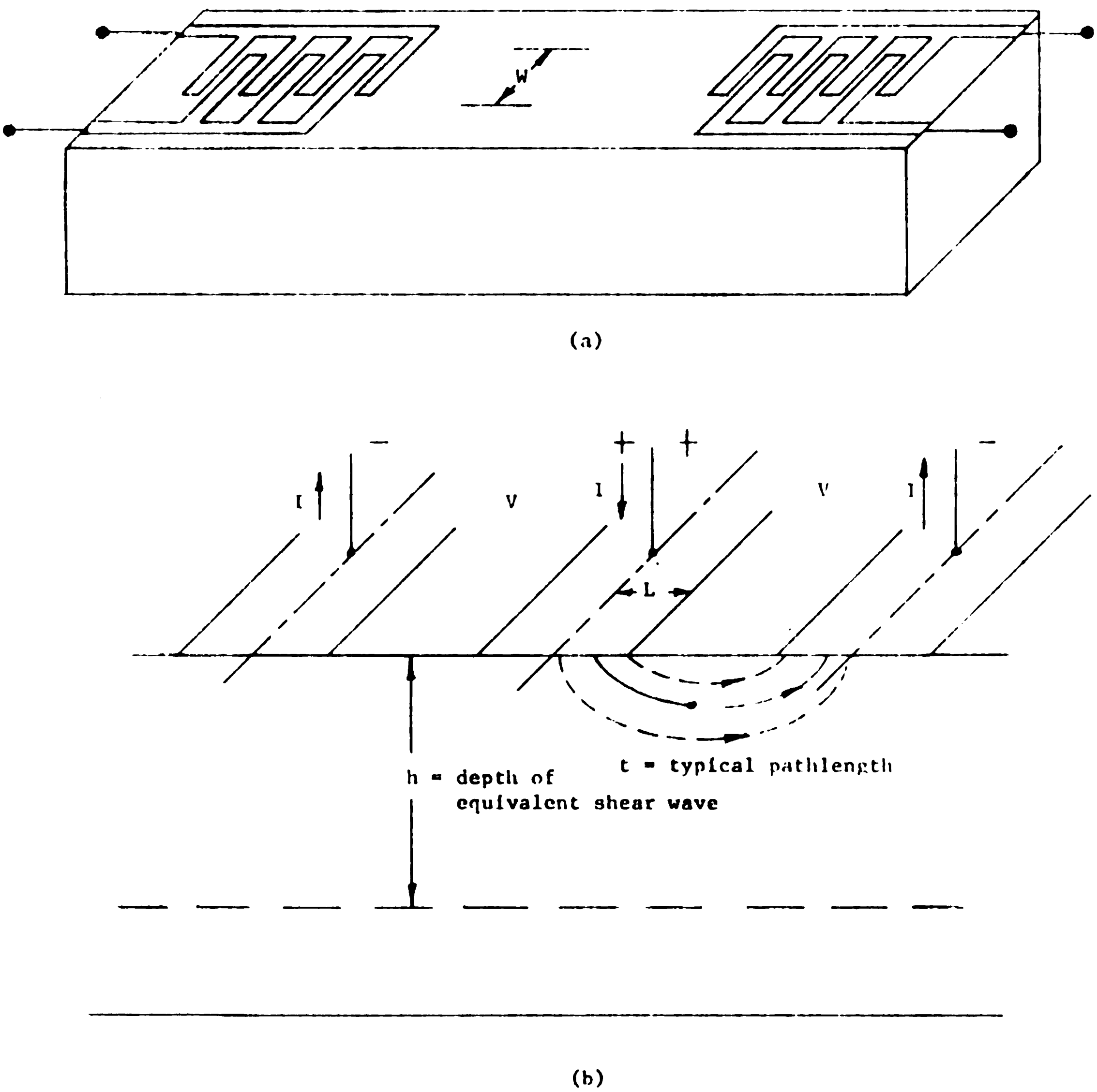


Figure 4.1 - Layout of surface-wave transducers.
(a) Overview.
(b) Detail showing field lines and equivalent depth.

y-direction:

$$\phi_s \sim \frac{j\, e_{26}\, C_2^{(2)}}{\sqrt{\varepsilon_{11}\varepsilon_{22}}} \quad . \tag{4.2}$$

Expression (4.2) is too large, but this is taken into account by suitable correction factors.

The main justification for this equivalent circuit is, however, that it predicts observed behavior [7], [13].

## 4.2 Development of the Model for One Electrode Section

The reference directions are shown in Fig. 4.2. It represents a "free-body" diagram. The thickness is $h = \lambda/4\pi\alpha_2$, the width W and the length L. It is assumed that a vertical shear wave can exist throughout this volume and that the E-field consists of $E_2$ only, where $E_2$ is assumed to be constant within the volume. For this case the constitutive Eqs. (2.4)-(2.5) are:

$$T_6 = C_{66}S_6 - e_{26}E_2 \tag{4.3}$$

$$D_2 = e_{26}S_6 + \varepsilon_2 E_2 \tag{4.4}$$

The standard assumption [12] is that the particle displacement $\xi(x)$ may be described by a standing wave. The same may then be said about the particle velocity $\dot{\xi}(x)$ and the strain Eq. (3.66):

$$S(x) = \frac{\partial \xi}{\partial x} \tag{4.5}$$

Let all of the variables be represented by complex exponents. By Euler's relation a standing wave may be expressed as the superposition of two waves:

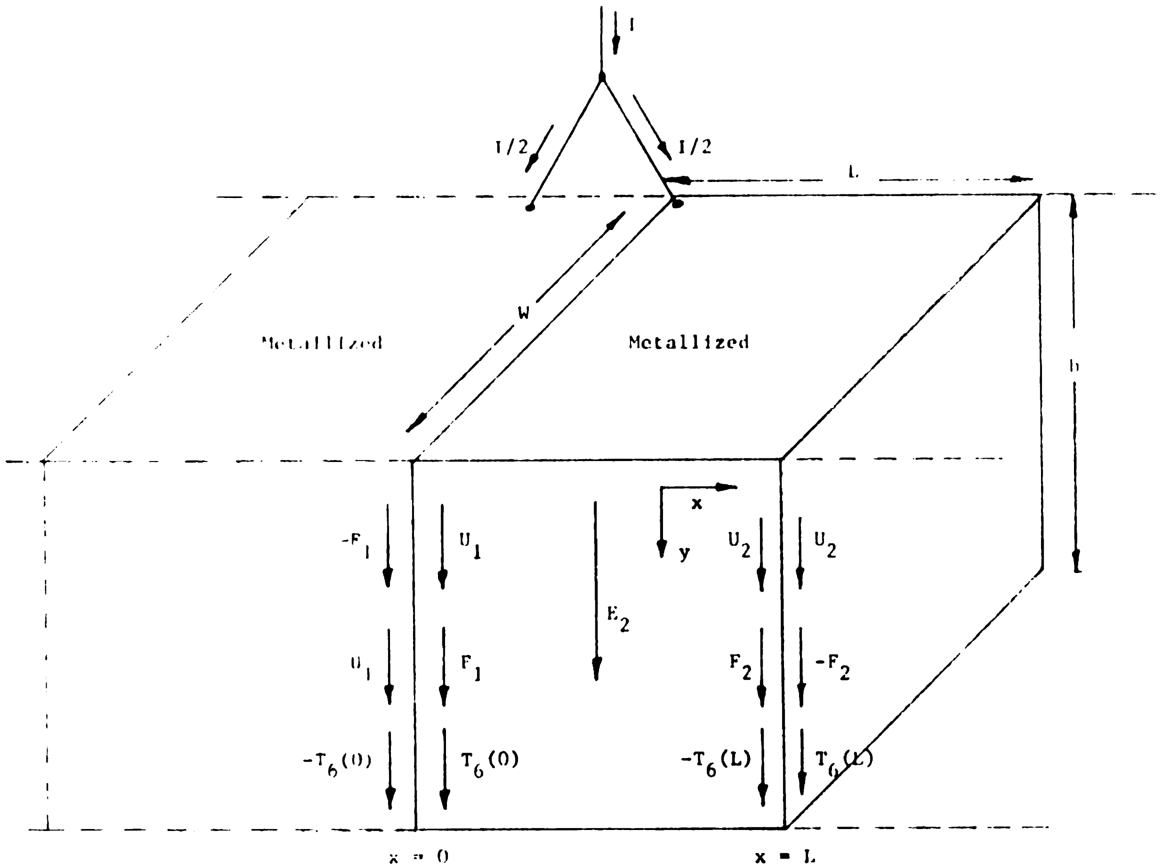


Figure 4.2 - Free-body diagram of section under a half electrode used for the development of the Mason circuit.

$$\dot{\xi}(x) = K_1\ e^{-jkx} + K_2\ e^{jkx}\ . \tag{4.6}$$

It follows that $U_1$ and $U_2$ are

$$\begin{Vmatrix} U_1 \\ \\ U_2 \end{Vmatrix} = \begin{Vmatrix} 1 & 1 \\ \\ e^{-jkL} & e^{jkL} \end{Vmatrix} \begin{Vmatrix} K_1 \\ \\ K_2 \end{Vmatrix} . \tag{4.7}$$

These relations yield $K_1$ and $K_2$ in terms of the terminal velocities $U_1$ and $U_2$

$$\begin{Vmatrix} K_1 \\ \\ K_2 \end{Vmatrix} = \frac{1}{2j\sin kL} \begin{Vmatrix} e^{jkL} & -1 \\ \\ -e^{-jkL} & 1 \end{Vmatrix} \begin{Vmatrix} U_1 \\ \\ U_2 \end{Vmatrix} . \tag{4.8}$$

By Eqs. (4.5)-(4.6) the strain is:

$$S_6(x) = \frac{\partial \xi}{\partial x} = \frac{1}{j\omega}\frac{\partial \dot{\xi}}{\partial x} = K_1\left(\frac{-jk}{j\omega}\right) e^{-jkx} + K_2\left(\frac{jk}{j\omega}\right) e^{jkx}\ . \tag{4.9}$$

With the aid of $k/\omega = V_p$, $S_6(0)$ and $S_6(L)$ may now be expressed as:

$$\begin{Vmatrix} S_6(0) \\ \\ S_6(L) \end{Vmatrix} = \begin{Vmatrix} -\frac{1}{V_p} & \frac{1}{V_p} \\ \\ -\frac{e^{-jkL}}{V_p} & \frac{e^{jkL}}{V_p} \end{Vmatrix} \begin{Vmatrix} K_1 \\ \\ K_2 \end{Vmatrix} \tag{4.10}$$

or

$$\begin{Vmatrix} S_6(0) \\ \\ S_6(L) \end{Vmatrix} = \frac{1}{2j\sin(kL)} \begin{Vmatrix} -\frac{1}{V_p} & \frac{1}{V_p} \\ \\ -\frac{e^{-jkL}}{V_p} & \frac{e^{jkL}}{V_p} \end{Vmatrix} \begin{Vmatrix} e^{jkL} & -1 \\ \\ -e^{-jkL} & 1 \end{Vmatrix} \begin{Vmatrix} U_1 \\ \\ U_2 \end{Vmatrix} \tag{4.11}$$

where the column matrix has been replaced by Eq. (4.8). These equations are multiplied by $C_{66}$ to obtain the stresses acting on a surface to the left, providing $E_2$ is held equal to zero:

$$\begin{Vmatrix} T_6(0) \\ \\ T_6(L) \end{Vmatrix} = \frac{C_{66}/V_p}{j\sin(kL)} \begin{Vmatrix} -\cos(kL) & 1 \\ \\ -1 & +\cos(kL) \end{Vmatrix} \begin{Vmatrix} U_1 \\ \\ U_2 \end{Vmatrix} . \qquad (4.12)$$

If $E_2$ is not zero, then the quantity $-e_{26}E_2$ is added to both equations. The internally acting forces at the left and right surface relate to those stresses by Wh for the left surface and -Wh for the right surface:

$$\begin{Vmatrix} F_1 \\ \\ F_2 \end{Vmatrix} = \frac{WhC_{66}/V_p}{j\sin(kL)} \begin{Vmatrix} -\cos(kL) & 1 \\ \\ 1 & -\cos(kL) \end{Vmatrix} \begin{Vmatrix} U_1 \\ \\ U_2 \end{Vmatrix} - \begin{Vmatrix} e_{26}WhE_2 \\ \\ -e_{26}WhE_2 \end{Vmatrix} \qquad (4.13)$$

The electric current I/2 is related to the displacement $D_2(x)$ by

$$I/2 = W\int_0^L \dot{D}_2(x)\,dx = j\omega W\int_0^L D_2\,dx \quad . \qquad (4.14)$$

The current is denoted by I/2 because the section in Fig. 4.2 shows only one-half of one electrode.

By Eqs. (4.8)-(4.9) $S_6(x)$ is

$$S_6(x) = \frac{1}{V_p}\,[-e^{-jkx} \quad e^{jkx}] \begin{Vmatrix} K_1 \\ \\ K_2 \end{Vmatrix} , \qquad (4.15)$$

or

$$S_6(x) = \frac{1}{2jV_p\sin kL}\,[-e^{-jkx} \quad e^{jkx}] \begin{Vmatrix} e^{jkL} & -1 \\ \\ -e^{-jkL} & 1 \end{Vmatrix} \begin{Vmatrix} U_1 \\ \\ U_2 \end{Vmatrix} , \qquad (4.16)$$

i.e.,

$$S_6(x) = \frac{-\cos k(L-x)}{jV_p \sin kL} U_1 + \frac{\cos kx}{jV_p \sin kL} U_2 \ . \tag{4.17}$$

Equation (4.4) combined with (4.14) results in:

$$I/2 = j\omega W \int_0^L \left[\frac{-U_1 e_{26}}{jV_p \sin kL} \cos k(L-x) + \frac{U_2 e_{26}}{jV_p \sin kL} \cos kx + \varepsilon_2 E_2\right] dx \tag{4.18}$$

or

$$I/2 = -We_{26}\, U_1 + We_{26}\, U_2 + j\omega WL\varepsilon_2 E_2 \ . \tag{4.19}$$

The actual field is not simply $E_2$. Let t be $\frac{1}{2}$ the effective path length to the adjacent electrode of opposite polarity such that

$$tE_2 = V/2 \ , \tag{4.20}$$

where V is the actual potential difference. Then Eqs. (4.13) and (4.19) may be reexpressed as follows:

$$\left\|\begin{matrix} -F_1 \\ F_2 \\ (\frac{I}{2}) \end{matrix}\right\| = \left\|\begin{matrix} \frac{Z_o}{j\tan(kL)} & \frac{Z_o}{j\sin(kL)} & e_{26}W \\ \frac{Z_o}{j\sin(kL)} & \frac{Z_o}{j\tan(kL)} & e_{26}W \\ -e_{26}W & -e_{26}W & \frac{j\omega\varepsilon_2 WL}{h} \end{matrix}\right\| \left\|\begin{matrix} U_1 \\ -U_2 \\ \frac{Vh}{2t} \end{matrix}\right\| \ . \tag{4.21}$$

This choice of algebraic signs is necessary to obtain for an electric short circuit (V = 0) transmission-line behavior identical to that derived in Section 3.6, Eq. (3.5). Here as there (Eq. (3.84)),

$$Z_o = Wh\, C_{66}/V_p = C_{66}\, W/2\alpha_2\omega \ . \tag{4.22}$$

Since $-F_1$ must now be used as the cross-variable at x = 0, it is apparent (see Fig. 4.2) that the cross-variable is always the force applied to the face of a "free body" to the right. This is consistent with the reference direction taken for the power flux in Chapter 3. Particle motion in the y-direction is represented by through-variable arrows pointing to the right for consistency with Eq. (3.5) and Fig. 3.4.

The depth h of the shear wave is not a constant, it rather decreases with frequency:

$$h = 0.52\lambda \ .$$

On the other hand, the effective path-length t, chosen to make

$$V/2 = tE_2,$$

is in no way related to frequency. But, the device will be used at a frequency where the separation of the electrodes is roughly half a wavelength. The quantities t and h will then be of the same order of magnitude. It is required to make the identification

$$h = t$$

in order to form the equivalent circuit in Fig. 4.3, on the basis of satisfying Kirchhoff's laws. The turns ratio N on the basis of Eq. (4.21) must be of the form

$$N = e_{26} W \ . \tag{4.23}$$

For convenience, the turns ratio is actually described as follows:

$$N = V_p k_e W\sqrt{\varepsilon_2 \rho} \ , \tag{4.24}$$

if $k_e$ is defined as $k_c$ before in Chapter 3 as

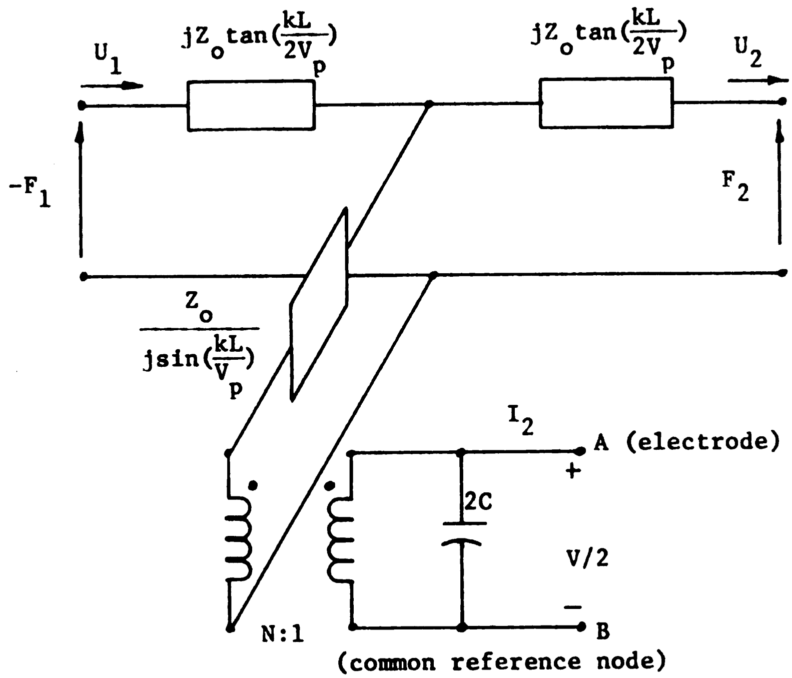


Figure 4.3 - Equivalent circuit for a half-electrode of a shear-wave transducer.

$$k_e = \frac{e_{26}}{\sqrt{\varepsilon_2 C_{66}}} \quad , \tag{4.25}$$

and $\sqrt{C_{66}}$ is expressed as

$$\sqrt{C_{66}} = v_p \sqrt{\rho} \quad ,$$

then Eqs. (4.23)-(4.24) are identical.

However, it was seen in Chapter 3, that the surface potential of a surface wave is smaller than the value produced by the vertical shear wave, which has been used for the development of the equivalent circuit. To correct this error, an appropriate value will be chosen for the piezoelectric coupling coefficient $k_e$ in the next section.

The expression $j\omega\varepsilon_2 WL/h$ relates half the current into one electrode to half the interelectrode potential difference. It is, therefore, equal to $j\omega$ times the capacitance between one electrode and its two neighbors. The capacitance to one neighbor, however, is of more practical interest and is defined as C,

$$C = \frac{\varepsilon_2 WL}{2t} \quad . \tag{4.26}$$

The values for the elements in the T-circuit are obtained from Eq. (4.21) as in Section 3.1, Eq. (3.8).

## 4.3 The Determination of the Effective Coupling Coefficient $k_e$

The turns ratio in the Mason circuit, Fig. 4.3, is proportional to the coupling coefficient $k_e$. In this section the surface potential, Eqs. (3.43) and (3.54), will be related to $k_e$ by means of the Mason equivalent circuit. Since the surface potential is known a value for $k_e$ may be obtained which yields results consistent with surface waves. This is true despite the fact that the Mason circuit was based on the shear-wave approximation.

In Fig. 4.4 two half-electrode sections are separated by an inactive transmission line section. This is an approximation since the area between the electrodes also has an applied electric field. This field is largely in the x-direction, as shown in Fig. 4.1b. The piezoelectric constant, $e_{16}$, which relates $E_1$ to $T_6$ is zero (Eq. (3.4)). This approximation is, therefore, consistent with the vertical shear-wave approximation.

The section is one half of a period D in the transducer structure Fig. 4.1a. The origin is chosen at the mid-point between any two electrodes. It was established at the end of Chapter 3 that the presence of an electric field has little effect on $V_p$, the speed of propagation, and on $Z_o$, the characteristic impedance. It is, therefore, reasonable to assume that a wave can travel through this section with a constant velocity and negligible reflections.

Let the complex amplitude be:

$$U(x) = U\, e^{-jkx} \quad . \tag{4.27}$$

The open circuit voltage is

$$V_{OC} = \frac{\phi}{j\omega 2C}\,[U_1 - U_2] - \frac{\phi}{j\omega 2C}\,[U_3 - U_4] \ , \tag{4.28}$$

where $U_1 = U\, e^{j\frac{kD}{4}}$ $\qquad U_2 = U\, e^{j\frac{kD(1-\eta)}{4}}$ $\qquad$ (4.29)

and $\quad U_4 = U\, e^{-j\frac{kD}{4}}$ $\qquad U_3 = U\, e^{-j\frac{kD(1-\eta)}{4}}$ . $\qquad$ (4.30)

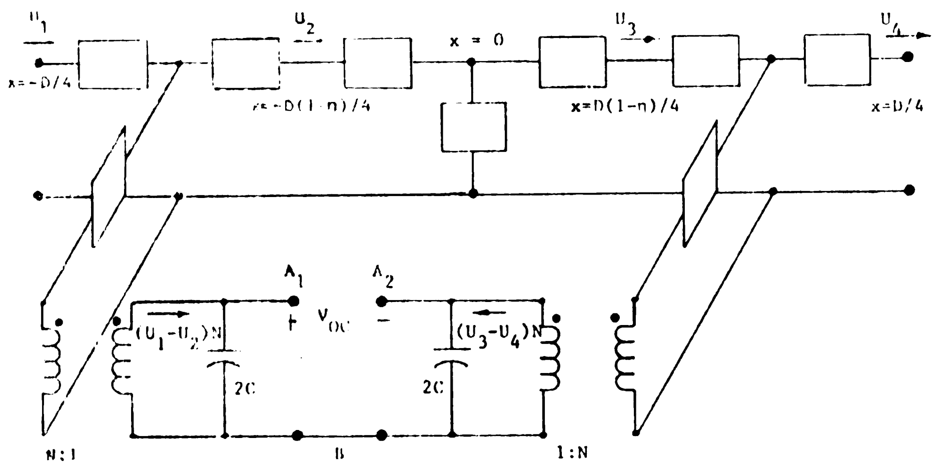


Figure 4.4 - Determination of the open circuit voltage between adjacent half electrodes for $U(x) - U\ e^{-jkx}$ employing sections of the equivalent shear-wave circuit.

The quantity $U_4 - U_3$ is multiplied by the complex conjugate of the quantity $U_1 - U_2$. It follows that Eq. (4.28) becomes

$$V_{OC} = \frac{NU}{j\omega C} \mathrm{Re}[e^{j\frac{kD}{4}} - e^{j\frac{kD(1-\eta)}{4}}] \tag{4.31}$$

i.e.

$$V_{OC} = \frac{NU}{j\omega C} [\cos\frac{kD}{4} - \cos\frac{kD(1-\eta)}{4}] \; . \tag{4.32}$$

This expression gives the open circuit response for any frequency

$$\omega = kV_p \; . \tag{4.33}$$

At present the attention will be focused on the special case when $\omega$ is the so-called synchronous frequency $\omega_o$. At this frequency the wavelength $\lambda$ equals the period in the comb structure D. It is clear that, when $\omega = \omega_o$ and the electrodes become very narrow, the open circuit voltage, $V_{OC}$, is twice the surface potential. This is used to specify the turns ratio N.

The open circuit voltage for infinitely narrow electrodes is:

$$V_{OC} = \frac{NU}{j\omega} \left\{ \lim_{\eta\to 0} \frac{1}{C} [\cos\frac{kD}{4} - \cos\frac{kD(1-\eta)}{4}] \right\}. \tag{4.34}$$

By trigonometric expansion, and the fact that for small $\theta$ $\cos\theta \simeq 1$ and $\sin\theta \simeq \theta$ the open circuit voltage becomes

$$V_{OC} = - NC_2^{(2)} \sin\frac{kD}{4} [\lim_{\eta\to 0} \frac{kD\eta}{4C}] \; . \tag{4.35}$$

U is also expressed here as $j\omega C_2^{(2)}$, consistent with the vertical shear-wave approximation. For $\omega = \omega_o$ k becomes $2\pi/D$. The ratio $\eta$ of the electroded part to the total length of the section is $\eta = 4L/D$. For very narrow electrodes the capacitance is proportional to L, since a change in L no longer affects t.

$$C = \frac{\varepsilon WL}{2t} \tag{4.36}$$

The exact nature of C will be studied in the next Chapter. At this time it will be sufficient to estimate the path length 2t to be somewhat longer than D/2. Under these circumstances Eq. (4.35) becomes

$$|V_{OC}| \simeq \pi \frac{N}{\varepsilon W} C_2^{(2)} \quad . \tag{4.37}$$

To find the correction factor for the turns ratio N (Eqs. (4.23) and (4.24)), let

$$N = A\, e_{26}\, W \ , \tag{4.38}$$

where A is the required correction factor. The open circuit voltage should be twice the surface potential, so that

$$|\Phi_S| = A \frac{\pi e_{26}}{2\varepsilon} C_2^{(2)} \quad . \tag{4.39}$$

Equation (3.89) gives the actual surface potential

$$|\Phi_S| = 0.215 \frac{e_{26}}{\varepsilon} C_2^{(2)} \quad . \tag{4.40}$$

It then follows that the correction factor A is

$$A = 0.14 \ . \tag{4.41}$$

The effective coupling coefficient $k_c$ in the turns ratio N should then be (Eq. (3.108)):

$$k_e = 0.14\, e_{26}/\sqrt{\varepsilon C_{66}} = 0.014 \ . \tag{4.42}$$

The equivalent circuit is now specified except for an analytical expression for the capacitance C. This will be obtained in a different context in the next Chapter. It could certainly be determined experimentally without difficulty.

## 4.4 Concluding Remarks

The development of the last three sections pointed out both the attractiveness of the Mason model and its flaws. The strength of the model lies in the orderly, analytical relation of the final matrix, Eq. (4.21), to the initial assumptions. The ease with which circuit sections were cascaded (see Fig. 4.4) to calculate the open-circuit voltage (Eq. (4.31)) illustrates the versatility and usefulness of the equivalent circuit. Its weakness lies in the fact that there are many farfetched assumptions associated with the development of the model; i.e. in both setting up the problem and in taking the matrix equations to the equivalent circuit form. First, in order to obtain the desired result, a surface wave is approximated by a vertical shear wave of finite thickness, even though the mechanical boundary conditions ($T_6 = 0$ at the surface) would not permit such a shear wave to exist in a finite medium. Secondly, the thickness h is frequency dependent, but it has to be canceled against the frequency independent representative path length t in Eq. (4.21), in order to facilitate synthesis with passive elements. Finally, the values of the capacitance and the turns ratio obtained in the mathematical development have to be modified in order to give correct results.

In the following chapters, an equivalent circuit for a complete section of an alternate phase array, as shown in Fig.

4.4, will be derived. In this derivation many of the assumptions made previously are relaxed. Even though the subsequent development lacks some of the elegance of that which led to the Mason circuit, it is conceptually and theoretically sound and results in an equivalent circuit which lends itself readily to analysis and design.

# CHAPTER 5

## THE DETECTION OF SURFACE WAVES BY AN ALTERNATE PHASE ARRAY

In this Chapter the frequency response will be formulated by extending the techniques used by Coquin and Tiersten [4].

### 5.1 The Residual Solution of the Potential Problem

It was established in Chapter 3 that the speed of propagation of an elastic wave in quartz changes very little with an applied electric field. It will be assumed here that the velocity under the electrodes, where $E_x$ is zero at the surface, is the same as between the electrodes or far away from them. In Chapter 3 a surface potential was developed and is of the form

$$\phi^P(x,o,t) = \phi^+ = \phi_S\ e^{j(\omega t-kx)}\ , \qquad (5.1)$$

for a wave traveling in the positive x-direction and far away from any electrode structure. As in Coquin and Tiersten [4], a residual solution $\phi^C$ is introduced so that right under an electrode at peak potential $\phi_o$

$$\phi^C(x,o,t) + \phi_S\ e^{j(\omega t-kx)} = \phi_o\ e^{j\omega t}\ . \qquad (5.2)$$

However, it should also apply at any point within the material and be of the following form:

$$\phi(x,y,t) = \phi^C(x,y,t) + \phi^P(x,y,t)\ . \qquad (5.3)$$

According to Coquin and Tiersten the electric current injected into an electrode of width W, extending from x = a to x = b, would be in the present notation

$$I = -j\omega\varepsilon_{22}W\int_a^b \frac{\partial\phi^C}{\partial y}\bigg|_{y=0^+} dx \ . \tag{5.4}$$

The proof will be developed here for completeness. It is assumed here, as there, that the $\overline{D}$-field outside the piezoelectric slab is zero. The error in this assumption can readily be corrected by appropriately increasing the final interelectrode capacitance. The conduction current into the electrode is then

$$I = j\omega W\int_a^b D_2\bigg|_{y=0^+} dx \ . \tag{5.5}$$

By Eq. (2.5) this becomes

$$I = j\omega W\int_a^b (e_{2kl}\ S_{kl} + \varepsilon_{22}E_2)\bigg|_{y=0^+} dx \ . \tag{5.6}$$

But $E_2$ may be expressed as

$$E_2 = -\frac{\partial\phi}{\partial y} = -\frac{\partial\phi^P}{\partial y} - \frac{\partial\phi^C}{\partial y} = E_2^{\ P} - \frac{\partial\phi^C}{\partial y} \tag{5.7}$$

where $E_2^{\ P}$ is the field in the absence of any metallization nearby. Therefore

$$I = -j\omega\varepsilon_{22}W\int_a^b \frac{\partial\phi^C}{\partial y}\bigg|_{y=0^+} dx + j\omega W\int_a^b (e_{2kl}S_{kl}+\varepsilon_{22}E_2^{\ P})\bigg|_{y=0^+} dx. \tag{5.8}$$

It is assumed that the strain wave is not affected by the electrode. The integrand of the last term is $D_2^{\ P}\big|_{y=0^+}$, the $D_2$ component at the surface in the absence of any metallization, which by continuity of the normal D-field is zero.

It seems that the integrand of Eq. (5.4) would be rather difficult to obtain. The potential $\phi$ anywhere is a solution of

$$\varepsilon_{11} \frac{\partial^2 \phi}{\partial x^2} + \varepsilon_{22} \frac{\partial^2 \phi}{\partial y^2} = e_{1kl} \frac{\partial S_{kl}}{\partial x} + e_{2kl} \frac{\partial S_{kl}}{\partial y} . \tag{5.9}$$

By Eq. (5.3) this may be rewritten as

$$\varepsilon_{11} \frac{\partial^2 \phi^C}{\partial x^2} + \varepsilon_{22} \frac{\partial^2 \phi^C}{\partial y^2} = - \varepsilon_{11} \frac{\partial^2 \phi^P}{\partial x^2} - \varepsilon_{22} \frac{\partial^2 \phi^P}{\partial y^2} + e_{1kl} \frac{\partial S_{kl}}{\partial x}$$

$$+ e_{2kl} \frac{\partial S_{kl}}{\partial y} . \tag{5.10}$$

Since the right hand side is zero it follows that the residual potential is a solution of Laplace's equation

$$\frac{\partial^2 \phi^C}{\partial x^2} + \frac{\partial^2 \phi^C}{\partial (ay)^2} = 0 \ , \quad a = \sqrt{\frac{\varepsilon_{11}}{\varepsilon_{22}}} \ , \tag{5.11}$$

in an x - ay coordinate system. The boundary condition is given by Eq. (5.2),

$$\phi^C(x,o,t) = \phi_o - \Phi_S \, e^{j(\omega t - kx)} \ , \tag{5.12}$$

under the electrodes, and in the interspace by

$$\left. \frac{\partial \phi^C}{\partial (ay)} \right|_{y=0} = 0 . \tag{5.13}$$

This relation follows from Eq. (5.4) since, for any interval a to b on the interspace, there is no externally injected conduction current, yet the mathematical proof for Eq. (5.4) applies there equally well.

In Coquin and Tiersten [4], Eqs. (5.11)-(5.13) are solved for the geometry shown in Fig. 5.1 at the synchronous frequency $\omega_o$. In this thesis that method will be extended to other frequencies. Such an extension is a significant contribution to the theory of the detection of surface waves because it will make possible the construction of useful equivalent circuit models. In order to appreciate the details of the technique, it is essential that the reader become familiar with the method used at $\omega_o$ in [4]. This development is presented in the next section.

## 5.2 The Detection at Synchronous Frequency

Consider a surface wave traveling to the right at synchronous frequency through the infinite array. It is assumed that the velocity of propagation $V_p = \omega_o/k$ is constant, and that the wave is unreflected and unattenuated. From the discussion at the end of Chapter 3 these assumptions are reasonable for the AC cut in quartz. Let the mid-point of the electrode, at potential $\phi_M$ with respect to the piezoelectric bulk, be the origin as shown in Fig. 5.1. At the synchronous frequency $\omega_o$ a wavelength $\lambda$ is exactly equal to D, the periodic distance of the array. The portion of D which is metallized is denoted by $\eta D$. The usual value of $\eta$ is one-half. The electrodes to the left and right are at a potential $\phi_L$ and $\phi_R$ respectively. Because they are directly interconnected $\phi_L = \phi_R$ and this in turn equals $-\phi_M$. All electrodes at potential $\phi_M$ are also directly connected. The potential difference V between the electrodes at potential $\phi_M$ and those at $\phi_L$ is $2\phi_M = \phi_M - \phi_L$.

The residual potential right under the central electrode

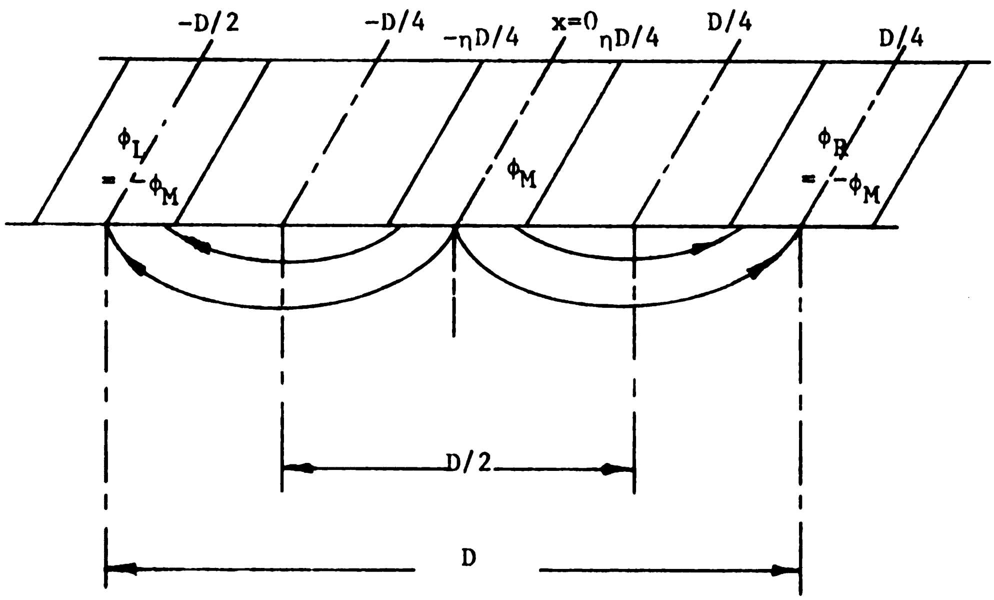


Figure 5.1 - Geometry used for the Coquin and Tiersten analysis.

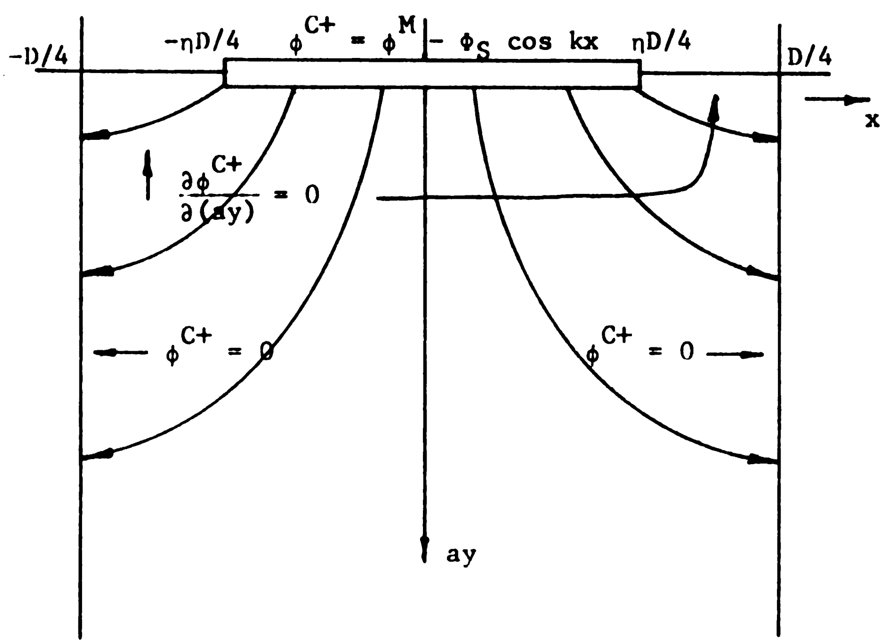


Figure 5.2a - Boundary conditions in the x-ay plane.

is by Eq. (5.2)

$$\phi^{C}(x,o,t) = \phi_M e^{j\omega t} - \phi_S e^{j(\omega t - kx)} \quad . \tag{5.14}$$

Equation (5.4) becomes

$$I = -j\omega\sqrt{\epsilon_{11}\epsilon_{22}}\, W \int_{-\eta D/4}^{\eta D/4} \left.\frac{\partial\phi^{C}}{\partial(ay)}\right|_{ay=0} dx \ . \tag{5.15}$$

Only the even part of the integrand can contribute to the integral. The pertinent part of Eq. (5.14) is therefore in complex amplitude form (phasors):

$$\phi^{C+}(x,o) = \phi_M - \phi_S \cos kx \ . \tag{5.16}$$

The superscript (+) denotes that $\phi^{C+}$ is the even part of $\phi^{C}$.

$$\phi^{C+} = \frac{\phi^{C}(x) + \phi^{C}(-x)}{2} \quad . \tag{5.17}$$

In general $\phi^{C+}$ is not known, but since the even part of the surface potential $\phi_S \cos kx$ is zero at synchronous frequency at $x = \pm D/4$ and $\phi_R = \phi_L = -\phi_M$ there is a virtual ground at $x = \pm D/4$ for all values of y. It follows that $\phi^{C+}$ must be zero there

$$\phi^{C+}(\pm D/4, y) = 0 \ . \tag{5.18}$$

A further boundary condition on the field $\phi^{C+}(x,y)$ is that on $\eta D/4 < x < D/4$ and $-D/4 < x < -\eta D/4$

$$\left.\frac{\partial\phi^{C+}}{\partial(ay)}\right|_{ay=0} = 0 \ , \tag{5.19}$$

because there is no current injected into the unmetallized surface area. These conditions are illustrated in Fig. 5.2.

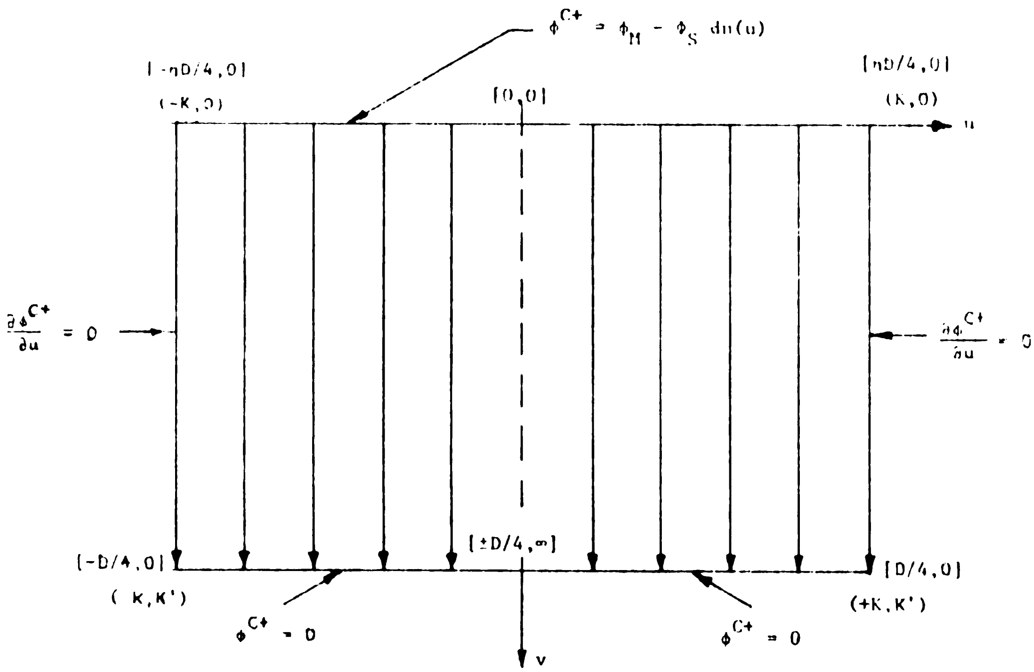


Figure 5.2b - Map of the infinite strip in Fig. 5.2. The corresponding points of Fig. 5.2 are indicated by [ ]. The boundary conditions are also indicated.

The mapping function

$$\sqrt{m}\ \mathrm{sn}(w|m) = \sin(2\pi z/D) \tag{5.20}$$

is used to map the geometry of Fig. 5.2 in the z = x + jay plane into the w = u + jv plane, where the infinite strip in Fig. 5.2 becomes a rectangle shown in Fig. 5.3. The quantity m, the modulus of the sn-function, must be

$$m = \sin^2(\eta\tfrac{\pi}{2}) \ . \tag{5.21}$$

The reader familiar with [4] will find it difficult to identify each step used here in comparison with that article. It was found more convenient to use the notation of Abramowitz [14] for the Jakobian Elliptic Functions. Figure 5.3 shows the result of the mapping. By Eq. (5.20) the value of x in the boundary condition Eq. (5.16) must be replaced by

$$x = \frac{D}{2\pi} \sin^{-1}[\sqrt{m}\ \mathrm{sn}(u|m)] \ , \tag{5.22}$$

so that Eq. (5.16) becomes:

$$\phi^{C+} = \phi_M - \phi_S \cos \sin^{-1}[\sqrt{m}\ \mathrm{sn}(u)] \ . \tag{5.23}$$

sn(u) is used from now on instead of sn(u|m) where the context leaves no doubt about the modulus. Equation (5.23) may be expressed in shorter form by recognizing that [14]:

$$\cos \sin^{-1}[\sqrt{m}\ \mathrm{sn}(u)] = \sqrt{1 - m\ \mathrm{sn}^2(u)} \quad , \tag{5.24}$$

which by definition is dn(u), another elliptic function. The quantity K is the complete elliptic integral of modulus m. It is a quarter period of the sn- and the dn-functions. The quantity K' is

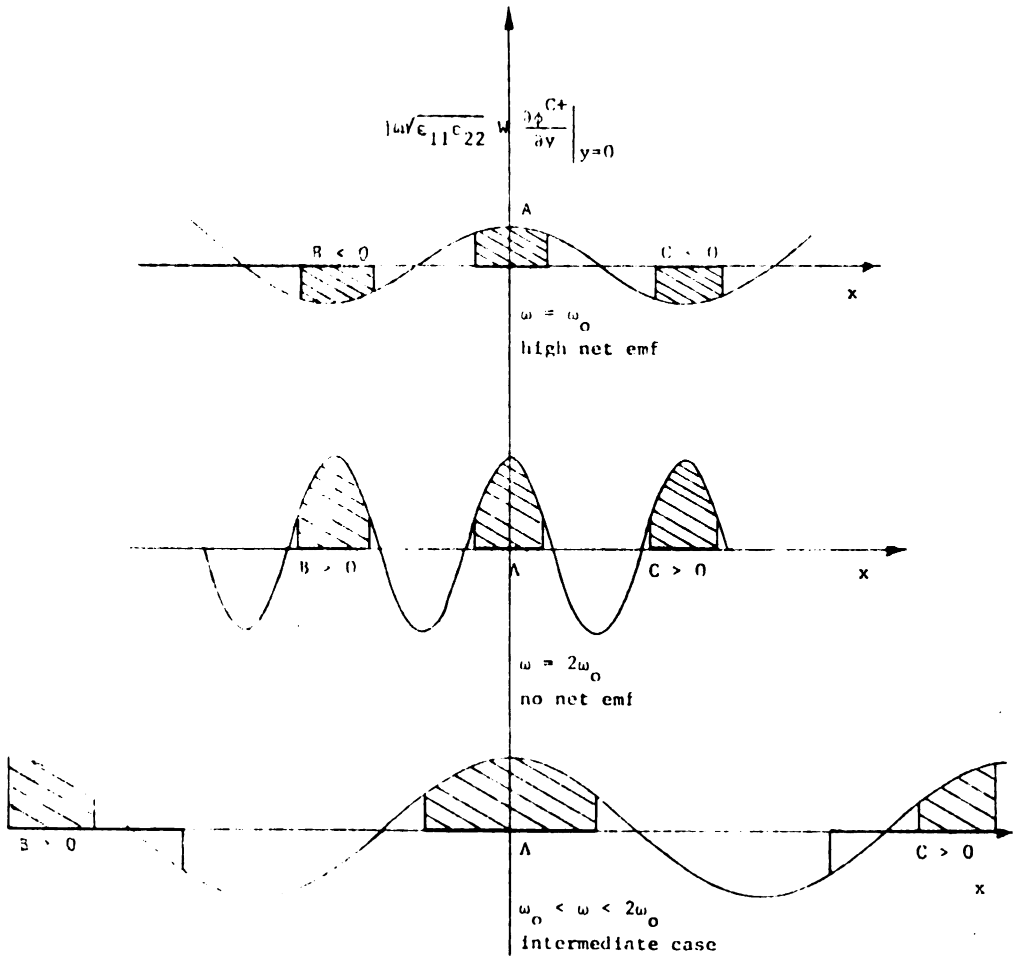


Figure 5.3 - Illustration of the net induced emf in relation to its nearest neighbors, $\frac{1}{2}$ [A - (B + C)/2].

the complete elliptic integral of m', which is related to m by

$$m' = 1 - m \ . \tag{5.25}$$

The value of the dn-function at u = 0 is one, and at a quarter period K is

$$dn(K) = \sqrt{m'} = \sqrt{1 - m} \quad . \tag{5.26}$$

Laplace's equation becomes in the u-v plane

$$\frac{\partial^2 \phi^{C+}}{\partial u^2} + \frac{\partial^2 \phi^{C+}}{\partial v^2} = 0 \ . \tag{5.27}$$

Following the method of separation of variables the solution is of the form

$$\phi^{C+} = A_o(1 - \frac{v}{K'}) + \sum_{n=1}^{\infty} A_n \sinh[\frac{n\pi}{K} (K' - v)] \cos(\frac{n\pi u}{K}) \ . \tag{5.28}$$

Equation (5.15) becomes in the u-v plane

$$I = -j\omega\sqrt{\varepsilon_{11}\varepsilon_{22}} \ W\int_{-K}^{K} \left.\frac{\partial\phi^{C+}}{\partial v}\right|_{v=0} du \tag{5.29}$$

From Eq. (5.28) it is seen that $\frac{\partial\phi^{C+}}{\partial v}$ is also a Fourier series in u for any value of v:

$$\frac{\partial\phi^{C+}}{\partial v} = -\frac{A_o}{K'} + \sum_{n=1}^{\infty} a_n(v) \cos(\frac{n\pi u}{K}) \ . \tag{5.30}$$

Of principal interest is the average value over u of $\frac{\partial\phi^{C+}}{\partial v}$ [see Eq. (5.29)], the coefficient $a_o = -\frac{A_o}{K'}$ [see Eq. (5.30)]. It turns out to be independent of v.

$$-\frac{A_o}{K'} = \frac{1}{2K} \int_{-K}^{K} \frac{\partial\phi^{C+}}{\partial v} du \ . \tag{5.31}$$

Equation (5.29) is therefore:

$$I = j\omega\sqrt{\varepsilon_{11}\varepsilon_{22}}\ W\ 2K\ A_o/K' \ . \tag{5.32}$$

By Eq. (5.28) $A_o$ is, in turn, the average value of $\phi^{C+}(u,o)$, which is the upper boundary condition:

$$\phi^{C+}(u,o) = \phi_M - \phi_S\ dn(u) \ , \tag{5.33}$$

hence,

$$A_o = \frac{1}{2K}\int_{-K}^{K} [\phi_M - \phi_S\ dn(u)]\ du \ . \tag{5.34}$$

The equation relating the electrical quantities I and $V = 2\phi_M$ to the surface wave is then:

$$I = j\omega[\sqrt{\varepsilon_{11}\varepsilon_{22}}\ WK/K']V - j\omega\sqrt{\varepsilon_{11}\varepsilon_{22}}\ W\ \phi_S[\frac{1}{K'}\int_{-K}^{K} dn(u)du] \ . \tag{5.35}$$

By the integral relations listed in Abramowitz [14]

$$\int dn(u)du = \sin^{-1}[sn(u)] \ , \tag{5.36}$$

but sn(K) = 1 and sn(-K) = -1, so that the square bracket in Eq. (5.35) becomes

$$\frac{1}{K'}\int_{-K}^{K} dn(u)du = \frac{\pi}{K'} \ . \tag{5.37}$$

With this simplification Eq. (5.35) becomes

$$I = j\omega CV - j\omega\sqrt{\varepsilon_{11}\varepsilon_{22}}\ W\pi\ \phi_S/K' \ . \tag{5.38}$$

The quantity $\sqrt{\varepsilon_{11}\varepsilon_{22}}\ WK/K'$ has been identified as C, the capacitance of one electrode to its neighbors. The relation shows how the current into the electrode depends on both the applied potential difference V and the amplitude of the surface wave $\phi_S$. The shortcoming of Eq. (5.38) is that it holds only at the synchronous frequency. At other frequencies the current I will still depend on V by $j\omega C$ but the second term will have to change drastically, for it is reported by other investigators [15,16] that, for example, the response is zero at twice the synchronous frequency, or it is also clear that the response should peak somewhere near synchronous frequency. None of this can be deduced from Eq. (5.38). However, with care, the preceding procedure can be generalized to other frequencies. This is done in the next section.

## 5.3 The Frequency Response of the Short Circuit Current from Electrode to its Nearest Neighbors

Recall that the ultimate objective of this research is to obtain a useful equivalent circuit for an individual section of the array. The correct overall effect can then be accounted for by cascading individual sections. In the next Chapter such a section will be properly defined and its equivalent circuit will be developed. To lead up to that development the frequency response of the short circuit current from an individual electrode to its next two neighbors will be studied here. In the following Chapter this idea will be extended to account for the current to all electrodes of opposite polarity.

In order to study the response at frequencies other than the synchronous frequency $\omega_o$ Eq. (5.38) must be generalized. Referring back to Fig. 5.2 it is seen that $\phi^{C+} = 0$ at $x = \pm D/4$. This is so because of two reasons: First of all, at $x = \pm D/4$

$$kx = \pm \frac{2\pi}{\lambda} \cdot \frac{D}{4} = \pm \frac{\pi}{2} , \tag{5.39}$$

so that cos(kx) is zero there, and secondly D/4 is the mid-point between the applied potentials $\phi_M$ and $-\phi_M = \phi_R$, so that it is a virtual ground from the point of view of the externally applied potentials with respect to the piezoelectric bulk.

If the frequency is somewhat higher than $\omega_o$, $\lambda/4$ will fall short of D/4, but the mid-point between the electrodes at potentials $\phi_M$ and $-\phi_M$ respectively would remain at D/4. The latter problem can be resolved easily by considering the short circuit response, i.e. the current when $\phi_M = \phi_R = 0$. Then $\phi^{C+}$ will be of the form $-A\cos kx$ and the lines given by $\phi^{C+} = 0$ in Fig. 5.2 would occur at $\lambda/4$. The next difficulty is now that the current $I_{SC}$, determined in this fashion, would be a current between the electrode and the bulk of the piezoelectric material since it has been assumed to be the reference node all along. At the synchronous frequency this causes no problem; the current injected into it by one electrode was equal to that taken out by one of its neighbors. A connection to the bulk was implied but it made no difference.

An extension of that reasoning to other frequencies is to assume at first that a fictitious short circuit current still flows from each electrode to the bulk based on Eq. (5.4).

$$I_{SCM} = +j\omega\sqrt{\epsilon_{11}\epsilon_{22}}\, W \int_{-\eta D/4}^{\eta D/4} \left.\frac{\partial \phi^C}{\partial (ay)}\right|_{ay=0} dx , \tag{5.40}$$

but really there is no such connection, so the actual current from the electrode to its neighbors [see Fig. 5.1] depends on the difference between the induced emf on the electrode under consideration and the average emf induced in the two neighbors. If again only the even part with respect to the origin is considered the waves shown in Fig. 5.3 illustrate that point very well. Areas above the x-axis are positive and correspond to the fictitious current from electrode to the bulk. Areas below the axis represent current from the bulk to the electrode. The actual current from the center electrode is then

$$I_{SC} = \frac{I_{SCM} - (I_{SCL} + I_{SCR})/2}{2} \quad . \tag{5.41}$$

To be more general consider a superposition of a wave to the right and the left. At the surface under the electrode, $\phi^C$ is simply the negative of $\phi^P$:

$$\phi^C(x,o) = -[\phi_S^+ e^{-jkx} + \phi_S^- e^{jkx}] \ . \tag{5.42}$$

Equation (5.40) becomes now for the three electrodes:

$$I_{SCM} = + j\omega\sqrt{\varepsilon_{11}\varepsilon_{22}}\, W \int_{-\eta D/4}^{\eta D/4} \left.\frac{\partial\phi^C}{\partial(ay)}\right|_{ay=0} dx \ , \tag{5.43}$$

$$I_{SCL} = + j\omega\sqrt{\varepsilon_{11}\varepsilon_{22}}\, W \int_{-\eta D/4-D/2}^{\eta D/4-D/2} \left.\frac{\partial\phi^C}{\partial(ay)}\right|_{ay=0} dx \ , \tag{5.44}$$

$$I_{SCR} = + j\omega\sqrt{\varepsilon_{11}\varepsilon_{22}}\, W \int_{-\eta D/4+D/2}^{\eta D/4+D/2} \left.\frac{\partial\phi^C}{\partial(ay)}\right|_{ay=0} dx \ . \tag{5.45}$$

In order to comply with Eq. (5.41) a change in variables in the last two integrals will result in the same limits of integration as that of the first integral (Eq. (5.43)). Equation (5.44) will get the integral

$$\int_{-\eta D/4}^{\eta D/4} \frac{\partial}{\partial(ay)} \phi^C(x - D/2,ay)\Big|_{ay=0} dx \tag{5.46}$$

and Eq. (5.45) will get the integral

$$\int_{-\eta D/4}^{\eta D/4} \frac{\partial}{\partial(ay)} \phi^C(x + D/2,ay)\Big|_{ay=0} dx \ . \tag{5.47}$$

The actual short circuit current by Eq. (5.41) is now:

$$I_{SC} = +j\omega\sqrt{\varepsilon_{11}\varepsilon_{22}}\, W\Big[\frac{\partial}{2\partial(ay)} \int_{-\eta D/4}^{\eta D/4} [\phi^C(x,ay) - \frac{1}{2}\phi^C(x-D/2,ay)$$

$$- \frac{1}{2}\phi^C(x+D/2,ay)]dx\Big]_{ay=0} \ . \tag{5.48}$$

The value of $\phi^C(x,o)$ is given in Eq. (5.42). In general, it is reasonable to assume that $\phi^C$ is of the form

$$\phi^C(x,ay) = -[\phi^+(x,ay)\, e^{-jkx} + \phi^-(x,ay)\, e^{jkx}] \tag{5.49}$$

where the wave amplitudes $\phi^+$ and $\phi^-$ may be functions of both x and ay, but, because all electrodes are at zero potential they must be periodic in x with period D/2, and they are symmetric about x=0.

$$\phi^{\pm}(x \pm D/2,ay) = \phi^{\pm}(x,ay) \tag{5.50}$$

The integrand of Eq. (5.48) is then, if the argument of the amplitudes is left out:

$$-[\phi^+e^{-jkx} + \phi^-e^{jkx} - \frac{1}{2}\phi^+e^{-jkx}(e^{jkD/2} + e^{-jkD/2}) - \frac{1}{2}\phi^-e^{jkx}$$

$$(e^{-jkD/2} + e^{jkD/2})] \ , \tag{5.51}$$

or

$$-[\phi^{+}e^{-jkx}[1 - \cos kD/2] + \phi^{-}e^{jkx}[1 - \cos kD/2]] \ . \qquad (5.52)$$

The identities

$$1 - \cos 2\theta = 2 \sin^2\theta \qquad (5.53)$$

and

$$kD/4 = \frac{2\pi}{\lambda} \cdot \frac{D}{4} = \frac{\pi\omega}{2\omega_o} \qquad (5.54)$$

simplify Eq. (5.52), the integrand of Eq. (5.48), to

$$2\phi^{C}(x,ay) \sin^2(\frac{\pi\omega}{2\omega_o}) \ . \qquad (5.55)$$

The short circuit current from the middle electrode is then

$$I_{SC} = +j\omega\sqrt{\epsilon_{11}\epsilon_{22}}\, W \sin^2(\frac{\pi\omega}{2\omega_o}) \int_{-\eta D/4}^{\eta D/4} \frac{\partial}{\partial(ay)} \phi^{C}(x,ay)\Big|_{ay=0} dx \ . \qquad (5.56)$$

The integral is solved by the procedure outlined in Section 5.2. As mentioned earlier the infinite strip shown in Fig. 5.2 does not extend from $-D/4$ to $+D/4$ but rather from $-\lambda/4$ to $+\lambda/4$ (see Fig. 5.4) and $\phi^{C+}$ on the electrode is now by Eq. (5.42)

$$\phi^{C+} = -(\phi_S^{+} + \phi_S^{-}) \cos kx \ . \qquad (5.57)$$

By Eqs. (5.35), (5.37) the result will then be

$$I_{SC} = j\omega\sqrt{\epsilon_{11}\epsilon_{22}}\, W(\phi_S^{+} + \phi_S^{-})[\pi/K'(\omega)]\sin^2(\frac{\pi\omega}{2\omega_o}) \ . \qquad (5.58)$$

The elliptic integral $K'(\omega)$ is now a function of frequency since the infinite strip in Fig. 5.2 changes width with frequency (see Fig. 5.4). The validity of Eq. (5.58) extends only to a frequency

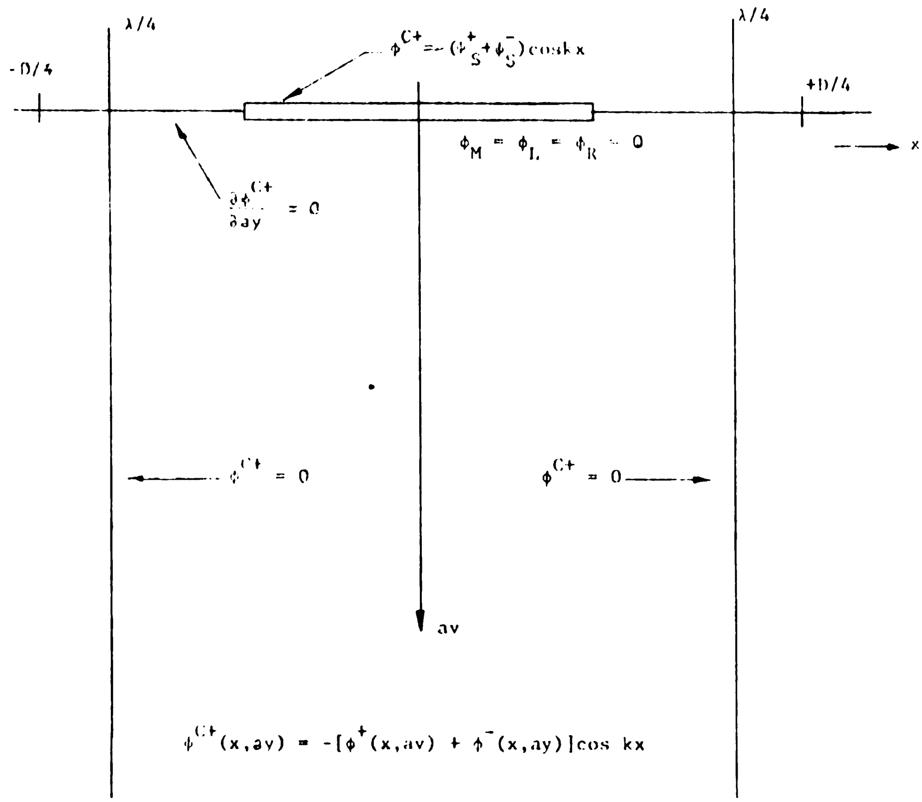


Figure 5.4 - The geometry for the field problem with no external potential applied and $\omega \neq \omega_o$.

less than that which would produce a quarter wavelength equal to $\eta D/4$, the edge of the electrode, i.e.

$$\lambda > \eta D$$

or

$$\frac{2\pi V_p}{\omega} > \eta \frac{2\pi V_p}{\omega_o}$$

or

$$\frac{\omega}{\omega_o} < 1/\eta \quad .$$

Furthermore, since the boundary condition requires on the range

$$\eta D/4 < x < \lambda/4$$

that $\frac{\partial \phi^{C+}}{\partial(ay)} = 0$ there is also an upper limit on $\lambda/4$:

$$\lambda/4 < D/2 - \eta D/4 \ ,$$

which defines the edge of the next electrode. In terms of a frequency restriction this means

$$\frac{\omega}{\omega_o} > \frac{1}{2-\eta} \quad .$$

The combined statement of the frequency range over which Eq. (5.58) is valid is then

$$\frac{1}{2-\eta} < \frac{\omega}{\omega_o} < \frac{1}{\eta} \ . \tag{5.59}$$

The frequency dependence of $K'(\omega)$ is caused by the modulus $m'=1-m$ of the elliptic functions (Eq. (5.21)),

$$m' = 1 - \sin^2(\eta\frac{\pi}{2}) \ . \tag{5.60}$$

Here, this relation must be modified, because $\eta$ represents no longer the ratio of electrode width to interelectrode distance but rather electrode width to $\lambda/2$, half a wave length. Hence

$$m'(\omega) = 1 - \sin^2\left(\frac{\eta\pi\omega}{2\omega_o}\right) \tag{5.61}$$

The complete elliptic integrals K' are listed in Abramowitz [14] as a function of

$$\alpha = \frac{\eta\pi\omega}{2\omega_o} \quad .$$

In Table 5.1 the normalized form of Eq. (5.58), $F(\omega/\omega_o)$, is computed for $\eta = 1/2$, where

$$F(\omega/\omega_o) = I_{SC}/j\omega_o\sqrt{\varepsilon_{11}\varepsilon_{22}}\, W(\Phi_S^{\,+} + \Phi_S^{\,-}), \tag{5.62}$$

i.e.

$$F(\omega/\omega_o) = \frac{\omega}{\omega_o} \sin^2\left(\frac{\pi\omega}{2\omega_o}\right)[\pi/K'(\omega/\omega_o)] \quad . \tag{5.63}$$

The frequency response is plotted in Fig. 5.5 for $\eta = 1/2$ for frequencies between $2\omega_o/3$ and $2\omega_o$. Most applications fall in this range. It is seen that the value of F at $\omega/\omega_o = 1$ is equal to that obtained in Section 5.2. In addition it should be noted that the functional form of Eq. (5.58) is identical to Eq. (5.35) if $\omega = \omega_o$ and $V = 0$. It is furthermore seen that the response is zero at $\omega = 2\omega_o$ as it must be. The peak for the short circuit current response occurs near $\omega = 1.2\ \omega_o$, i.e. higher than the synchronous frequency. This will not be the case in the open circuit voltage frequency response, which is derived next.

TABLE 5.1 - Normalized Frequency Response of a Single Section for $\eta = 1/2$, $2\omega_o/3 < \omega < 2\omega_o$

| $\omega/\omega_o$ | $\alpha = \frac{\eta\pi\omega}{2\omega_o}$ | $K'(\omega/\omega_o)$ | $F(\omega/\omega_o)$ | $[F(\omega/\omega_o)/(\omega/\omega_o)]\frac{K'}{K}$ |
|---|---|---|---|---|
| 0.8 | 36° | 2.01327 | 1.12915 | 1.41144 |
| 1.0 | 45° | 1.85407 | 1.69443 | 1.69443 |
| 1.2 | 54° | 1.741499 | 1.95804 | 1.63170 |
| 1.4 | 63° | 1.66272 | 1.73131 | 1.23665 |
| 1.6 | 72° | 1.61045 | 1.07835 | 0.67397 |
| 1.8 | 81° | 1.58054 | 0.34165 | 0.18980 |
| 2.0 | 90° | 1.57080 | 0.0 | 0 |

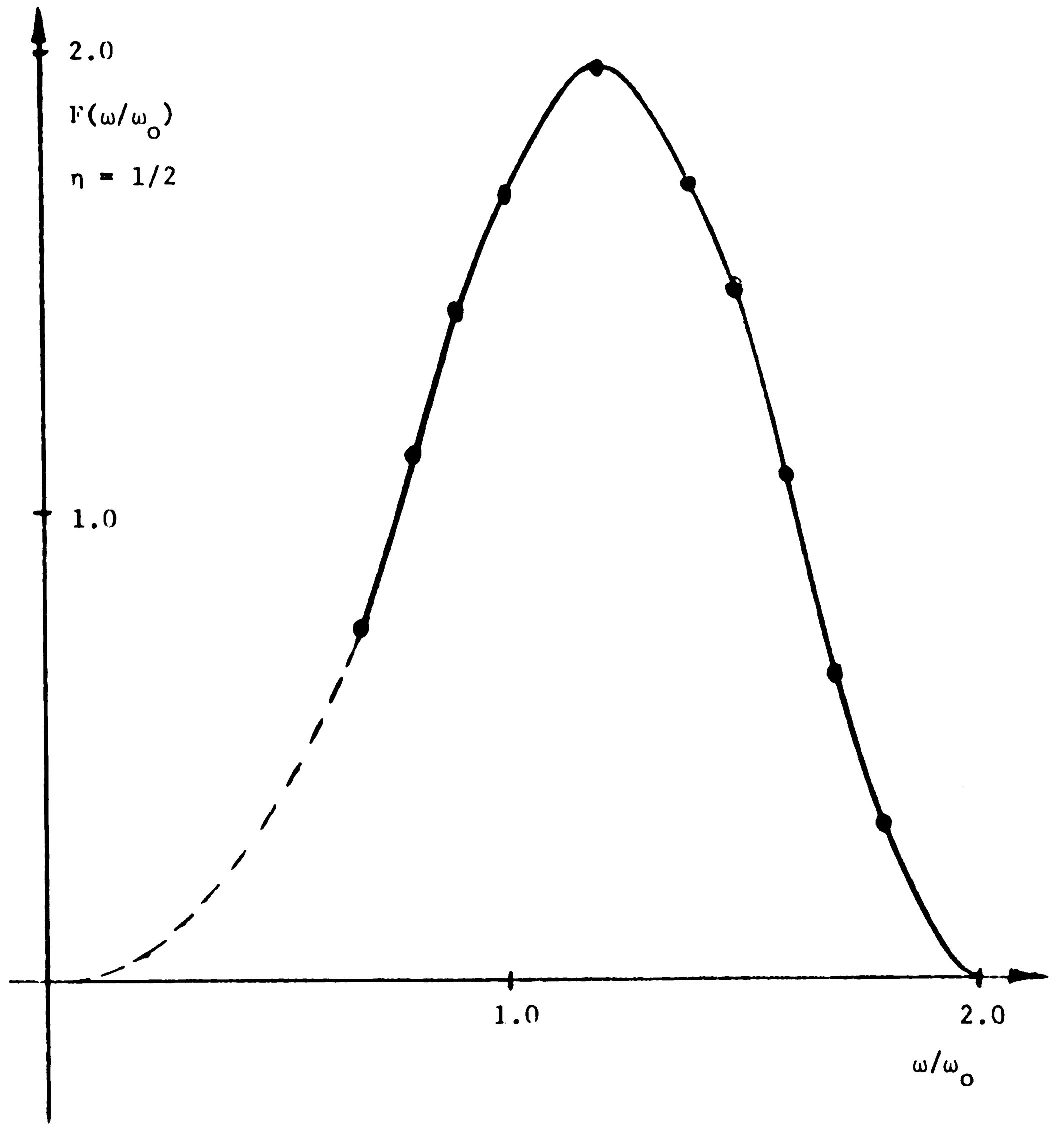


Figure 5.5 - Normalized frequency response of the short circuit current from an electrode to its nearest neighbors.

## 5.4 The Norton Equivalent Circuit

By Thevenin's theorem the product of the short circuit current times the output impedance is the open circuit voltage. The output impedance is obtained from Eq. (5.38). All independent sources are set to zero, in this case $\Phi_S$, then the ratio of the externally applied voltage to the current is the output impedance. This is clearly $1/j\omega C$. A Norton equivalent circuit for a section consisting of a single electrode at $x = 0$ with the potential referred to its neighbors is then shown in Fig. 5.6. The voltage current relation for other than short circuit terminations follows directly:

$$I = j\omega CV - j\omega_o\sqrt{\varepsilon_{11}\varepsilon_{22}}\, W(\Phi_S^{+} + \Phi_S^{-})\, F(\omega/\omega_o) \ . \tag{5.64}$$

It is seen from this that the open circuit voltage response equals

$$V_{OC} = (K'/K)(\Phi_S^{+} + \Phi_S^{-})\, F(\omega/\omega_o)/(\omega/\omega_o) \ . \tag{5.65}$$

The value of C used here is given by $\sqrt{\varepsilon_{11}\varepsilon_{22}}\ W\ K/K'$.

The normalized open circuit voltage response is plotted in Fig. 5.7. The peak has indeed shifted to the left in relation to the peak of the short circuit current response.

The technique used here in this Chapter is an important extension of the work by Coquin and Tiersten, since it will lead to equivalent circuits which apply specifically to surface waves and are not based on analogies to bulk waves.

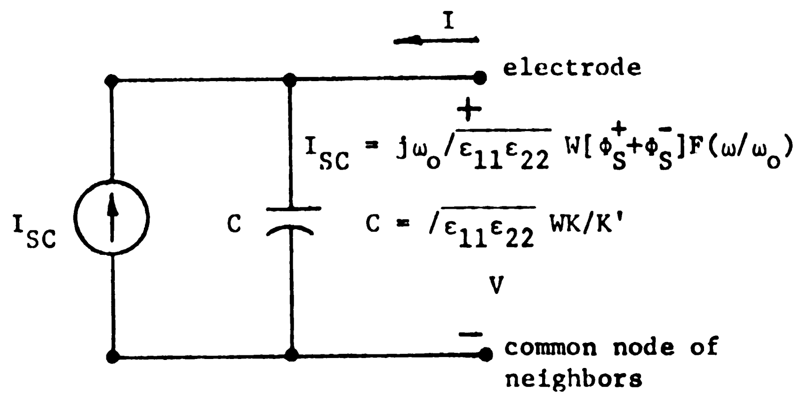


Figure 5.6 - Norton equivalent circuit of a single electrode and its nearest neighbors.

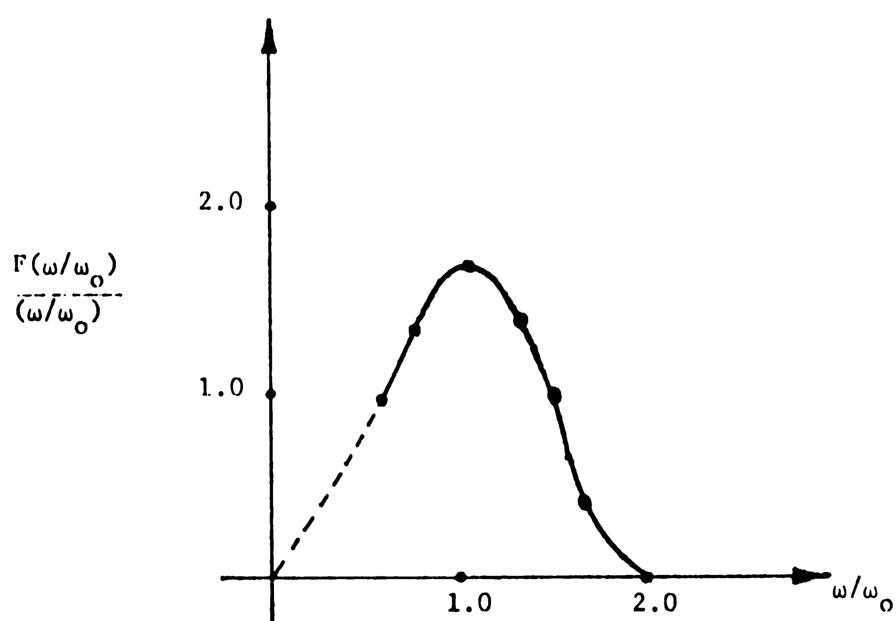


Figure 5.7 - The normalized frequency response of the open circuit voltage.

# CHAPTER 6

# EQUIVALENT CIRCUIT MODELS FOR SURFACE-WAVE TRANSDUCERS

The transducer models presented in this Chapter have been developed specifically for surface waves and do not rely on an equivalent bulk-wave behavior. The two circuit models derived here are one with dependent generators and the other, derived from the first, with an ideal transformer similar in form to the Mason model. The starting point is Eq. (5.43) in addition to various surface-wave transmission line models of Chapter 3.

## 6.1 An Equivalent Circuit with Dependent Sources

With Eq. (5.58) an expression was obtained for the short-circuit current from an electrode centered at $x = 0$ to its next neighbors. This led to a Norton equivalent circuit from which Eq. (5.65) was derived, which in turn gave rise to the frequency response plot [Fig. 5.7] of the open-circuit voltage of the electrode with respect to its neighbors.

In order to arrive at a valid equivalent circuit for a suitably small section, that can serve as a building block for a larger array, the constraint that the current exchange only occurs between an electrode and its next neighbors [see Eq. (5.41)] will be lifted. The nature of the final equivalent circuit will be such that short-circuit calculations based on it result automatically in the current between electrodes rather than current from an electrode to the grounded bulk implied by Eq. (5.40).

Nevertheless, the current from an electrode to the grounded bulk is obtained first. By comparing Eqs. (5.40), (5.56) and (5.58) the conclusion can be drawn that the current to the bulk for an electrode at $x = 0$ will be:

$$I_{SCM} = j\omega\sqrt{\epsilon_{11}\epsilon_{22}}\, W[\pi/K'(\omega/\omega_o)](\phi_S^{\ +} + \phi_S^{\ -}) \ . \tag{6.1}$$

If the electrode is located at a point $x_n = nD/2$, i.e. n half periodic lengths to the right of the origin, the equation becomes

$$I_n = j\omega\sqrt{\epsilon_{11}\epsilon_{22}}\, W[\pi/K'(\omega/\omega_o)][\phi_S^{\ +}\, e^{-jkx_n} + \phi_S^{\ -}\, e^{+jkx_n}]. \tag{6.2}$$

An array of N electrodes shorted to the bulk is shown in Fig. 6.1. All odd numbered electrodes are interconnected first before this is done. The same is done with the even numbered electrodes. Thus the total current into the bulk would be $I_1 + I_2 + I_3 + \ldots . I_N$. This is suggested by the mathematical formulation of Eq. (6.2), but it is physically not the case. By analogy to Eq. (5.41) the actual short-circuit current from the upper half of the array [see Fig. 6.1] to the lower half is determined by one-half the difference in emf's, which leads to

$$I_{SC} = \frac{1}{2}\,[I_1 - I_2 + I_3 - I_4 + \ldots \ldots - I_N] \ . \tag{6.3}$$

By Kirchhoff's current law this result is simply achieved by connecting the upper electrodes directly to the lower electrodes, bypassing the bulk node. The strength of each generator must also be cut in half. Figure 6.2 shows this connection as a hatched line. To guarantee the correct output impedance between terminals

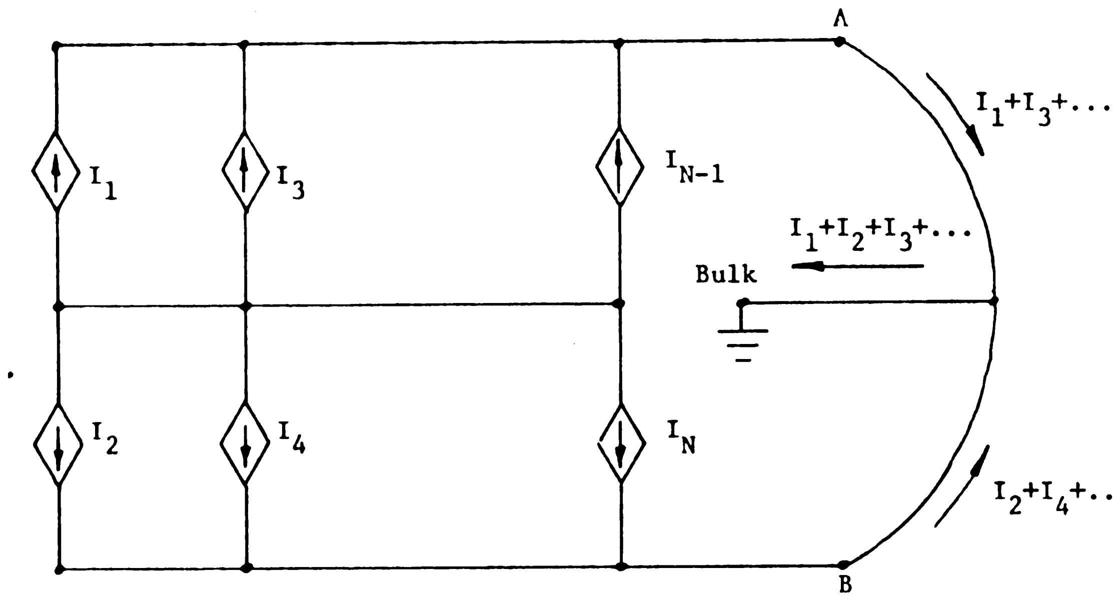


Figure 6.1 - Connection of generators consistent with the meaning of Eq. (6.2). The resulting short circuit current is physically incorrect.

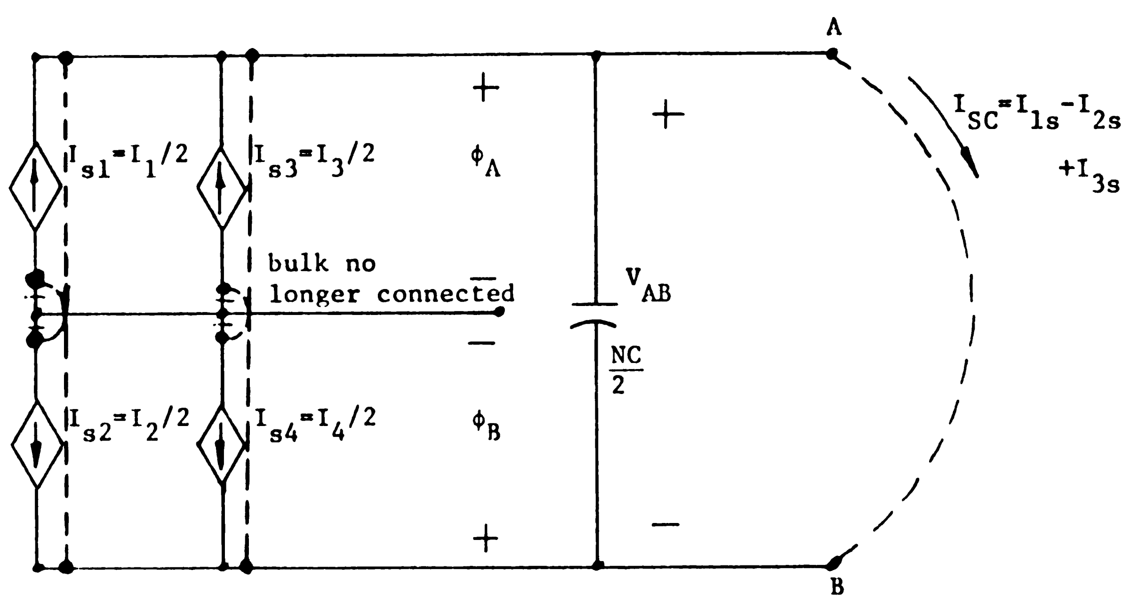


Figure 6.2 - Choice of circuit interconnection to obtain a meaningful expression for the electric terminal behavior.

A-B a capacitance of value C must be added as shown for each pair of current sources. The terminal voltage $V_{AB}$ is now the difference between the potentials referred to the bulk, $\phi_A$ and $\phi_B$. The effect of the field above the slab must finally be included so that the value of C is given by [16]:

$$C = (\varepsilon_o + \sqrt{\varepsilon_{11}\varepsilon_{22}})WK/K' \ , \tag{6.4}$$

and the strength of each current source is

$$I_{sn} = j\omega\sqrt{\varepsilon_{11}\varepsilon_{22}}\, W[\pi/2K'(\omega/\omega_o)][\phi_S{}^{+}\, e^{-jn\theta} + \phi_S{}^{-}\, e^{jn\theta}] \ , \tag{6.5}$$

where

$$\theta = kD/2 = \pi\omega/\omega_o \ . \tag{6.6}$$

The current sources depend on the surface potential at points $x_n$.

In Chapter 5, it was assumed that under short-circuit conditions the transducer behaves as a piezoelectric transmission line, without losses or reflections and a constant velocity of propagation. Consistent with this assumption will be the equivalent circuit in Fig. 6.3 from which $\phi^P(x_n)$ may be determined, where

$$\phi^P(x_n) = \phi_S{}^{+}\, e^{-jkx_n} + \phi_S{}^{-}\, e^{+jkx_n} = \phi_S{}^{+}\, e^{-jn\theta} + \phi_S{}^{-}\, e^{jn\theta} \ .$$

The circuit, however, applies only if the electric terminals A-B are shorted. Since the array is a linear, passive system the reciprocity theorem must apply to any three-port network formed from it. For this purpose cut out a section between the center of two adjacent electrodes at $x_n$ and $x_{n+1}$ respectively. The current sources $I_{sn}$ and $I_{s(n+1)}$ should then be halved. The appropriate

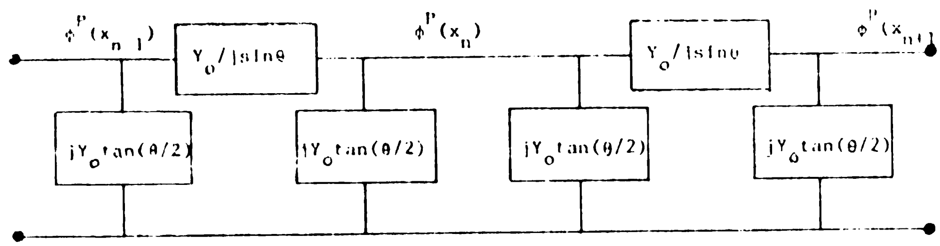


Figure 6.3 - Equivalent circuit to determine $\phi^P(x_n)$ when terminals A-B are shorted.

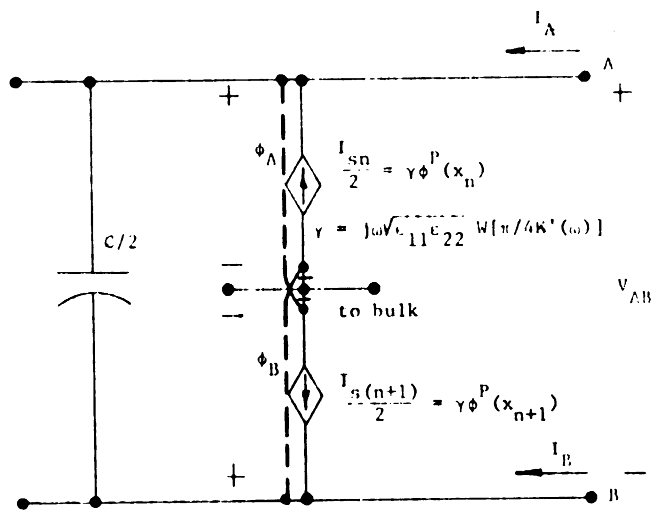


Figure 6.4 - Temporary equivalent circuit of the electrical part of a basic section extending from the mid-point of one electrode to its neighbor.

capacitance is then also C/2. The electrical part of the section is shown in Fig. 6.4.

The symbol $\gamma$ has been introduced for the sake of brevity.

$$\gamma = j\omega\sqrt{\varepsilon_{11}\varepsilon_{22}}\, W[\pi/4K'(\omega/\omega_o)] \tag{6.7}$$

It may be interpreted as a transconductance. The difficulty with the circuit model shown in Fig. 6.4 is that it is not a one-port network but rather a two-port network because of the presence of the connection to the bulk. However, it was seen in the development that led to Fig. 6.2 that the contribution to the short-circuit current out of terminal A and into terminal B is

$$I_{SC} = I_{sn}/2 - I_{s(n+1)}/2 = \gamma[\phi^P(x_n) - \phi^P(x_{n+1})] \; . \tag{6.8}$$

Since the output impedance is determined by C/2 the Norton equivalent circuit for this section will be that of Fig. 6.5. The terminal equation for this is

$$I/2 = j\omega C\, V_{AB}/2 - \gamma\phi^P(x_n) + \gamma\phi^P(x_{n+1}) \; . \tag{6.9}$$

The equations for the transmission line part under shorted conditions are by Eq. (3.6)

$$\left\|\begin{matrix} I^P(x_n) \\ \\ -I^P(x_{n+1}) \end{matrix}\right\| = \left\|\begin{matrix} \dfrac{Y_o}{j\tan\theta} & \dfrac{-Y_o}{j\sin\theta} \\ \\ \dfrac{-Y_o}{j\sin\theta} & \dfrac{Y_o}{j\tan\theta} \end{matrix}\right\| \times \left\|\begin{matrix} \phi^P(x_n) \\ \\ \phi^P(x_{n+1}) \end{matrix}\right\| . \tag{6.10}$$

Equations (6.9) and (6.10) are next combined. By the reciprocity theorem $Y_{13} = Y_{31}$ and $Y_{23} = Y_{32}$:

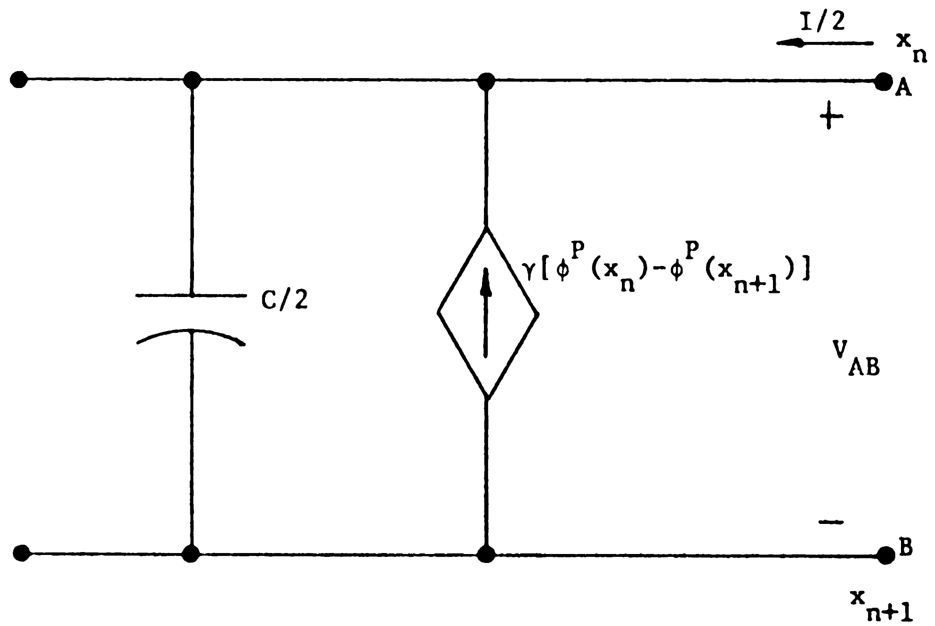


Figure 6.5 - Norton equivalent circuit of the electrical part of a basic section between $x_n$ and $x_{n+1}$. The current is denoted by the symbol I/2 because it represents approximately one-half the current into the electrode at $x_n$.

$$\begin{Vmatrix} I^P(x_n) \\ \\ -I^P(x_{n+1}) \\ \\ I/2 \end{Vmatrix} = \begin{Vmatrix} \dfrac{Y_o}{j\tan\theta} & \dfrac{-Y_o}{j\sin\theta} & -\gamma \\ \\ \dfrac{-Y_o}{j\sin\theta} & \dfrac{Y_o}{j\tan\theta} & \gamma \\ \\ -\gamma & \gamma & j\omega C/2 \end{Vmatrix} \times \begin{Vmatrix} \phi^P(x_n) \\ \\ \phi^P(x_{n+1}) \\ \\ V_{AB} \end{Vmatrix} \tag{6.11}$$

Because the effect of the electrical part on the transmission line part is now known, the complete equivalent circuit, valid under all conditions, is now obtained and shown in Fig. 6.6.

When such sections are interconnected, proper polarities must be observed. All current sources associated with terminal A, i.e. $(x_n)$, point up; all current sources associated with terminal B, i.e. $(x_{n+1})$, point down. In the next section an example will be presented to demonstrate the utility of this equivalent circuit model. It will be used to study the detection of a surface wave by an array and the excitation of surface waves from the electric terminals.

## 6.2 Analysis of the Detection and Excitation Problem with the Equivalent Circuit

Consider an array made up of twenty identical electrodes. The field distribution at the end sections is quite different from that for the other sections. It is therefore uncertain whether to account for 19, 20 or 21 sections. For a large array it won't matter. In this case the mathematically most convenient value will be chosen. The array has an equivalent circuit as shown in Fig.

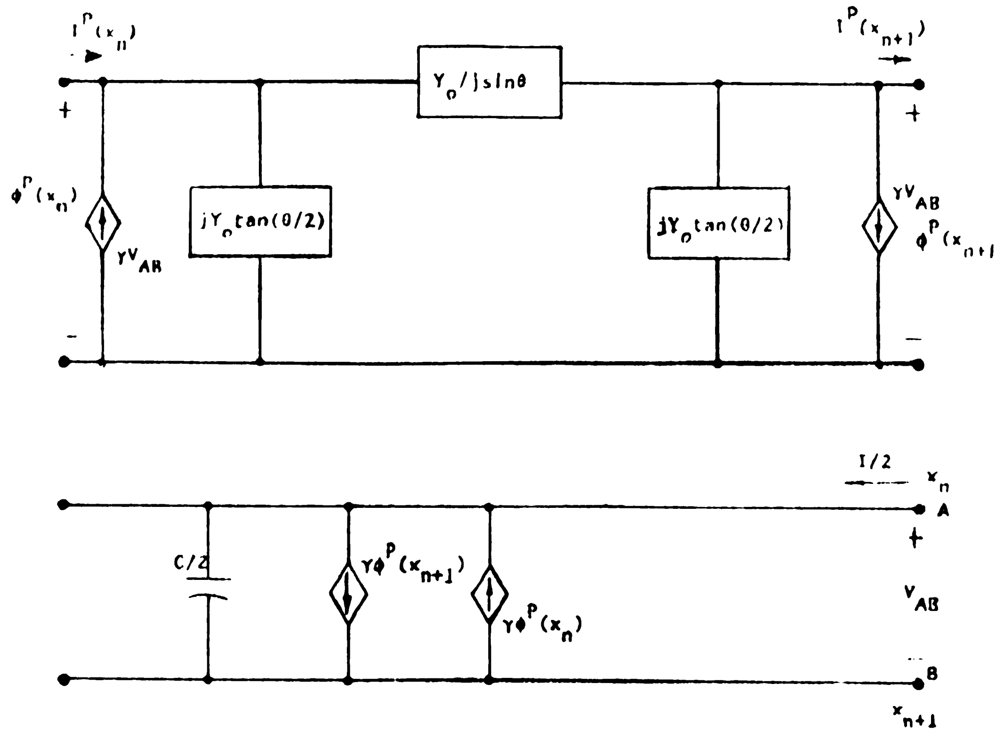


Figure 6.6 - Equivalent circuit of a section shown in Fig. 6.7.

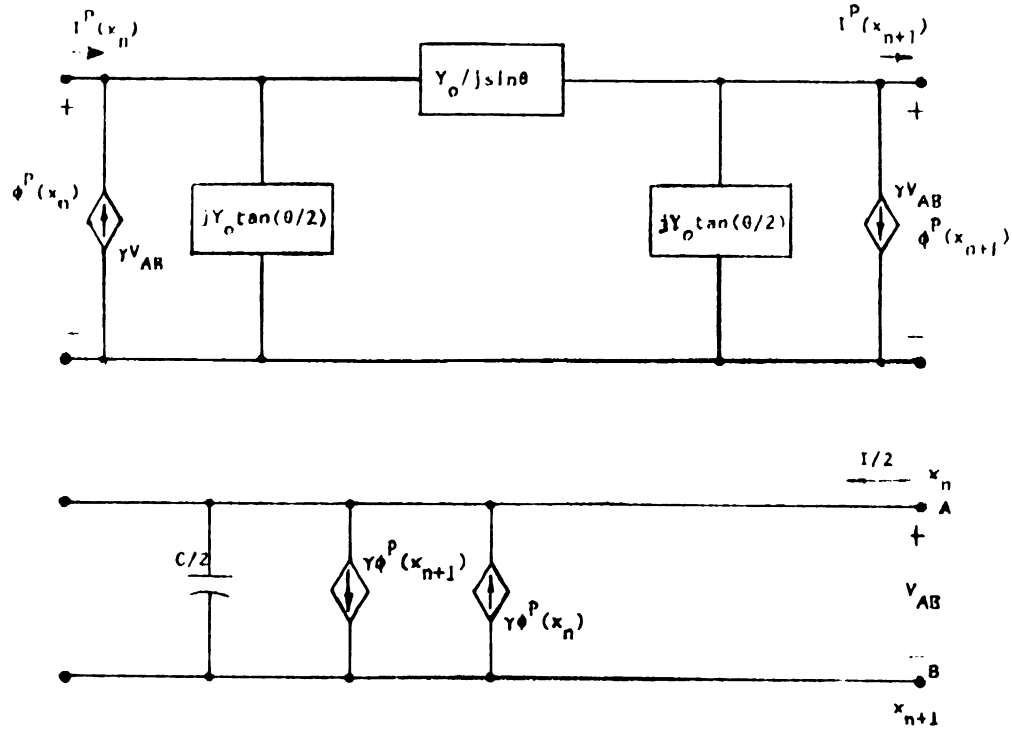


Figure 6.6 - Equivalent circuit of a section shown in Fig. 6.7.

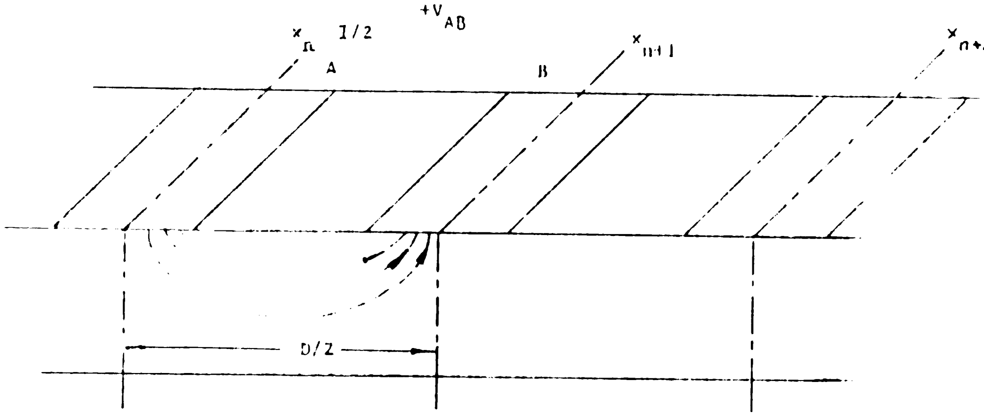


Figure 6.7 - A basic section for which the equivalent circuit in Fig. 6.6 is applicable.

6.8. In the electrical part of the equivalent circuit, the value of the current sources $\gamma\phi^P(x_1)$ and $\gamma\phi^P(x_{20})$ has been doubled. This is mathematically convenient and corresponds to an assumption that the 19 sections of the array are terminated on both ends by half-sections. Apart from this convenience, it is also consistent with the results obtained from Fig. 6.2, which originally gave rise to the present equivalent circuit. The procedure to be extracted from this is stated below:

> Each <u>electrode</u> has a dependent current source of strength $2\gamma\phi^P(x_n)$ in the lower part of the equivalent circuit, and a source of $2\gamma V_{AB}$ in the upper part. If the particular electrode is connected to node A, the terminal labeled with a (+) sign, the reference arrows must point up. For node B, they point down. Now, without resorting further to matrix equations, the model is put together by giving each space between the electrode centers a $\pi$-section of characteristic admittance $Y_o$ and transit angle $\theta = \pi\omega/\omega_o$ in the upper part, and a capacitor of value C/2 in the lower part. Then each electrode is accounted for as described above.

This procedure extends easily to unequal electrode spacings and apodized arrays [ 7 ], i.e. arrays where the "acoustic aperture" is changed by letting adjacent electrodes overlap only partially. An apodizing function w(x) is defined [13]. It determines the fraction of overlap. The generators in the upper part of Fig. 6.8 each become

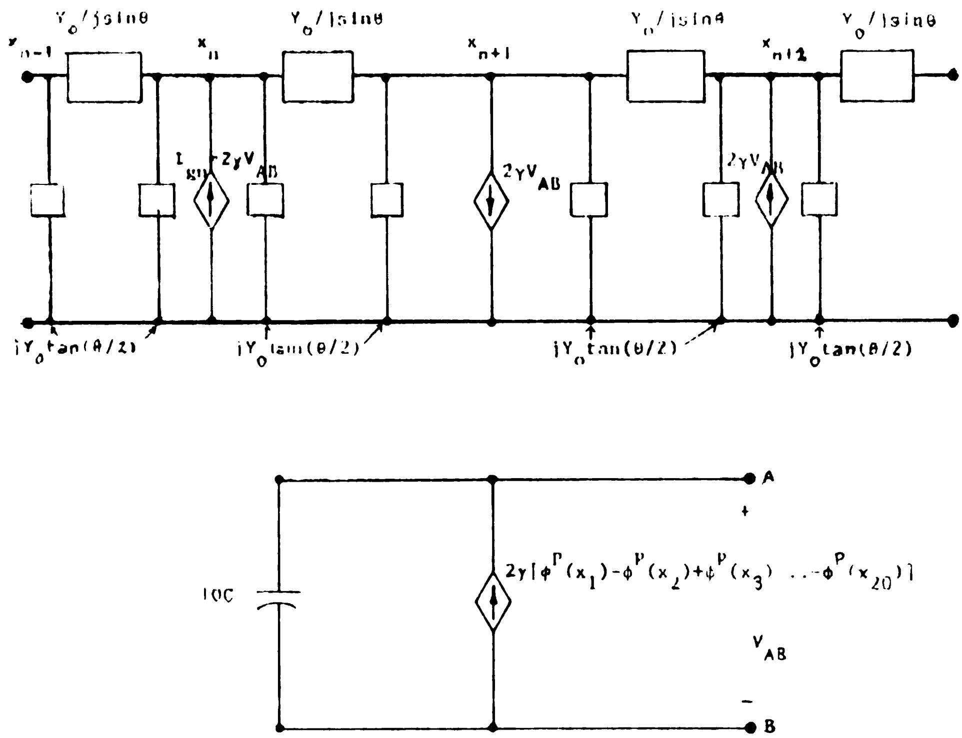


Figure 6.8a - Equivalent circuit of twenty electrodes.

$$Y = j\omega\sqrt{\epsilon_{11}\epsilon_{22}}\ W[\pi/4K'(\omega/\omega_o)]$$

$$C = (\epsilon_o + \sqrt{\epsilon_{11}\epsilon_{22}})\ WK/K'$$

$$\theta = \pi\omega/\omega_o = kD/2$$

$$Y_o = \omega W \times 2.68 \times 10^{-7}\ \mho\ \text{(AC cut)}$$

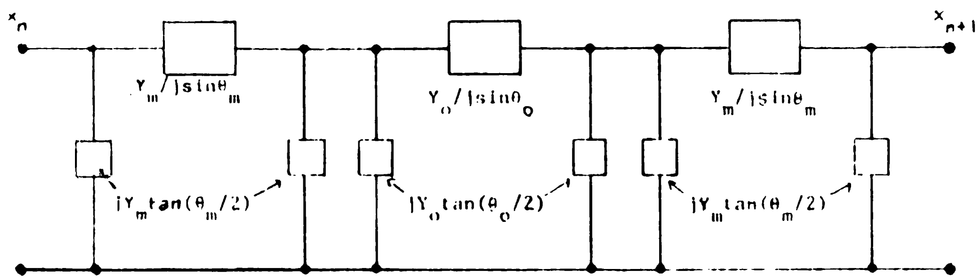


Figure 6.8b - Interspaces are broken down each into three sections to account for difference in velocity and $Y_o$ under metallized surfaces for materials with stronger coupling.

$$I_{gn} = 2\gamma w(x_n)\ V_{AB}\ (-1)^{n+1}\ , \qquad (6.12)$$

with the reference arrows pointing up and the total strength of the current source in the lower part becomes

$$I_{SC} = -2\gamma \sum_{n=1}^{N} (-1)^n\ \phi^P(x_n)\ w(x_n)\ . \qquad (6.13)$$

Each capacitance value is also multiplied by $w(x_n)$, which has some value between zero and one.

In the present discussion the sections are identical so that $w(x) = 1$. But here too a more sophisticated model could be employed to account for the difference in $V_p$ and $Y_o$ under the metallized parts as compared with the unmetallized interspaces. By the discussion of Section 3.7 this is not worth the effort in the case of quartz, but in materials with stronger coupling, such as lithium niobate, the section between the electrode centers could be broken down into three parts [see Fig. 6.8b]. The change in velocity, and therefore of $Y_o$, under the surface metallization has been investigated for lithium niobate by Campbell and Jones [ 3]. Their tabulated values could be used in connection with this equivalent circuit. Smith et al have produced a similarly composite equivalent circuit based on the Mason model [12]. Usually these complications are ignored. Back to the analysis problem, for $\eta = 1/2$ (half the surface area is metal plated) the elliptic integrals K and K' are equal. If the width is 2mm then the total capacitance 10C equals only 1 pF. A high frequency probe with an input capacitance of 9 pF is connected to the array. This will lower the measured voltage to one-tenth its theoretical open circuit value, but because of this it will lower the strength of the current generators $I_{gn}$ so that it is quite reasonable to assume that the wave is unaffected by the array. The form of $\phi^P(x)$ throughout is taken to be

$$\phi^P(x_n) = \phi_S^+ e^{-jkx_n} = \phi_S^+ e^{-j(n-1)\theta} \quad . \qquad (6.14)$$

The value of $x_1$ was taken to be zero and $\theta = \pi\omega/\omega_o$. The terminal voltage is then

$$V_{AB} = \frac{0.02\gamma\phi_S^+}{j\omega C} [1 - e^{-j\theta} + e^{j2\theta} - \ldots - e^{-j19\theta}] \; , \qquad (6.15)$$

or

$$V_{AB} = \frac{0.02\gamma\phi_S^+}{j\omega C} \cdot \frac{1 - e^{-j20\theta}}{1 + e^{-j\theta}} = \frac{.02\gamma}{\omega C} e^{-j19\theta/2} \frac{\sin(10\theta)}{\cos(\theta/2)} \phi_S^+ \; .$$

With the form of $\gamma$ and C inserted, this becomes

$$V_{AB} = \frac{K'}{K} \cdot \phi_S^+ \cdot \frac{\pi \times 0.01}{2K'(\omega/\omega_o)} \cdot \frac{\sin(10\pi\omega/\omega_o)}{\cos(\pi\omega/2\omega_o)} \; . \qquad (6.16)$$

At $\omega = \omega_o$ the value of $\sin(10\pi\omega/\omega_o)/\cos(\pi\omega/2\omega_o)$ is 20. At $\eta = 1/2$ $K' = K = 1.85407$, so that $V_{AB}/\phi_S^+$ has a peak value of 0.16944. This value is essentially independent of the number of electrodes used, provided the load capacitance seen by the array is nine times its own output capacitance. The value is identical to that obtained in Chapter 5. The advantage of many electrodes is the decrease in output impedance and the very selective frequency response. For general values of $\omega/\omega_o$ the function has been programmed in Appendix F. The quantity $K'(\omega/\omega_o)$ is by Eqs. (5.59)-(5.62) the complete elliptic integral of modulus

$$m' = 1 - \sin^2(\eta\pi\omega/2\omega_o) \; . \qquad (6.17)$$

According to Abramowitz [14] K' may be calculated with the "geometric-arithmetic" mean $a_N$:

$$\pi/K' = 2a_N \ . \tag{6.18}$$

The geometric-arithmetic mean is found to great accuracy within very few steps of the following algorithm. As an example, $\omega/\omega_o$ is taken to be 1.2:

$$a_o = 1 \qquad b_o = \sin(\eta\pi\omega/2\omega_o) = .809017 \tag{6.19}$$

$$a_1 = \frac{a_o + b_o}{2} = .904508 \qquad b_1 = \sqrt{a_o b_o} = .899454 \tag{6.20}$$

$$a_2 = \frac{a_1 + b_1}{2} = .901981 \qquad b_2 = \sqrt{a_1 b_1} = .901977 \tag{6.21}$$

$$a_3 = \frac{a_2 + b_2}{2} = .901979 \qquad b_3 = \sqrt{a_2 b_2} = .901979 \tag{6.22}$$

The quantity $2a_N = 2a_3$, so that $\pi/K' = 1.803958$, for $\omega/\omega_o = 1.2$. The frequency response could only be computed for the range $\frac{2}{3} < \omega/\omega_o < 2$, because the validity of Eq. (6.1) has not been established outside of that frequency range. Figure 6.9 is a computer plot of Eq. (6.16). The general shape of the frequency response is quite similar to that obtained by Tseng [16], who used a flat-field approximation between the electrodes for the excitation of surface waves. It will be shown next that, within a constant of proportionality, the frequency response of the array used for excitation of surface waves is the same as that developed here in Eq. (6.16) for the detection of surface waves.

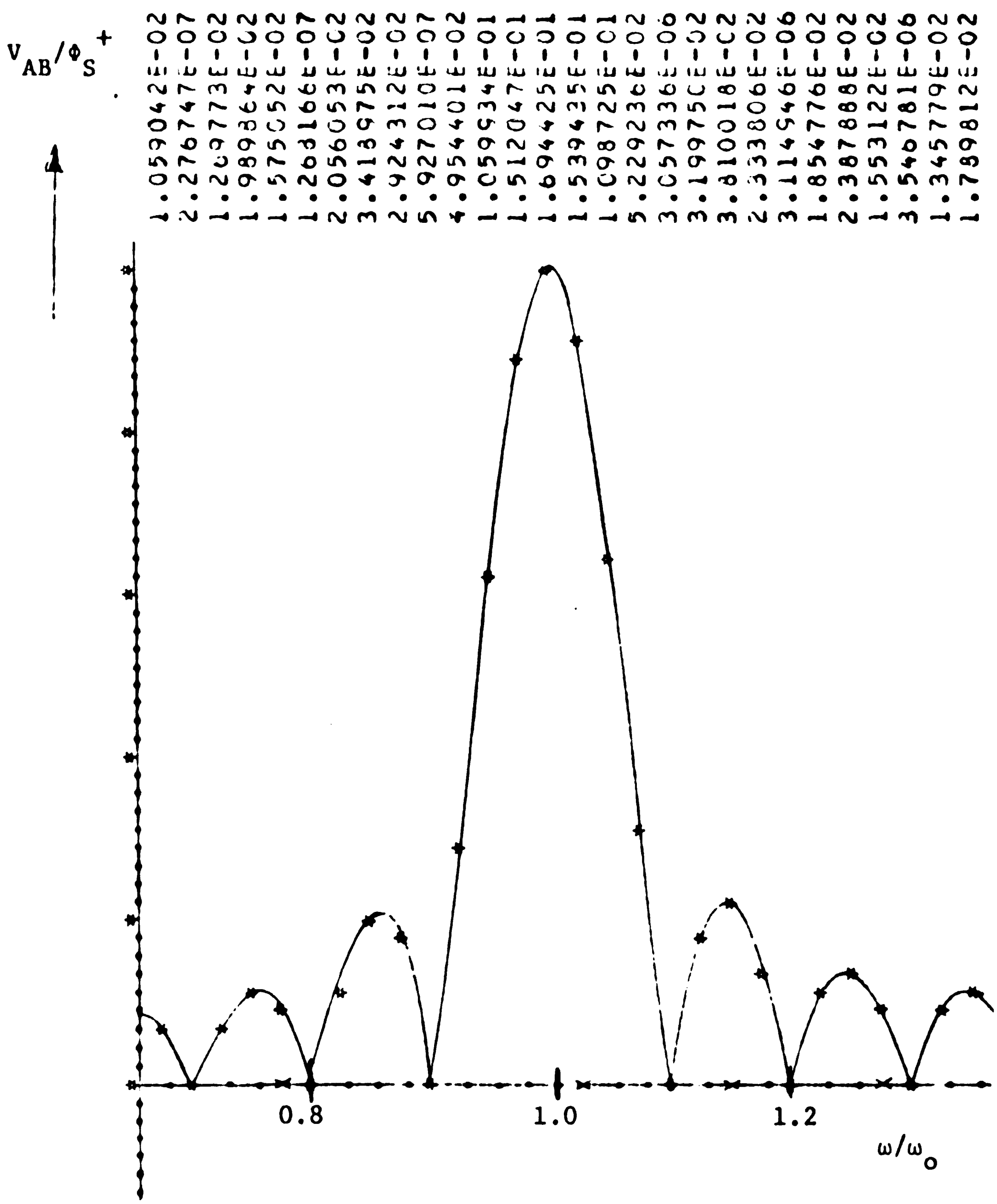


Figure 6.9a - Frequency response of a 20 element array terminated in a relatively large capacitor.

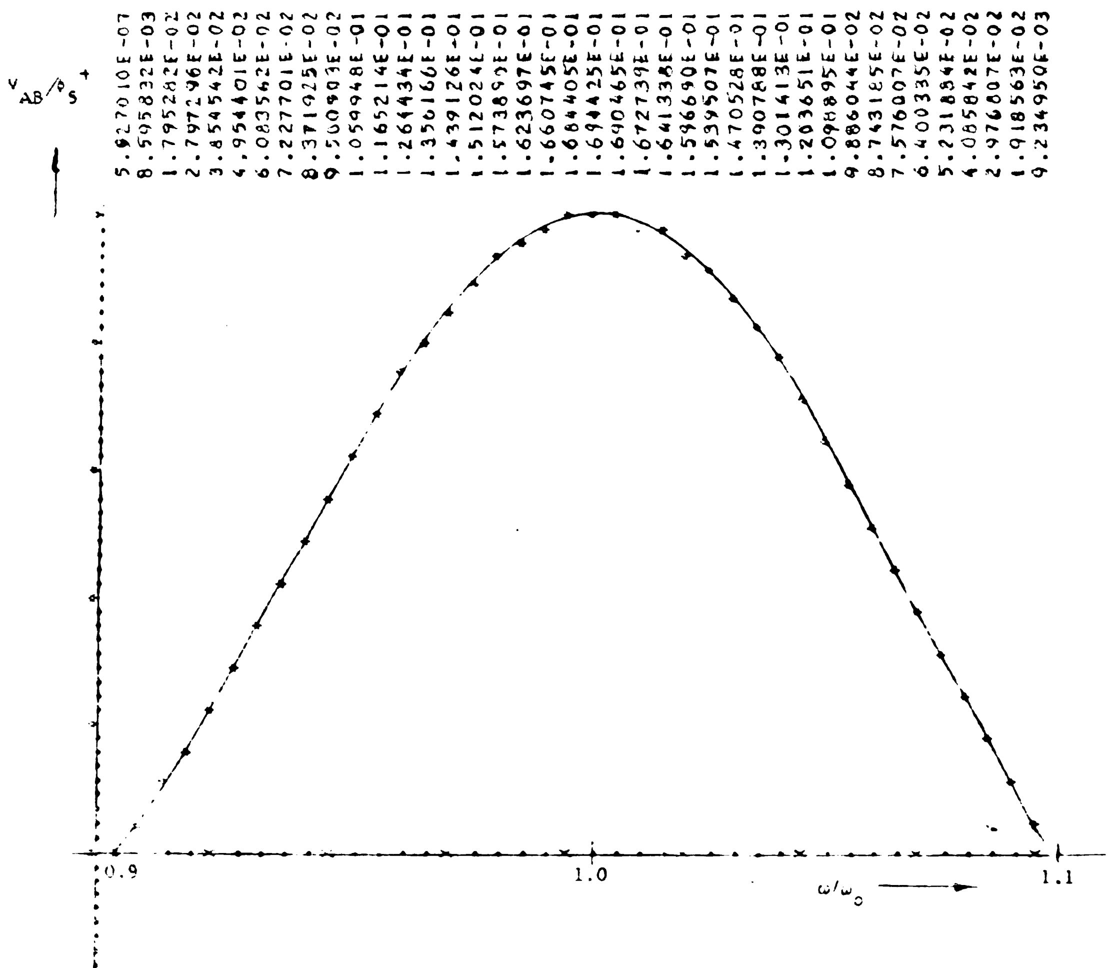


Figure 6.9b - Central peak of the frequency response of a 20 element array.

Let it be assumed that the transducer is terminated on both sides by an infinite piezoelectric line with a characteristic admittance $Y_o$ equal to that of the transducer array.

The line generators are each of strength

$$I_{gn} = (-1)^{n+1}\, 2\gamma\, V_{AB}\ , \tag{6.23}$$

[see Fig. 6.8], all reference directions pointing up.

By the principle of superposition the response to the generator connected to $x_n$ is considered first with all others set to zero. The total input impedance seen at point $x_n$ is, because of the matched conditions, $1/2\ Y_o$. The line potential at this point is therefore:

$$\phi^P(x_n) = (-1)^{n+1}\, 2\gamma\, V_{AB}/2Y_o \quad . \tag{6.24}$$

From this point a wave spreads in both directions. At a point x to the right of the array the line potential will be:

$$\phi_n^{\,P}(x) = (-1)^{n+1}\, \frac{\gamma V_{AB}}{Y_o}\, e^{-jk(x-x_n)} \quad . \tag{6.25}$$

The complete response at x is then by superposition:

$$\phi^P(x) = \sum_{n=1}^{20} \phi_n^{\,P}(x)\ ,$$

or

$$\phi^P(x) = \frac{\gamma V_{AB}}{Y_o}\, e^{-jkx}\, [e^{jkx_1} - e^{jkx_2} + e^{jkx_3} \,.\,.\,.\,.\,.\, - e^{jkx_{20}}]. \tag{6.26}$$

Once more, let $x_1 = 0$ and $kx_{n+1} - kx_n = \theta$, the result is the identical progression, but with positive exponents, as in Eq. (6.15).

It sums therefore to

$$\phi^P(x) = \frac{\gamma V_{AB}}{Y_o} e^{-jkx} \frac{1 - e^{j20\theta}}{1 + e^{j\theta}} \quad . \tag{6.27}$$

This simplifies to

$$\phi^P(x) = -j\ e^{j19\theta/2}\ \gamma V_{AB}\ e^{-jkx}\ \sin(10\theta)/Y_o\ \cos(\theta/2)\ , \tag{6.28}$$

or

$$\phi^P(x) = -j\ e^{j19\pi\omega/2\omega_o}\ V_{AB}\ \Lambda(\omega/\omega_o)\ e^{-jkx}/Y_o\ . \tag{6.29}$$

The function $\Lambda(\omega/\omega_o)$ is

$$\Lambda(\omega/\omega_o) = \frac{\gamma \sin(10\theta)}{\cos(\theta/2)} = j\omega\sqrt{\varepsilon_{11}\varepsilon_{22}}\ W[\pi/4K'(\omega/\omega_o)]\ \frac{\sin(10\pi\omega/\omega_o)}{\cos(\pi\omega/2\omega_o)}\ . \tag{6.30}$$

From Eq. (3.58) the value of $Y_o$ is for the AC cut:

$$Y_o = \omega W \times 2.68 \times 10^{-7} \mho\ . \tag{6.31}$$

This results in a cancellation of the term $\omega W$:

$$\phi^P(x) = \sqrt{\varepsilon_{11}\varepsilon_{22}}\ e^{j19\pi\omega/2\omega_o}\ V_{AB}\ e^{-jkx} \times 4.7 \times 10^5$$

$$\times\ \frac{2\pi\ \sin(10\pi\omega/\omega_o)}{K'(\omega/\omega_o)\cos(\pi\omega/2\omega_o)}\ . \tag{6.32}$$

Comparing the last fraction with Eq. (6.16) shows that the shape of the frequency response is identical here. At $\omega = \omega_o$ the absolute value of Eq. (6.32) is

$$|\phi^P(x)/V_{AB}| = 1.2 \times 10^{-3} \tag{6.33}$$

which means it takes an excitation of 83 volts to produce a surface potential of only 0.1 volt, but the associated line current is rather high. At $\omega = 1.5 \times 10^9$/sec and W = 2.5 mm, typical values, the line admittance $Y_o$ equals 1 ℧, so that $|I^P(x)|$ is 100 milliamps. However, the purpose here was merely to demonstrate the versatility of the equivalent circuit, not to judge the efficiency of the transducer.

## 6.3 An Equivalent Circuit Model with Ideal Transformers

In the last section it was shown how readily the equivalent circuit developed in this Chapter lends itself to mathematical analysis. The dependent generators are no drawback. In the excitation problem they offered, in fact, an advantage over the ideal transformers found in the Mason model because of the principle of superposition, by which all but one of the sources may be set to zero at any time. This facilitates the calculation of the response. No direct equivalent procedure exists for transformers which are passive circuit elements. Nevertheless, for the sake of interest an equivalent circuit will be developed in this section that resembles the Mason model with its ideal transformer. The principal difference lies in the fact that, in Chapter 4, the equivalent circuit is developed for half-electrodes; here, the equivalent circuit will be centered on the interspace with one-half of the adjacent electrodes on either side as illustrated in Fig. 6.7. The Mason model of Smith et al [10] is centered around the interspace as in the present treatment.

In order to accomplish this the dual of the upper part of the circuit of Fig. 6.6 is found first. The technique is illustrated in Fig. 6.10. The admittances become impedances with the same numerical value; meshes become nodes. When a current source pointing right is encountered by a path linking the mesh centers, it is replaced by a voltage source with a "- +" orientation. The voltage across the current source becomes the current through the voltage source. The reference directions must be such that the power relations are maintained for that source. The short linking two sections becomes an open circuit. The current through the short will be the voltage across the open circuit. The equations resulting from the dual circuit shown in Fig. 6.11 are identical to those obtained from the original circuit in Fig. 6.10. However, the physical units are all wrong. This can be easily corrected by multiplying $\phi^P(x_n)$ by the factor $-j\omega\sqrt{\varepsilon_{11}\varepsilon_{22}}\,W$, similar to Eq. (3.44). The quantity $j\omega\sqrt{\varepsilon_{11}\varepsilon_{22}}\,W\phi^P(x_n)$ has units of electric current and it points to the right [see Fig. 6.11]. In order to maintain the equality in any conceivable circuit equation, all possible ratios of "voltages" to "impedances" $Z_o' = Y_o$ must be multiplied by the same factor $-j\omega\sqrt{\varepsilon_{11}\varepsilon_{22}}\,W$. In particular, consider $\gamma V_{AB}/Z_o'$, where $\gamma$ is defined in Eq. (6.7),

$$\frac{j\omega\sqrt{\varepsilon_{11}\varepsilon_{22}}\,W\gamma V_{AB}}{Z_o'} = \frac{\omega^2\,\varepsilon_{11}\varepsilon_{22}\,W^2}{\omega W \times 2.68 \times 10^{-7}} \times \frac{\pi}{4K'(\omega/\omega_o)} \times V_{AB}\ . \qquad (6.34)$$

By Eq. (3.61) the value of $Z_o$ is determined uniquely for this new definition of electric current. It must be

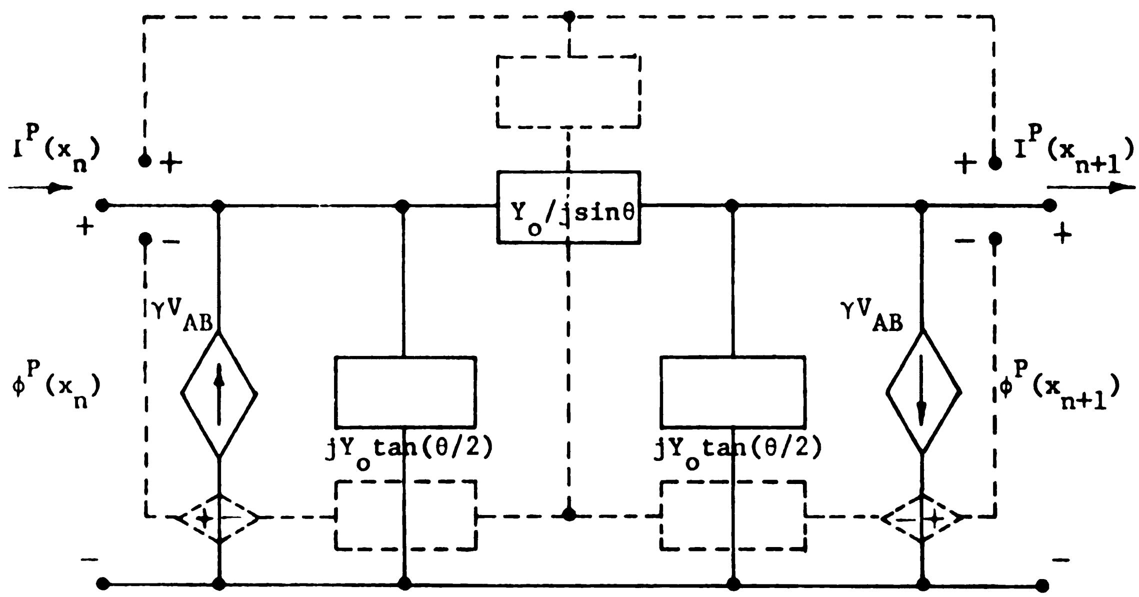


Figure 6.10 - Method to obtain the dual circuit.

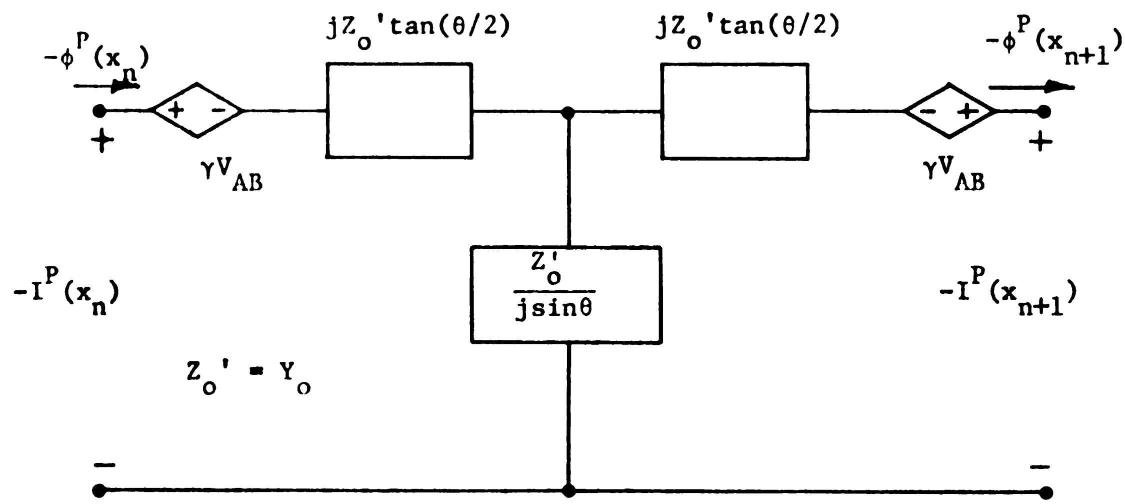


Figure 6.11 - Dual of the upper part of the equivalent circuit of Fig. 6.6. The negative of all dynamic variables corresponds to the most convenient reference directions.

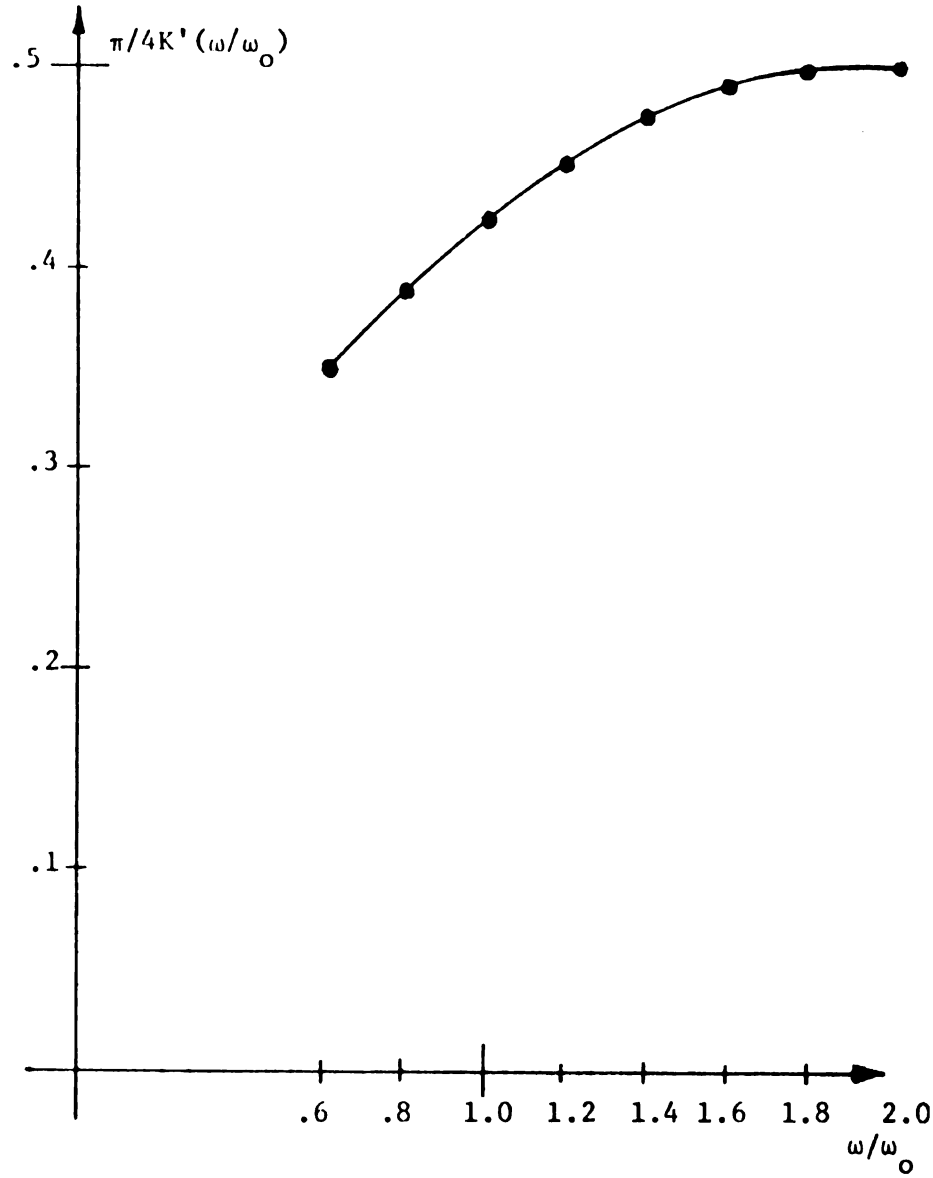


Figure 6.12 - The variation of the turns ratio with frequency. $\eta = 1/2$.

$$Z_o = 1.72 \times 10^{14}/\omega W \ \Omega \tag{6.35}$$

for the AC cut in quartz. An examination of Eq. (6.34) shows that the first part of the tripple product has exactly the right value:

$$\frac{\omega \varepsilon_{11} \varepsilon_{22} W}{2.68 \times 10^{-7}} = \frac{\omega W}{1.72 \times 10^{14}} = \frac{1}{Z_o} \ . \tag{6.36}$$

The voltage dependent voltage source now has a strength of

$$\frac{\pi}{4K'(\omega/\omega_o)} \cdot V_{AB} \ . \tag{6.37}$$

It is only slightly frequency dependent over the frequency range of interest. Fig. 6.12 shows a plot of $\pi/4K'(\omega/\omega_o)$. A reasonable approximation for the function would be $\pi/4K'$ which for $\eta = 1/2$ equals

$$\pi/4K' = 0.4236 \ . \tag{6.38}$$

Such an approximation, however, is not essential if an ideal transformer with a "slightly frequency dependent turns-ratio" is acceptable.

The ideal transformer comes about as follows: First, by the Blakesley shift, the dependent voltage sources are moved into the center leg. This situation together with the new dynamic variables and line impedance is depicted in Fig. 6.13. Since the rigorous procedure of Chapter 3 was strictly adhered to, the new line voltages, $V^P(x_n)$, will have units of voltage.

Next, the lower part of Fig. 6.6 [or 6.5] must be examined. It contains a dependent current source of strength

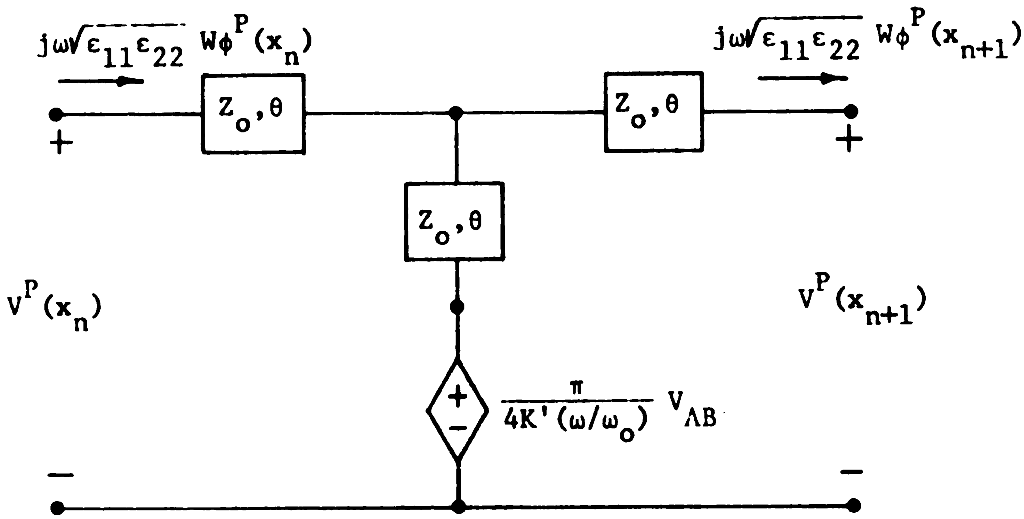


Figure 6.13 - The modified dual of the upper part of Fig. 6.6. Both circuits yield the same circuit equations.

$$\gamma[\phi^P(x_n) - \phi^P(x_{n+1})] = \frac{\pi}{4K'(\omega/\omega_o)} [j\omega\sqrt{\varepsilon_{11}\varepsilon_{22}}\, W\phi^P(x_n)$$

$$- j\omega\sqrt{\varepsilon_{11}\varepsilon_{22}}\, W\phi^P(x_{n+1})] \ . \qquad (6.39)$$

Any ideal transformer with turns ratio a:1 may be represented by the dependent voltage-current-source configuration shown in Fig. 6.14. The converse is also true. This follows directly from the fact that the transmission matrix for an ideal transformer may be implemented by the circuit shown in Fig. 6.14.

$$\left\|\begin{matrix} V_1 \\ \\ I_1 \end{matrix}\right\| = \left\|\begin{matrix} a & 0 \\ & \\ 0 & 1/a \end{matrix}\right\| \times \left\|\begin{matrix} V_2 \\ \\ I_2 \end{matrix}\right\| \qquad (6.40)$$

The final equivalent circuit follows immediately. It is shown in Fig. 6.15. The "dots" must be reversed for every alternate section, because the dependent generators in Fig. 6.6 would be reversed also. Since the frequency variation of the turns ratio is not strong, replacement by the constant $\pi/4K'$ will lead to good results. This then is the justification for the usage of the Mason model [10]. It should also be noted that the new "line current" $j\omega\sqrt{\varepsilon_{11}\varepsilon_{22}}W\phi^P(x_n)$ is much smaller than in calculations performed on the basis of the model in Fig. 6.6. In the excitation problem at the end of Section 6.2 the line voltage $\phi^P$ was 0.1 volt and the line current 100 ma. In this new model the line current would be for the values given there

$$|\omega\sqrt{\varepsilon_{11}\varepsilon_{22}}\, W\phi^P| = 1.5 \times 10^9 \times 40 \times 10^{-12} \times 2.5 \times 10^{-3} \times 0.1$$
$$= 15\mu A \ . \qquad (6.41)$$

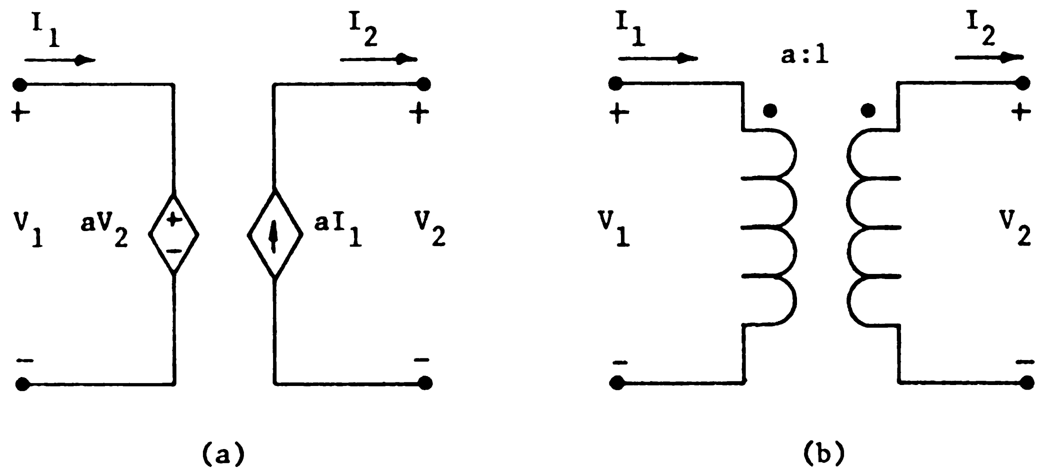


Figure 6.14 - Equivalent representations of an ideal transformer.

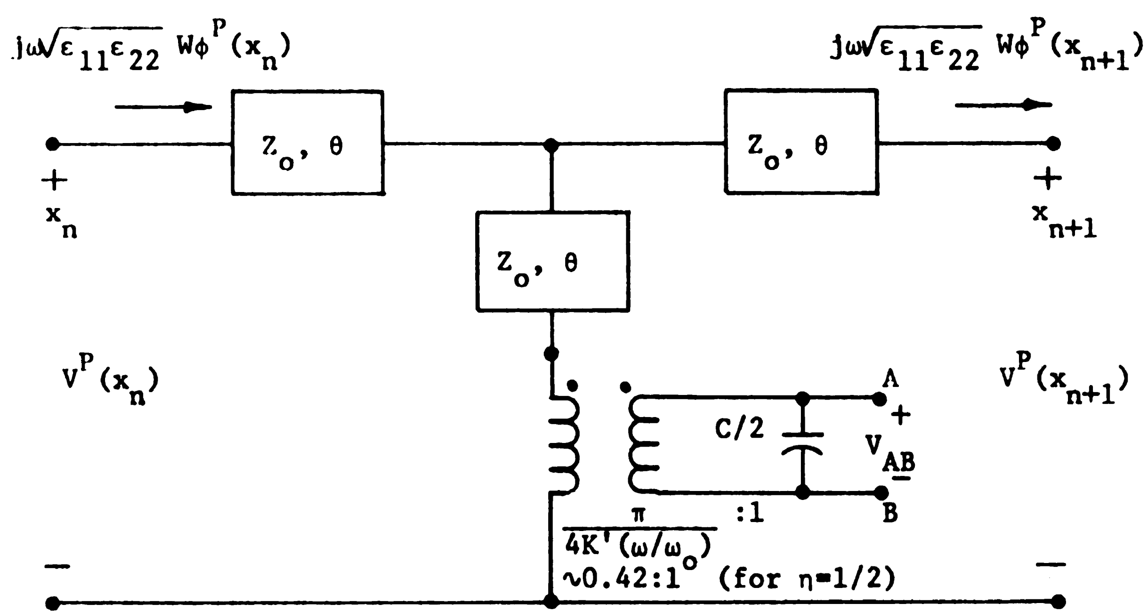


Figure 6.15 - Alternate equivalent circuit for a basic section of 1 interspace and 2 half electrodes. The location of electrode A is point $x_n$.

The line-impedance $Z_o$ would be

$$Z_o = \frac{1.72 \times 10^{14}}{\omega W} = 45.9 \text{ M}\Omega. \qquad (6.42)$$

The line-voltage $V^P$ must then be

$$V^P = Z_o \times \left| \omega\sqrt{\varepsilon_{11}\varepsilon_{22}} \, W\phi^P \right| = 688 \text{ volts}. \qquad (6.43)$$

In spite of the vastly different values, the effect on any measurable quantity is the same. Neither model is therefore superior to the other from a physical point of view; unless the interspace section shown in Fig. 6.8b is used in conjunction with the first circuit, in which case that circuit will account for the effect of the metallization, whereas the present circuit cannot do that. Otherwise, any preference should be based on mathematical advantages offered by a particular model in the context of the external terminations under study.

As mentioned in Chapter 4, for very narrow electrodes and a single wave of the form

$$\phi^P(x) = \phi_S^+ \, e^{-j \frac{\omega_o}{V_p} x} \qquad (6.44)$$

a potential difference $V_{AB}$ of $2\phi_S^+$ should be observed across the basic section [see Fig. 6.7]. The equivalent circuit of Fig. 6.15 will account for that effect correctly, as shown presently. The current into the dot of the primary is

$$I_{pr} = j\omega\sqrt{\varepsilon_{11}\varepsilon_{22}} \, W[\phi_S^+ \, e^{-j\frac{\omega_o x_n}{V_p}} - \phi_S^+ \, e^{-j\frac{\omega_o x_{n+1}}{V_p}}] \, . \qquad (6.45)$$

At the synchronous frequency $x_{n+1}$ is greater than $x_n$ by half a wave length, so that

$$I_{pr} = j\omega\sqrt{\varepsilon_{11}\varepsilon_{22}}\, W\, 2\Phi_S^{+}\, e^{-j\frac{\omega_o x_n}{V_p}} . \qquad (6.46)$$

At the synchronous frequency $K'(\omega/\omega_o) = K'$, the secondary current is then $\pi/4K'$ times the primary current, and $V_{AB}$ becomes

$$V_{AB} = (\pi/4K')\, I_{pr}/j\omega\sqrt{\varepsilon_{11}\varepsilon_{22}}\, WK/2K' . \qquad (6.47)$$

The effect of the field above the piezoelectric slab on the value of $C/2$ has been ignored. The quantity $2K'$ will cancel, and $V_{AB}$ becomes then:

$$V_{AB} = (\pi/2)\, j\omega\sqrt{\varepsilon_{11}\varepsilon_{22}}\, W\, 2\Phi_S^{+}\, e^{-j\omega_o x_n/V_p}/j\omega\sqrt{\varepsilon_{11}\varepsilon_{22}}\, KW . \qquad (6.48)$$

For very narrow electrodes K is $\pi/2$, so that $V_{AB}$ reduces to the desired result:

$$V_{AB} = 2\Phi_S^{+}\, e^{-j\omega_o x_n/V_p} . \qquad (6.49)$$

This certainly does not represent a proof of the validity of the equivalent circuit, but it is gratifying to see that the postulates which led to these equivalent circuits do not create a conflict with this expected physical behavior of the device. More supporting evidence for the correctness of the theory presented here will be established in later sections of this Chapter where the radiation conductance and scattering parameters of the array are calculated on the basis of the last model [see Fig. 6.15]. The outcome fits the experimental results of Smith et al [10]. In order to perform these calculations, it is first necessary to obtain the three-port admittance matrix for the whole array.

## 6.4 The Admittance Matrix for an Array of an Even Number of Inter-electrode Spaces

The equivalent circuit of Fig. 6.15 is similar in form to that used by Smith et al [10]. The turns ratio and the characteristic impedance are frequency dependent in this investigation; in Smith et al, they are not. Since, however, the configuration is the same, the identical steps may be followed for the derivation. It will be particularly convenient to change the impedance level by a factor of the square of the turns ratio a

$$a^2 = [\pi/4K'(\omega/\omega_o)]^2, \tag{6.50}$$

so that the resulting characteristic impedance is

$$1/G_o \equiv R_o \equiv Z_o[\frac{4K'(\omega/\omega_o)}{\pi}]^2 , \tag{6.51}$$

and the new line-current will then be

$$I_n = j\omega[\sqrt{\varepsilon_{11}\varepsilon_{22}}\, W\pi/4K'(\omega/\omega_o)]\phi^P(x_n) \equiv \gamma\phi^P(x_n) . \tag{6.52}$$

First, two adjacent sections are cascaded as shown in Fig. 6.16 and the y-parameters for this combination are obtained. The symbol $\theta$ stands here for the transit angle for an interdigital period. It has therefore twice the value of the $\theta$ used previously. The calculations are based directly on the procedure suggested by Smith et al and are repeated for completeness in Appendix G. The results are listed below in Eq. (6.53):

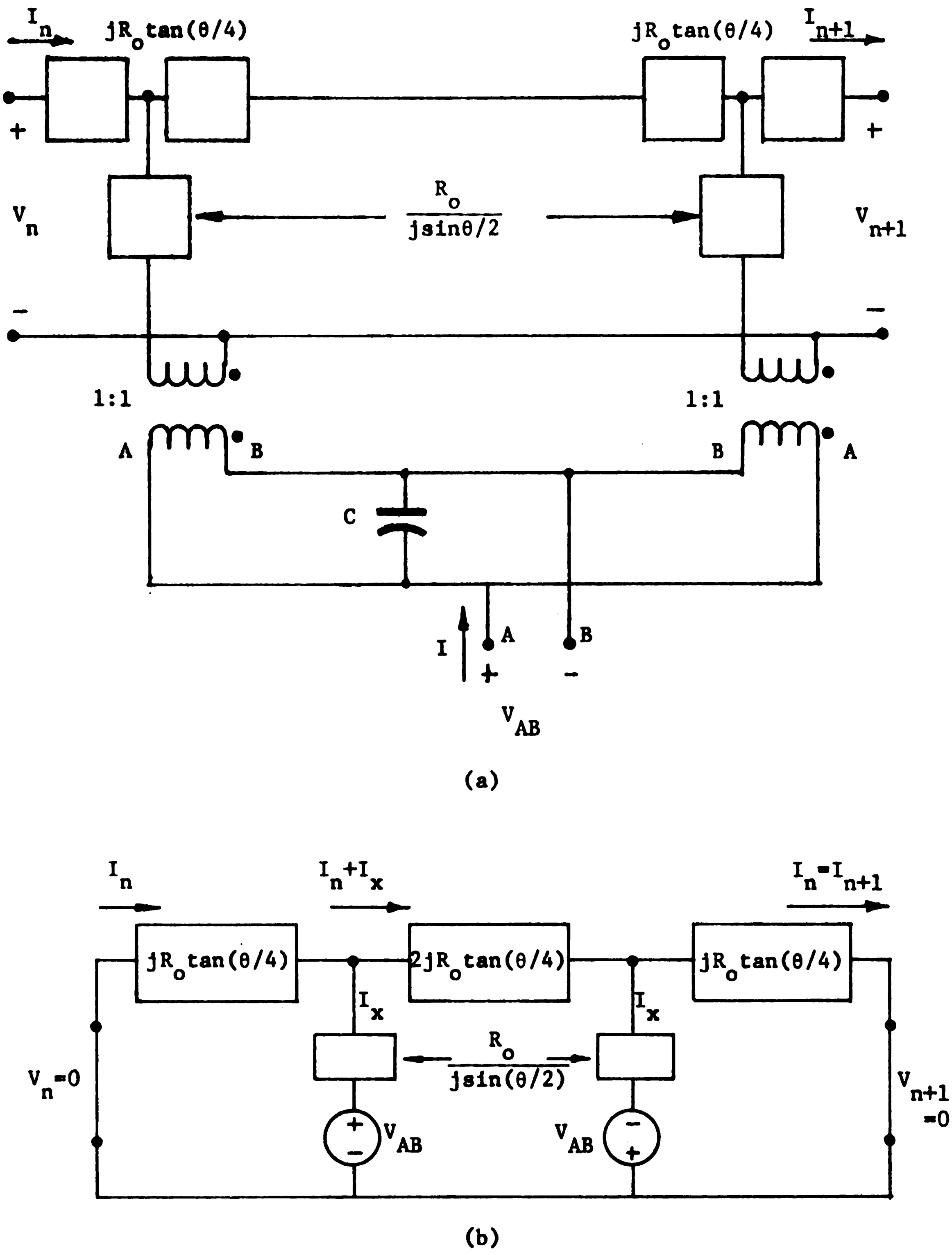


Figure 6.16 - (a) Equivalent circuit used to obtain the y-parameters for one interdigital period according to procedure by Smith et al. (b) Connection to find $y_{13}$, $y_{23}$ and $y_{33}$.

$$\begin{Vmatrix} I_n \\ \\ -I_{n+1} \\ \\ I \end{Vmatrix} = \begin{Vmatrix} \dfrac{G_o}{j\tan\theta} & \dfrac{-G_o}{j\sin\theta} & -jG_o\tan(\theta/4) \\ \\ \dfrac{-G_o}{j\sin\theta} & \dfrac{G_o}{j\tan\theta} & jG_o\tan(\theta/4) \\ \\ -jG_o\tan(\theta/4) & jG_o\tan(\theta/4) & j\omega C+j4G_o\tan(\theta/4) \end{Vmatrix} \begin{Vmatrix} V_n \\ \\ V_{n+1} \\ \\ V_{AB} \end{Vmatrix} . \tag{6.53}$$

When N such interdigital periods are cascaded, the resulting current $I_T$ will be by Eq. (6.53):

$$I_T = -jG_o\tan(\theta/4)\ V_1 + jG_o\tan(\theta/4)\ V_N$$

$$+ (j\omega C_T + j4NG_o\tan(\theta/4))\ V_{AB} \tag{6.54}$$

The total capacitance NC has been denoted $C_T$. The reason for this simplicity is that in Eq. (6.53)

$$y_{31} = -y_{32}\ . \tag{6.55}$$

This causes cancellations of the contribution from all $V_n$ except $V_1$ and $V_N$.

Equation (6.54) is sufficient for the determination of the overall admittance matrix, since for $V_{AB} = 0$ all sections behave like a transmission line, and because of the required symmetry about the main diagonal $y_{13}$ and $y_{23}$ are known through Eq. (6.54). The final result is then:

$$\begin{Vmatrix} I_1 \\ \\ -I_N \\ \\ I_T \end{Vmatrix} = \begin{Vmatrix} \dfrac{G_o}{j\tan(N\theta)} & \dfrac{-G_o}{j\sin(N\theta)} & -jG_o\tan(\theta/4) \\ \\ \dfrac{-G_o}{j\sin(N\theta)} & \dfrac{G_o}{j\tan(N\theta)} & jG_o\tan(\theta/4) \\ \\ -jG_o\tan(\theta/4) & jG_o\tan(\theta/4) & j\omega C_T+j4NG_o\tan(\theta/4) \end{Vmatrix} \times \begin{Vmatrix} V_1 \\ \\ V_N \\ \\ V_{AB} \end{Vmatrix} , \tag{6.56}$$

where

$$C_T = NC , \tag{6.57}$$

$$\theta = 2\pi(\omega/\omega_o) \tag{6.58}$$

and

$$G_o = \frac{1}{Z_o} \left[\frac{\pi}{4K'(\omega/\omega_o)}\right]^2 . \tag{6.59}$$

This admittance matrix for the whole transducer may now be used to determine various properties of the array. Since further verification of the theory developed in the last two Chapters is desirable, the radiation conductance will be calculated in the next section since it can be compared with experimentally measured frequency response curves for that quantity.

## 6.5 Calculation of the Radiation Admittance of an Array Made Up of N Identical Interdigital Periods

For the purpose of calculating the radiation admittance the array is terminated in $G_o$ on both ends, so that

$$I_1 = - G_o V_1 \tag{6.60}$$

and $$I_N = G_o V_N \; . \tag{6.61}$$

With this modification, Eq. (6.56) is rewritten as:

$$\left\|\begin{matrix} 0 \\ \\ 0 \\ \\ I_T \end{matrix}\right\| = \left\|\begin{matrix} Y_{11} + G_o & Y_{12} & Y_{13} \\ \\ Y_{12} & Y_{11} + G_o & -Y_{13} \\ \\ Y_{13} & -Y_{13} & Y_{33} \end{matrix}\right\| \times \left\|\begin{matrix} V_1 \\ \\ V_N \\ \\ V_{AB} \end{matrix}\right\| \; . \tag{6.62}$$

The input admittance under these conditions is the radiation admittance:

$$Y_a = I_T/V_{AB} = \frac{\Delta}{\Delta_{33}} \; . \tag{6.63}$$

The quantities $\Delta$ and $\Delta_{33}$ are the determinant of Eq. (6.62) and the co-factor of $Y_{33}$ respectively. These are worked out in Appendix H. The result of that calculation is summarized below:

$$G_a = 2G_o[\tan \frac{\theta}{4} \sin \frac{N\theta}{2}]^2 \tag{6.64}$$

and

$$B_a = G_o \tan \frac{\theta}{4} \; [4N + \tan \frac{\theta}{4} \sin N\theta] + \omega C_T \; . \tag{6.65}$$

These results are identical to those found in Smith et al [10] except for the frequency dependency of $G_o$ given by Eq. (6.59):

$$G_o = \frac{1}{Z_o} \; [\frac{\pi}{4K'(\omega/\omega_o)}]^2 = \frac{1}{Z_o(\omega_o)} \cdot (\frac{\omega}{\omega_o}) \; [\frac{\pi}{4K'(\omega/\omega_o)}]^2 \; . \tag{6.66}$$

The last substitution has been made on the basis of Eq. (3.61):

$$Z_o(\omega) = 1.72 \times 10^{14}/\omega W \; \Omega \; . \tag{6.67}$$

These relations are programmed for the digital computer in Appendix I. The resulting frequency response plots [see Figs. 6.17, 6.18a] for $N = 15$ show negligible difference between this theory and the assumption of a constant $G_o$ made by Smith et al, who used the Mason model for the corresponding development. The reason is that for larger arrays the central peak, where $G_a$ has a significant value, is so narrow that variations with frequency of $G_o$ are not noticeable, although $G_o$ increases monotonically with frequency because of $(\omega/\omega_o)$ as well as the factor $[\pi/4K'(\omega/\omega_o)]^2$, [see Fig. 6.12].

The direct comparison of the shape of the frequency response of $G_a$ with experimental data gathered [10] for a transducer laid out on YZ lithium niobate is made in Fig. 6.18b. An important conclusion to be drawn from this comparison is that it is now possible to deduce the value of the characteristic impedance $Z_o$ for YZ lithium niobate without resorting to the complicated calculations performed in Chapter 3. It is seen from Eqs. (6.64) and (6.66) that

$$G_a Z_o(\omega_o) = 2(\frac{\omega}{\omega_o})[\frac{\pi}{4K'(\omega/\omega_o)}]^2 \; [\tan(\frac{\pi\omega}{2\omega_o}) \; \sin(15\pi\omega/\omega_o)]^2 . \quad (6.68)$$

At $\omega = \omega_o$ this becomes numerically:

$$G_a Z_o(\omega_o)\Big|_{\omega_o} = 2[\frac{\pi}{4K'}]^2 \times 900 = 323 . \quad (6.69)$$

The experimental result [10] for a transducer with $N = 15$, $W = 1.25$ mm, $C_T = 8.5$ pF and $f_o = 105$ MHz yielded for $G_a = 4.2$ m℧. It follows that for YZ lithium niobate the characteristic impedance is

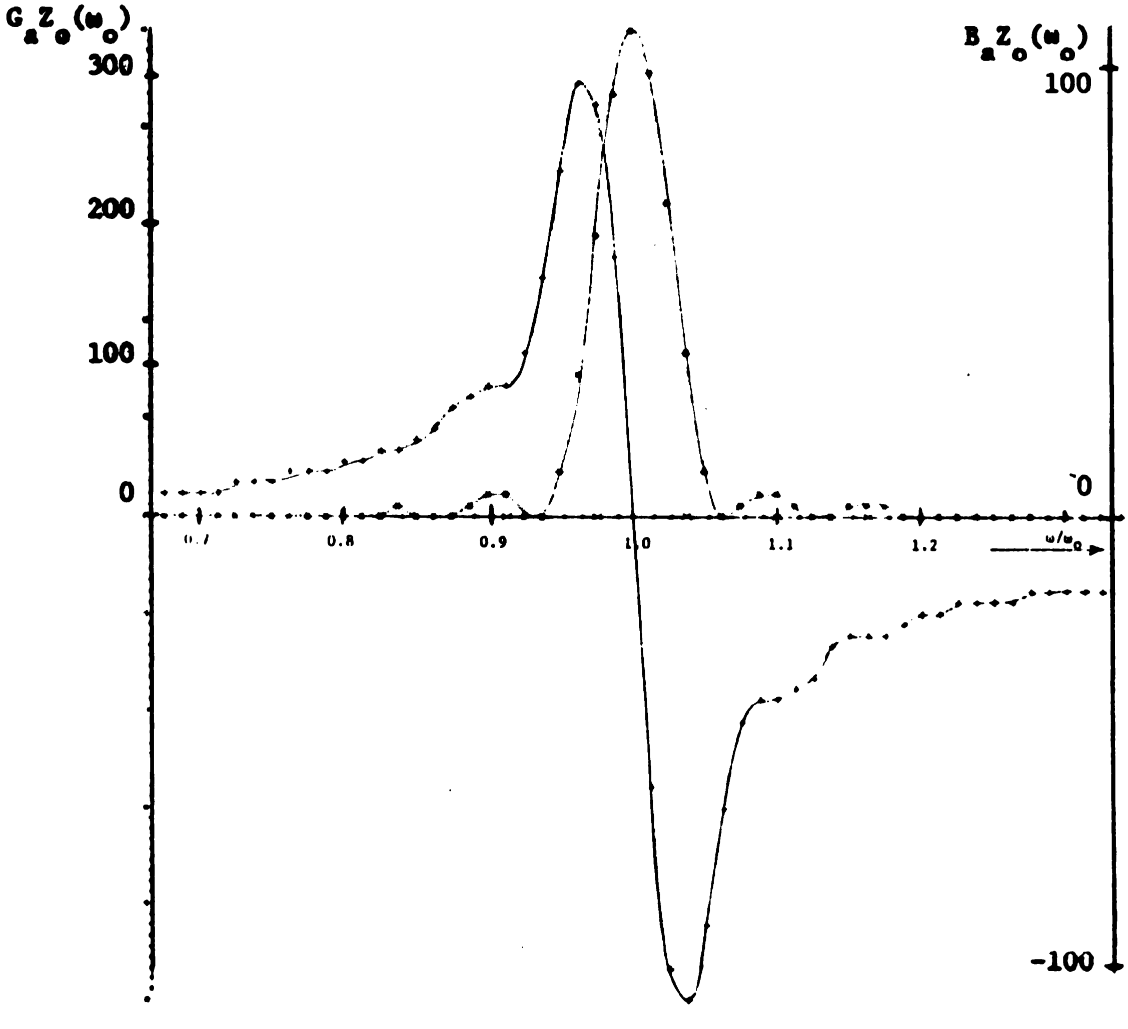


**Figure 6.17 - Normalized radiation admittance of a 30 element array.**

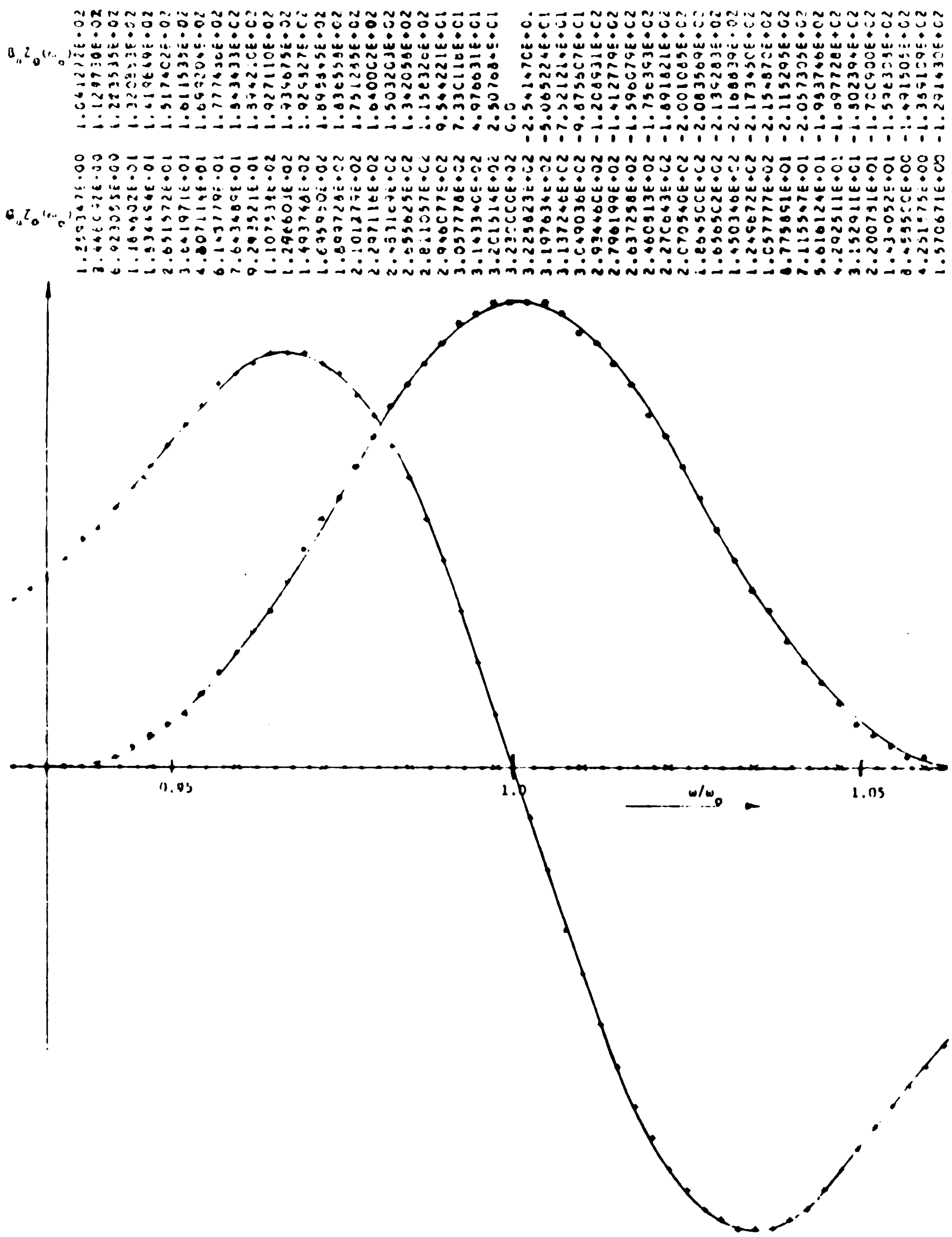


Figure 6.18a - Central portion of frequency response of radiation admittance.

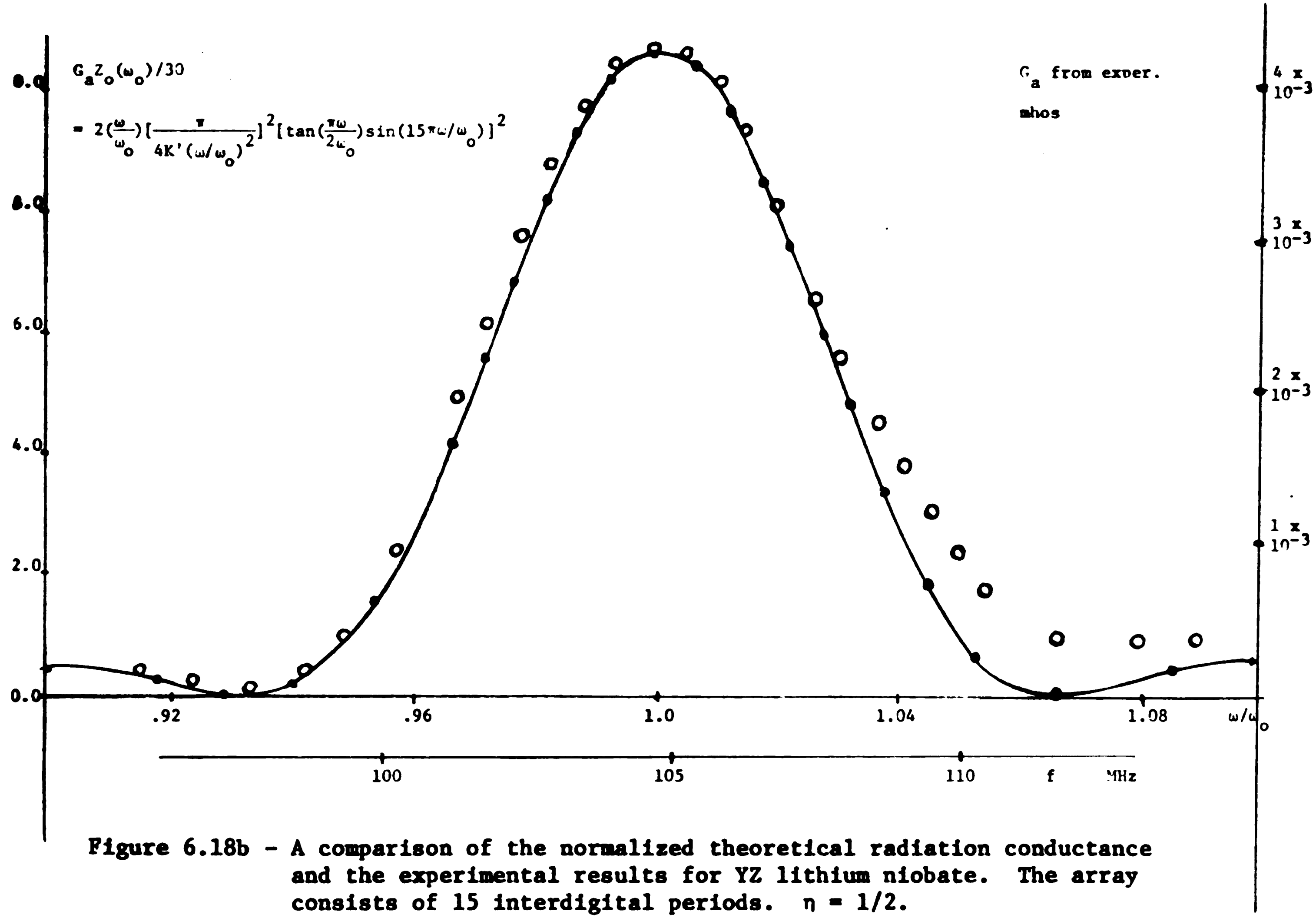


**Figure 6.18b - A comparison of the normalized theoretical radiation conductance and the experimental results for YZ lithium niobate. The array consists of 15 interdigital periods. $\eta = 1/2$.**

$$Z_o(\omega_o) = 323/4.2 \times 10^{-3} = 77000\ \Omega.$$

It is reasonable to assume the same functional relation to $\omega$ and W here as in the AC cut of quartz. Hence,

$$Z_o(\omega) = Z_o(\omega_o)\ \omega_o W/\omega W = \frac{77000 \times 2\pi \times 105 \times 10^6 \times 0.00125}{\omega W},$$

i.e.

$$Z_o(\omega) = \frac{6.35 \times 10^{10}}{\omega W} \quad . \tag{6.70}$$

To complete the equivalent circuit of Fig. 6.15 only C/2 is required in addition to $Z_o(\omega)$. From the experimental data in this case that would be

$$C/2 = C_T/30 = 0.28\ \text{pF} . \tag{6.71}$$

Otherwise it could be calculated from:

$$C/2 = \frac{(\varepsilon_o + \sqrt{\varepsilon_{11}\varepsilon_{22}})\ WK}{2K'} \quad . \tag{6.72}$$

The dielectric constants are listed in Warner et al [19]. They are also required to obtain the surface potential from the line current:

$$I^P(x) = j\omega\sqrt{\varepsilon_{11}\varepsilon_{22}}\ W\phi^P(x) . \tag{6.73}$$

In lithium niobate the propagation velocity shows a greater change under the metallized parts of the surface [ 3 ] than in quartz. Such a change in velocity implies by the investigation in Section 3.7 a change in $Z_o$:

$$V_{po} = V_{pm}\sqrt{1 + k_c^2} \tag{6.74}$$

and $$Z_{oo} = Z_m(1 + k_c^2) \ , \tag{6.75}$$

where the subscripts m and o mean metal and interspace respectively. It follows from these equations that the relative change in $Z_o$ may be determined if the change in $V_p$ is obtained

$$\frac{Z_{oo}}{Z_m} = (\frac{V_{po}}{V_{pm}})^2 \ . \tag{6.76}$$

In Campbell and Jones [ 3 ], both $V_{po}$ and $V_{pm}$ are given for various cuts of lithium niobate. Since even here that change in $V_p$ is only a few percent it does not really matter whether Eq. (6.70) is used for $Z_{oo}$ or $Z_{om}$ since the relative change in $Z_o$ would cause reflections and that can be determined from Eq. (6.76) with the data obtained from [ 3 ]. However, the T-model in which $Z_o$ is used will not accommodate a variation in $Z_o$. On the other hand, the modified $\pi$-model [see Fig. 6.8b] will account for both a change in $Z_o$ as well as a change in $V_p$ through the quantities $\theta_o$ and $\theta_m$ respectively:

$$\theta_m = \frac{\omega}{V_{pm}} \eta D/4 \tag{6.77}$$

and

$$\theta_o = \frac{\omega}{V_{po}} (1 - \eta) \ D/2 \ . \tag{6.78}$$

The quantity $D\eta$ is the length of an interdigital period times the fraction $\eta$ which gives the relative length of metallization. To complete this $\pi$-equivalent circuit $Y_o$ must be determined from Eqs. (6.70), (3.56) and (3.59):

$$Y_o = 2P_x/|\Phi_S|^2 ,$$

and

$$Z_o = 2P_x/\omega^2\epsilon_{11}\epsilon_{22}|\Phi_S|^2 W^2 ,$$

hence

$$Y_o = Z_o\, \omega^2 W^2\, \epsilon_{11}\epsilon_{22} , \tag{6.79}$$

or

$$Y_o = \omega W\, \epsilon_{11}\epsilon_{22} \times 6.35 \times 10^{10} . \tag{6.80}$$

The dielectric constants [19] are also required for the transconductance $\gamma$ shown in Fig. 6.8:

$$\gamma = j\omega\sqrt{\epsilon_{11}\epsilon_{22}}\, W[\pi/4K'(\omega/\omega_o)] . \tag{6.81}$$

This completes the $\pi$-model for YZ lithium niobate.

It has been shown in this section that the equivalent circuits developed in this investigation are quite adaptable to other piezoelectric materials. Originally they were developed for the AC cut in quartz only as a matter of mathematical convenience because the solution of the surface wave problem could be performed for that particular crystal cut in closed form. Later on in Chapter 3 the result was used for the determination of $Y_o$ and $Z_o$. In this Chapter, by comparison of the computed radiation conductance with experimental results, it became possible to determine $Y_o$ and $Z_o$ independently of the complicated procedure of solving numerically for the power flux of a piezoelectric surface wave. The circuit model may thus be determined by direct experimental procedure, which is analogous to finding transistor equivalent circuits from measurement rather than from a detailed knowledge of the geometry and physical properties of the material.

## 6.6 The Scattering Parameters of the Array at Synchronous Frequency With a Tuned Load

In the detection problem of Section 6.2 it was assumed that the array does not reflect nor attenuate a surface wave. The assumption was justified there because the load constitutes, for all practical purposes, a short circuit in which case the array behaves by assumption as a transmission line section.

In this section a resistive load in parallel with an inductance in resonance with $C_T$ at the synchronous frequency will be considered. It will be of interest to find out how much energy can be extracted from the wave at synchronous frequency. The scattering parameters are found from the admittance matrix of the two-port resulting from the termination described above by calculating [8]:

$$[\hat{S}] = [\hat{I} - \frac{\hat{y}_{ik}}{G_o}]\ [\hat{I} + \frac{\hat{y}_{ik}}{G_o}]^{-1} \ . \tag{6.82}$$

$\hat{I}$ is the identity matrix.

The matrix $\hat{y}_{ik}$ is derived from the admittance matrix of the three-port (Eqs. (6.56)) by eliminating $V_{AB}$ from the first two lines by means of the third line:

$$V_{AB} = \frac{jG_o \tan(\theta/4)[V_1 - V_N]}{G_L + j4NG_o \tan(\theta/4)} \ . \tag{6.83}$$

The elements of $\hat{y}_{ik}$ are then

$$y_{11} = y_{22} = \frac{G_oG_L + jG_o^2\tan(\theta/4)[4N+\tan(\theta/4)\tan(N\theta)]}{G_Lj\tan(N\theta) - 4NG_o\tan(N\theta)\ \tan(\theta/4)} , \quad (6.84)$$

and

$$y_{12} = y_{21} = -\frac{G_oG_L + jG_o^2\tan(\theta/4)[4N + \tan(\theta/4)\sin(N\theta)]}{G_Lj\sin(N\theta) - 4NG_o\sin(N\theta)\ \tan(\theta/4)} . \quad (6.85)$$

Unlike the elements of the three-port matrix these y-parameters remain finite at synchronous frequency, where

$$\sin(N\theta)\ \tan(\theta/4) = \tan(N\theta)\ \tan(\theta/4) = -4N . \quad (6.86)$$

Let

$$\alpha = G_L/16N^2\ G_o . \quad (6.87)$$

With this definition $[\hat{y}_{ik}]$ is at synchronous frequency

$$\hat{y}_{ik} = G_o \left\|\begin{matrix} \alpha & -\alpha \\ -\alpha & \alpha \end{matrix}\right\| . \quad (6.88)$$

The matrix $[\hat{I} + \hat{y}_{ik}/G_o]$ is in terms of $\alpha$:

$$[\hat{I} + \hat{y}_{ik}/G_o] = \left\|\begin{matrix} 1+\alpha & -\alpha \\ -\alpha & 1+\alpha \end{matrix}\right\| . \quad (6.89)$$

Its inverse is required in Eq. (6.82) which becomes:

$$[\hat{S}] = \left\|\begin{matrix} 1-\alpha & \alpha \\ \alpha & 1-\alpha \end{matrix}\right\| \times \left\|\begin{matrix} \frac{1+\alpha}{1+2\alpha} & \frac{\alpha}{1+2\alpha} \\ \frac{\alpha}{1+2\alpha} & \frac{1+\alpha}{1+2\alpha} \end{matrix}\right\| , \quad (6.90)$$

or

$$S_{11}\ (= S_{22}) \equiv \frac{V_1^-}{V_1^+} = \frac{1}{1 + 2\alpha} = \frac{1}{1 + G_L/8N^2G_o} \quad , \tag{6.91}$$

and

$$S_{21}\ (= S_{12}) \equiv \frac{V_2^+}{V_1^+} = \frac{2\alpha}{1 + 2\alpha} = \frac{G_L/8N^2G_o}{1 + G_L/8N^2G_o} \quad . \tag{6.92}$$

If $G_L$ is zero, there will be complete reflection off the array. It must be remembered, of course, that there is still the parallel inductance in resonance with $C_T$. This corresponds exactly to both the experimental and theoretical results of Smith et al [10]. By Eq. (6.64) the radiation conductance is at synchronous frequency

$$G_a = 8N^2\ G_o \quad . \tag{6.93}$$

With this identification $S_{11}$ and $S_{12}$ are rewritten respectively as power scattering coefficients

$$p_{11} = S_{11}{}^2 = 1/(1 + G_L/G_a)^2 = P_1^-/P_1^+ \ , \tag{6.94}$$

and

$$\begin{aligned} p_{21} = S_{21}{}^2 &= (G_L/G_a)^2/(1 + G_L/G_a)^2 \\ &= P_2^+/P_1^+ \ . \end{aligned} \tag{6.95}$$

The load power will be found from

$$P_L = P_1^+ - P_1^- - P_2^+ \quad , \tag{6.96}$$

or

$$P_L = P_1^+ - \frac{P_1^+}{(1 + G_L/G_a)^2} - \frac{(G_L/G_a)^2\ P_1^+}{(1 + G_L/G_a)^2} \quad , \tag{6.97}$$

i.e.

$$P_L = \frac{(2G_L/G_a)}{(1 + G_L/G_a)^2} P_1^+ \quad . \tag{6.98}$$

The result of maximizing this is

$$G_L = G_a \quad . \tag{6.99}$$

Under these optimum conditions, Eq. (6.98) implies that only one-half of the incoming power can be extracted from the electrical terminals. By Eqs. (6.94)-(6.95) one-quarter will be reflected and another quarter transmitted. Numerically the optimum termination for the lithium niobate transducer discussed earlier would be

$$R_L = 1/G_a = 238\ \Omega \ .$$

If the identical transducer were laid out on AC quartz it would be by Eq. (6.68) 2700 times larger, because that is the ratio of the $Z_o$'s of quartz to lithium niobate. At frequencies above 100 MHz practical impedance levels tend to be lower. Any realistic termination to the quartz transducer would therefore appear as a short circuit to the line, supporting the initial assertion made by Coquin and Tiersten that the wave is unaffected by the quartz transducer.

It should be pointed out here that these are not original conclusions. They are the same as those found in [10], as they should be by necessity, since the definition of the quantity $G_o$ in Eq. (6.51) led to the identical equivalent circuits in terms of this $G_o$ [see Fig. 6.16 and [10]].

The development was made here for two reasons. The detailed calculations shown here are not given in that reference and they are an excellent example of the usefulness of the equivalent circuit model on which they were originally based. Furthermore, the equivalence of the results emphasizes that it was never the intention of this investigation to disprove the well-established analysis and design procedures of Smith et al [7,10], but rather to put their equivalent circuit model on a firm theoretical basis which admittedly it was not. It relied entirely on analogy to bulk waves, but not directly either, for the equivalent circuit developed in Chapter 4 by that analogy has a somewhat different frequency response from that used by Smith et al and the one developed here in Chapter 6. Smith et al anticipated the correct form without deriving it. They did not, however, realize the complexity of $R_o$ given in Eq. (6.51), which combined with Eq. (6.70) is for YZ lithium niobate

$$R_o = \frac{6.35 \times 10^{10}}{\omega W} \left[\frac{4K'(\omega/\omega_o)}{\pi}\right]^2 \quad . \qquad (6.100)$$

They use a constant for $R_o$, which gives good results for large arrays as seen by the comparison made in the last section.

# CHAPTER 7

# CONCLUSION

## 7.1 Historical Context

The objective of this investigation was to develop useful equivalent circuit models for piezoelectric surface-wave transducers from surface-wave theory. Because of the complex nature of the subject, many simplifications had to be made along the way. Nevertheless, they clarified rather than obscured the logical development of the subject, and they were never so gross as to make direct numerical calculations meaningless.

Before this research was undertaken, a successful circuit model indeed existed, and it has been widely used. It is the Mason model as adapted by Smith et al. However, it derived its justification really only from the fact that it correctly accounted for observed physical behavior. Its theoretical justification was based on the analogy between surface waves and bulk waves, for which transducer equivalent circuits have been in existence for some time.

The circuit models developed here account for the observed physical behavior, as they must, but their detailed logical development also specifically links them back to piezoelectric surface waves.

It has been shown, furthermore, how the elements of the equivalent circuits may be obtained from either the geometrical layout of the transducer, plus a knowledge of the fundamental physical properties of the material; or from direct measurement of the input admittance of an array when terminated by an infinite piezoelectric transmission line on both sides. This dual approach to modeling is analogous to the modeling of transistors, where either a knowledge of the geometry and the nature of the semiconductor material, or a few key measurements, will lead to the Ebers-Moll model. There, also, many simplifications are made in the theoretical development of the model, but it is very satisfying to have one mathematical model whose origins can be traced back to a fundamental starting point, well founded in physical theory; even if some physical phenomena are not completely accounted for by the model. The value of this research must be viewed in that light.

## 7.2 Summary of the Results

In Chapter 2 a simplified solution of the surface-wave problem has been performed in closed form for the AC cut in quartz. The results are numerical values for the propagation velocity

$$V_p = 3147 \text{ m/sec} , \qquad (2.70)$$

and the decay constants of the two dominant modes, together with their complex amplitudes. This information is expressed in terms of the normalized particle displacements at any depth y below the surface:

$$u(x,y,t) = 0.66\ e^{-1.4ky} \cos(\omega t - kx - \pi/2)$$

$$+\ 0.052\ e^{-0.147ky} \cos(\omega t - kx + \pi/2)\ , \qquad (2.68)$$

for the horizontal displacement and for the vertical displacement:

$$v(x,y,t) = 0.079\ e^{-1.4ky} \cos(\omega t - kx - \pi)$$

$$+\ 1.0\ e^{-0.147ky} \cos(\omega t - kx)\ ; \qquad (2.69)$$

the quantity k here is the propagation constant $\omega/V_p$. The equations show that the dominant behavior of this surface wave is similar to that of a vertical shear wave.

In Chapter 3, these expressions were used to calculate the time average power flux for the AC cut

$$P_x = \frac{1}{2}\,\omega W \times 90 \times 10^9 \times [C_2^{(2)}]^2\ , \qquad (3.32)$$

and the surface potential

$$\Phi_S = j5.8 \times 10^8\ C_2^{(2)}\ . \qquad (3.54)$$

It was shown that these two quantities lead to a physically proper expression for the characteristic admittance of the piezoelectric transmission line

$$Y_o = 2P_x/|\Phi_S|^2 = \omega W \times 2.68 \times 10^{-7}\ , \qquad (3.58)$$

if the surface potential is selected as the cross-variable:

$$\phi(x) = \phi^+(x) + \phi^-(x)\ , \qquad (3.55)$$

where

$$\phi^{\pm}(x) = \Phi_S^{\pm}\ e^{j(\omega t \mp kx)}\ . \qquad (3.47)$$

An alternate possibility was developed with the value for the characteristic impedance as

$$Z_o = 2P_x/\omega^2\varepsilon_{11}\varepsilon_{22}\, W^2|\phi_S|^2 = 1.72 \times 10^{14}/\omega W \quad . \tag{3.61}$$

Here the through-variable is related to the surface potential by

$$I^{\pm} = \pm j\omega\sqrt{\varepsilon_{11}\varepsilon_{22}}\, W\phi^{\pm} \quad , \tag{3.45}$$

and

$$I(x) = I^{+}(x) - I^{-}(x) \ . \tag{3.46}$$

By analogy to a vertical shear wave, transverse shear stress and vertical particle velocity were also considered as dynamic variables in order to justify the bulk-wave model used in the literature. Such a model was developed in Chapter 4. Since better models are developed in Chapter 6, it is of no further interest here except, perhaps, that it is shown in Section 3.7 that for this choice of dynamic variables the small relative change in characteristic impedance and velocity is not the same for both quantities if the vertical component of the electric field is forced upon the wave externally. This statement differs from views commonly held.

In Chapter 5 the theory of Coquin and Tiersten was extended to obtain an expression for the short-circuit current from an electrode to its nearest neighbors in an infinite array with a fraction $\eta$ of the surface metallized:

$$I_{SC} = j\omega\sqrt{\varepsilon_{11}\varepsilon_{22}}\, W(\phi_S^{\,+} + \phi_S^{\,-})[\pi/K'(\omega)]\ \sin^2(\frac{\pi\omega}{2\omega_o}) \ . \tag{5.58}$$

The quantity $K'(\omega)$ is the complete elliptic integral of modulus

$$m'(\omega) = 1 - \sin^2(\eta\pi\omega/2\omega_o) \quad . \tag{5.61}$$

The validity has been established for the frequency range

$$1/(2 - \eta) < \omega/\omega_o < 1/\eta \quad . \tag{5.62}$$

The quantity $\omega_o$ is the so-called synchronous frequency, where one wave length equals a periodic distance of the array D.

An essential assumption which led to the expression of the short-circuit current at frequencies other than $\omega_o$ is that this current is proportional to one-half the difference in the emf's between the electrode and its nearest neighbors. In Chapter 6 this concept was extended further. Here the emf's of all electrodes connected to each common terminal are summed, and the current from one common terminal to the other depends on one-half the difference in the combined emf's. This is stated in the form

$$I_{SC} = \frac{1}{2} \sum (-1)^{k+1} I_k \quad , \tag{6.3}$$

where $\frac{1}{2} I_k$ is the contribution from one electrode:

$$\frac{1}{2} I_k = j\omega\sqrt{\varepsilon_{11}\varepsilon_{22}}\, W[\pi/2K'(\omega)]\; \phi^P(x_n) = 2\gamma\phi^P(x_n) \quad . \tag{6.5}$$

Together with the transmission line sections of Chapter 3 this led to an equivalent circuit representation of the transducer array as shown in Fig. 6.8.

It was shown how weighting by an apodizing function of each dependent current generator makes this circuit model applicable to arrays with non-uniform electrode overlap. Different values of propagation velocity and characteristic admittance for the parts with surface metallization can be accounted for by breaking up the transmission line representation of the interspaces [see Fig. 6.8b].

By finding the dual of one section of the equivalent circuit array, an alternate equivalent circuit was produced for a section consisting of one interspace and its adjacent two-half electrodes [see Fig. 6.15]. The turns ratio of the ideal transformer is frequency dependent, but the line impedance may be reflected through this transformer so that it becomes

$$R_o = Z_o(\omega) \left[\frac{4K'(\omega)}{\pi}\right]^2 , \qquad (6.51)$$

where $Z_o$ is the characteristic impedance of Chapter 3

$$Z_o(\omega) = Z_o(\omega_o)(\omega_o/\omega) . \qquad (3.61)$$

Under these circumstances the through variable is given by

$$I_n = \gamma\phi^P(x_n) . \qquad (6.52)$$

This equivalent circuit was used to obtain the y-parameters for one interdigital period [see Fig. 6.16] which led to the calculation of the radiation admittance $Y_a$ and the scattering parameters of an array of N equal interdigital periods in cascade. The purpose of finding the radiation admittance was to adapt the equivalent circuits obtained in this investigation to other crystal cuts by comparing the normalized calculated frequency response with experimentally determined frequency response plots. This was done in particular with YZ lithium niobate. It was found that the characteristic impedance corresponding to that developed in Chapter 3 for the AC cut in quartz [Eq. (3.61)] is several orders of magnitude lower here

$$Z_o(\omega) = \frac{6.35 \times 10^{10}}{\omega W} \quad . \tag{6.70}$$

This should be viewed as a measure of the stronger electromechanical coupling in lithium niobate.

The evaluation of the scattering parameters showed that under conditions of optimum termination,

$$R_L = 1/G_a \quad , \tag{6.99}$$

one-half of the power contained in an incoming wave is extracted by the electrical terminals, one-quarter is reflected and one-quarter is transmitted. It was seen that while the optimum value for $R_L$ is only about 200Ω for a typical lithium niobate array, it becomes unreasonably large for a quartz transducer. A practical lower value of $R_L$ will leave the wave largely unaffected in its travel through the transducer.

It has been shown in various applications in Chapter 6 that the physical behavior predicted by the new models corresponds very well to either measured performance or the theoretical predictions by other authors based on the Mason model. If, in fact, the equivalent circuit of Fig. 6.16 is used with the value of $R_o$ for YZ lithium niobate,

$$R_o = \frac{6.35 \times 10^{10}}{\omega W} \left[\frac{4K'(\omega/\omega_o)}{\pi}\right]^2 \quad , \tag{6.100}$$

then it is clear in retrospect that the model developed by Smith et al is but a special case of the development presented here. This is true because, while their characteristic impedance was determined for the single frequency $\omega_o$, the characteristic impedance $R_o$

developed here is frequency dependent and reduces to their value at $\omega_o$.

## 7.3 Further Investigations

It would be of interest to show experimentally that under certain wide-band applications the frequency dependence of $R_o$ shown here would predict the correct behavior, where a constant $R_o$ would not. The radiation conductance,

$$G_a = \frac{2}{R_o} [\tan \frac{\theta}{4} \sin \frac{N\theta}{2}]^2 , \tag{6.64}$$

should be measured since the results of the experiment, for small N, will clearly demonstrate which theory is correct. The small N is necessary to achieve the required bandwidth. For large N, for example N = 15, there is no significant difference between this theory, that of Smith et al and measured performance.

It would be desirable, furthermore, to extend the frequency range for which this theory is valid. At the lower end of the frequency scale the expressions obtained here for the short-circuit current might be valid down to DC. At higher frequencies, when half a wave length is shorter than the width of an electrode, there will be partial cancellation of the emf developed under an electrode and the current should decrease for that reason. In either case, the present theory cannot be justified whenever a quarter wave length measured from the center of the electrode falls under a metallized part because of the boundary conditions in the conformal mapping problem of Chapter 5. The higher frequency end would particularly be of interest because third harmonic generation is, in fact, used to generate waves in the gigahertz region. However, the scope of the present investigation must be kept within reasonable bounds. Such research is therefore deferred to some future date.

# APPENDIX A

## DERIVATION OF THE PROPAGATION VELOCITY

It is shown here that Eqs. (2.44) and (2.45) lead to Eq. (2.46). When Eq. (2.45) is multiplied out with the definitions of the $\beta$'s inserted we obtain:

$$(\alpha_1 - \alpha_2)\left\{g_{22}[(q - g_{11}) + \alpha_1^2][(q - g_{11}) + \alpha_2^2] + g_{12}(\alpha_1\alpha_2 K^2)\right\}$$

$$+ (\alpha_1\alpha_2 g_{22} + g_{12})\left\{\alpha_1 K[(q - g_{11}) + \alpha_2^2]\right.$$

$$\left. - \alpha_2 K[(q - g_{11}) + \alpha_1^2]\right\} = 0 \quad . \tag{A.1}$$

This leads to an equation as described in [6] on page 670:

$$\alpha_1\alpha_2 K[g_{22}(q - g_{11}) + g_{12}(K - 1)] + \alpha_1^2\alpha_2^2(1 - K)g_{22}$$

$$+ (\alpha_1^2 + \alpha_2^2)(q - g_{11})\, g_{22} + (q - g_{11})^2\, g_{22}$$

$$+ g_{12}\, K(q - g_{11}) = 0 \ . \tag{A.2}$$

Equation (2.44) is of a form shown in Eq. (2.52):

$$\alpha^4 + \alpha^2 a + b = 0 \ . \tag{A.3}$$

In factored form this must equal:

$$(\alpha^2 - \alpha_1^2)(\alpha^2 - \alpha_2^2) = \alpha^4 + \alpha^2(-\alpha_1^2 - \alpha_2^2) + \alpha_1^2\alpha_2^2 \ . \tag{A.4}$$

It follows from Eq. (2.56) that we can make the following identifications:

$$\alpha_1^2 + \alpha_2^2 = -\frac{g_{22}(q-g_{11})+(q-1)+K^2}{g_{22}} \tag{A.5}$$

$$\alpha_1^2\alpha_2^2 = \frac{(q - g_{11})(q - 1)}{g_{22}} \quad . \tag{A.6}$$

These expressions are inserted into Eq. (A.2) to obtain, after some manipulation:

$$(q - g_{11})q^2 = \frac{q-1}{g_{22}} [g_{22}(q - g_{11}) + g_{12}{}^2]^2 \ . \qquad \text{(A.7)}$$

This is a cubic in q which simplifies eventually to Eq. (2.46).

# APPENDIX B

## THE TENSOR TRANSFORMATION OF THE STRESS COEFFICIENTS

The stress coefficients shown in Eqs. (2.1), (2.2) and (2.3) are really fourth rank tensors. The subscripts 1 to 6 used in engineering are a short form which convert as follows to tensor notation:

TABLE B.1 - Conversion from Engineering Notation to Tensor Notation

| Engineering Notation | Tensor Notation |
|---|---|
| 1 | 11 |
| 2 | 22 |
| 3 | 33 |
| 4 | 23 or 32 because of symmetry |
| 5 | 13 or 31 |
| 6 | 12 or 21 |

In order to obtain the stress coefficients for a rotated Y-cut by an angle $\theta$ one must use the transformation according to [5]:

$$\alpha_{ir} = \begin{bmatrix} 1 & 0 & 0 \\ 0 & \cos\theta & \sin\theta \\ 0 & -\sin\theta & \cos\theta \end{bmatrix} . \qquad \text{(B.1)}$$

The relation of the stress coefficients in the rotated system $C'_{ijkl}$ to those for the standard crystal axes is then given by:

$$C'_{ijkl} = \alpha_{ir}\alpha_{js}\alpha_{kt}\alpha_{eu}\, C_{rstu} . \qquad \text{(B.2)}$$

As an example it will be shown here that for $\theta = 31.62°$ $C'_{56}$ is zero. This is the coefficient that relates vertical shear strain $S_6(=S_{12})$ to face shear stress $T_5$ $(=T_{13})$.

$$C'_{56} = C'_{1312} = \alpha_{3s}\alpha_{2u}\, C_{1s1u} = \alpha_{32}\alpha_{22}\, C_{1212}$$

$$+ \alpha_{33}\alpha_{22}\, C_{1312} + \alpha_{32}\alpha_{23}\, C_{1213} + \alpha_{33}\alpha_{23}\, C_{1313} \tag{B.3}$$

$$C'_{56} = -\sin\theta\cos\theta\, C_{66} + \cos^2\theta\, C_{56} - \sin^2\theta\, C_{65} + \sin\theta\cos\theta\, C_{55} \tag{B.4}$$

There is further symmetry in the stress coefficients in engineering notation

$$C_{ij} = C_{ji}\ . \tag{B.5}$$

With values inserted which were taken from [4] $C'_{56}$ is:

$$C'_{56} = \cos\theta\sin\theta(57.94 - 39.88) - 17.91(\cos^2\theta - \sin^2\theta) \tag{B.6}$$

in units of $10^9$ N/m$^2$.

This becomes zero at a rotation of 31.62°. The other constants were obtained in a similar fashion.

# APPENDIX C

## DERIVATION OF THE TWO-PORT PARAMETERS FOR A LOSSLESS TRANSMISSION LINE

All pertinent quantities are defined in Fig. 3.2. Express first the terminal quantities at port 2 in terms of the cross-variable "waves" at port 1:

$$\begin{bmatrix} V_2 \\ I_2 \end{bmatrix} = \begin{bmatrix} V_1^+ e^{-st_o} + V_1^- e^{st_o} \\ Y_o V_1^+ e^{-st_o} - Y_o V_1^- e^{st_o} \end{bmatrix} = \begin{bmatrix} e^{-st_o} & e^{st_o} \\ Y_o e^{-st_o} & -Y_o e^{st_o} \end{bmatrix} \begin{bmatrix} V_1^+ \\ V_1^- \end{bmatrix} . \qquad \text{(C.1)}$$

Next this relation is inverted to yield:

$$\begin{bmatrix} V_1^+ \\ V_1^- \end{bmatrix} = \frac{1}{-2Y_o} \begin{bmatrix} -Y_o e^{st_o} & -e^{st_o} \\ -Y_o e^{-st_o} & e^{-st_o} \end{bmatrix} \begin{bmatrix} V_2 \\ I_2 \end{bmatrix} . \qquad \text{(C.2)}$$

The "through-variable waves" at port 1 are related to the "cross-variable waves" by $Y_o$:

$$\begin{bmatrix} I_1^+ \\ I_1^- \end{bmatrix} = Y_o \begin{bmatrix} V_1^+ \\ V_1^- \end{bmatrix} . \qquad \text{(C.3)}$$

The first equation is added to the second in relation (C.2) to result in $V_1$:

$$V_1 = V_1^+ + V_1^- = \frac{1}{2} [e^{st_o} + e^{-st_o}] V_2$$

$$+ (Z_o/2) [e^{st_o} - e^{-st_o}] I_2 \qquad \text{(C.4)}$$

$$V_1 = \cosh(st_o) V_2 + Z_o \sinh(st_o) I_2 . \qquad \text{(C.5)}$$

Also from relation (C.3) $I_1$ is obtained:

$$I_1 = I_1^+ - I_1^- = (Y_o/2)[e^{st_o} - e^{-st_o}]V_2 + \frac{1}{2}[e^{st_o} + e^{-st_o}]I_2 \tag{C.6}$$

$$I_1 = Y_o \sinh(st_o)\, V_2 + \cosh(st_o)\, I_2 \tag{C.7}$$

Equations (C.5) and (C.7) form the desired transmission equations as stated in Eqs. (3.1).

Next regroup these equations as follows:

$$1 \times V_1 - \cosh(st_o)V_2 = 0 \times I_1 - Z_o \sinh(st_o)\, [-I_2] \tag{C.8}$$

$$0 \times V_1 + Y_o \sinh(st_o)V_2 = 1 \times I_1 + \cosh(st_o)\, [-I_2]\ . \tag{C.9}$$

If the equations stated above in matrix form are next premultiplied by the inverse of the coefficient matrix of $V_1$ and $V_2$ one obtains the z-parameters. The y-parameters are obtained below that.

$$\begin{bmatrix} V_1 \\ V_2 \end{bmatrix} = \frac{1}{Y_o \sinh(st_o)} \begin{bmatrix} Y_o \sinh st_o & \cosh st_o \\ 0 & 1 \end{bmatrix} \begin{bmatrix} 0 & -Z_o \sinh(st_o) \\ 1 & \cosh(st_o) \end{bmatrix} \begin{bmatrix} I_1 \\ -I_2 \end{bmatrix} \tag{C.10}$$

$$\begin{bmatrix} V_1 \\ V_2 \end{bmatrix} = \begin{bmatrix} \dfrac{Z_o}{\tanh(st_o)} & \dfrac{Z_o}{\sinh(st_o)} \\ \dfrac{Z_o}{\sinh(st_o)} & \dfrac{Z_o}{\tanh(st_o)} \end{bmatrix} \begin{bmatrix} I_1 \\ -I_2 \end{bmatrix} \tag{C.11}$$

$$\begin{bmatrix} I_1 \\ -I_2 \end{bmatrix} = \frac{1}{Z_o \sinh(st_o)} \begin{bmatrix} \cosh(st_o) & Z_o \sinh(st_o) \\ -1 & 0 \end{bmatrix} \begin{bmatrix} 1 & -\cosh(st_o) \\ 0 & Y_o \sinh(st_o) \end{bmatrix} \begin{bmatrix} V_1 \\ V_2 \end{bmatrix} \tag{C.12}$$

$$\begin{bmatrix} I_1 \\ \\ -I_2 \end{bmatrix} = \begin{bmatrix} \dfrac{Y_o}{\tanh(st_o)} & \dfrac{-Y_o}{\sinh(st_o)} \\ \\ \dfrac{-Y_o}{\sinh(st_o)} & \dfrac{Y_o}{\tanh(st_o)} \end{bmatrix} \begin{bmatrix} V_1 \\ \\ V_2 \end{bmatrix} \qquad \text{(C.13)}$$

# APPENDIX D

# CALCULATION OF THE POWER FLUX

The integrand of Eq. (3.21) becomes:

$$T_1\dot{u}^* + T_6\dot{v}^* = -j\omega[C_1^{(1)*}\, e^{-\alpha_1 ky} + C_1^{(2)*}\, e^{-\alpha_2 ky}]\Big\{-jkC_{11}[C_1^{(1)}\, e^{-\alpha_1 ky}$$

$$+ C_1^{(2)}\, e^{-\alpha_2 ky}] + C_{12}[-\alpha_1 kC_2^{(1)}\, e^{-\alpha_1 ky} - \alpha_2 kC_2^{(2)}\, e^{-\alpha_2 ky}]\Big\}$$

$$-j\omega[C_2^{(1)*}\, e^{-\alpha_1 ky} + C_2^{(2)*}\, e^{-\alpha_2 ky}]\, C_{66}\Big\{-jk[C_2^{(1)}\, e^{-\alpha_1 ky}$$

$$+ C_2^{(2)}\, e^{-\alpha_2 ky}] + [-\alpha_1 kC_1^{(1)}\, e^{-\alpha_1 ky} - \alpha_2 kC_1^{(2)}\, e^{-\alpha_2 ky}]\Big\} \qquad \text{(D.1)}$$

$$= -\omega kC_{11}[C_1^{(1)}C_1^{(1)*}\, e^{-2\alpha_1 ky} + (C_1^{(1)*}C_1^{(2)} + C_1^{(1)}C_1^{(2)*})e^{-(\alpha_1+\alpha_2)ky}$$

$$+ C_1^{(2)}C_1^{(2)*}\, e^{-2\alpha_2 ky}]$$

$$+ j\omega kC_{12}[\alpha_1 C_2^{(1)}C_1^{(1)*}\, e^{-2\alpha_1 ky} + (\alpha_2 C_2^{(2)}C_1^{(1)*} + \alpha_1 C_2^{(1)}C_1^{(2)*})$$

$$\times\, e^{-(\alpha_1+\alpha_2)ky} + \alpha_2 C_2^{(2)}C_1^{(2)*}\, e^{-2\alpha_2 ky}]$$

$$+ j\omega kC_{66}[\alpha_1 C_1^{(1)}C_2^{(1)*}\, e^{-2\alpha_1 ky} + (\alpha_2 C_1^{(2)}C_2^{(1)*} + \alpha_1 C_1^{(1)}C_2^{(2)*})$$

$$\times\, e^{-(\alpha_1+\alpha_2)ky} + \alpha_2 C_1^{(2)}C_2^{(2)*}\, e^{-2\alpha_2 ky}]$$

$$- \omega kC_{66}[C_2^{(1)}C_2^{(1)*}\, e^{-2\alpha_1 ky} + (C_2^{(1)*}C_2^{(2)} + C_2^{(1)}C_2^{(2)*})e^{-(\alpha_1+\alpha_2)ky}$$

$$+ C_2^{(2)}C_2^{(2)*}\, e^{-2\alpha_2 ky}] \qquad \text{(D.2)}$$

We integrate this as prescribed by Eq. (3.21).

$$\overline{P}_x = C_{11}\frac{W\omega}{2}\left[\frac{C_1^{(1)}C_1^{(1)*}}{2\alpha_1} + \frac{C_1^{(1)*}C_1^{(2)} + C_1^{(1)}C_1^{(2)*}}{\alpha_1 + \alpha_2} + \frac{C_1^{(2)}C_1^{(2)*}}{2\alpha_2}\right]$$

$$+ C_{12}\frac{W\omega}{2}\left[\frac{C_2^{(1)}C_1^{(1)*}}{2j} + \frac{\alpha_2 C_2^{(2)}C_1^{(1)*} + \alpha_1 C_2^{(1)}C_1^{(2)*}}{j(\alpha_1 + \alpha_2)} + \frac{C_2^{(2)}C_1^{(2)*}}{2j}\right]$$

$$+ C_{66}\frac{W\omega}{2}\left[\frac{C_1^{(1)}C_2^{(1)*}}{2j} + \frac{\alpha_2 C_1^{(2)}C_2^{(1)*} + \alpha_1 C_1^{(1)}C_2^{(2)*}}{j(\alpha_1 + \alpha_2)} + \frac{C_1^{(2)}C_2^{(2)*}}{2j}\right]$$

$$+ C_{66}\frac{W\omega}{2}\left[\frac{C_2^{(1)}C_2^{(1)*}}{2\alpha_1} + \frac{C_2^{(1)*}C_2^{(2)} + C_2^{(1)}C_2^{(2)*}}{\alpha_1 + \alpha_2} + \frac{C_2^{(2)}C_2^{(2)*}}{2\alpha_2}\right] \quad \text{(D.3)}$$

Expression (D.3) is a special case of Eq. 28 in [4]. For the values derived in Chapter 1:

$C_1^{(1)} = -j0.66$

$C_1^{(2)} = j0.052$

$C_2^{(1)} = -0.079$

$C_2^{(2)} = 1$ (the vertical amplitude of mode 2 is taken as reference)

$C_{11} = 86.74 \times 10^9$ N/m$^2$

$C_{12} = -7.65 \times 10^9$ N/m$^2$

$C_{66} = 28.85 \times 10^9$ N/m$^2$

$\alpha_1 = 1.40$

$\alpha_2 = 0.147$

$$\overline{P}_x = \frac{1}{2}\,\omega W|C_2^{(2)}|^2 \Bigg\{ \Big[\frac{0.66^2}{2x1.4} + \frac{-2 \times 0.66 \times 0.052}{1.55} + \frac{0.052^2}{2x0.147}\Big](86.74)$$

$$+ \Big[\frac{-0.66 \times 0.079}{2} + \frac{0.147 \times 0.66 + 1.4 \times 0.052 \times 0.079}{1.55} + \frac{-0.052}{2}\Big](-7.65)$$

$$+ \Big[\frac{0.66 \times 0.079}{2} + \frac{0.147 \times (-0.079)(0.052) + 1.4(-0.66)}{1.55} + \frac{0.052}{2}\Big](28.85)$$

$$+ \Big[\frac{0.079^2}{2x1.4} + \frac{-0.079 \times 2}{1.55} + \frac{1}{2 \times 0.147}\Big](28.85)\Bigg\} \times 10^9 \qquad \text{(D.4)}$$

$$\overline{P}_x = \frac{1}{2}\,\omega W|C_2^{(2)}|^2 \left\{ \begin{array}{lll} 13.5 & - \;\; 3.8 & + \;\; 0.8 \\ + \; 0.2 & - \;\; 0.5 & + \;\; 0.2 \\ + \; 0.8 & - 17.2 & + \;\; 0.8 \\ + \; 0.1 & - \;\; 2.9 & + 98.1 \end{array} \right\} \times 10^9 \qquad \text{(D.5)}$$

These numbers are arranged in the same order in which they appear in Eq. (D.3). It is seen that by far the largest contribution to the power comes from the vertical component of mode 2:

$$P_2^{(2)} = \frac{1}{2}\,\omega W|C_2^{(2)}|^2 \times 98 \times 10^9 \text{ watts .} \qquad \text{(D.6)}$$

Equation (D.5) yields

$$\overline{P}_x = \frac{1}{2}\,\omega W|C_2^{(2)}|^2 \times 90 \times 10^9 \text{ watts .} \qquad \text{(D.7)}$$

$P_2^{(2)}$ taken alone actually results in a value which is slightly too high (8.8%). This suggests that a surface wave is in a lower energy state than a shear wave.

It should be noted furthermore that $\overline{P}_x$ is real, which will produce a real $Z_o$ (or $Y_o$) so that the through-variable and cross-variable are in phase, whatever their choice.

Since $C_2^{(2)}$ might be of the order of only $10^{-10}$ m $P_x$ will be rather small. For W = 3 mm and $\omega = 10^9$/sec we obtain

$$P_x = 1.3 \text{ mW}.$$

# APPENDIX E

## SOLUTION OF THE POTENTIAL EQUATION

Equations (2.6), (2.7) and (2.8) are inserted into Eq. (3.41)

$$\varepsilon_{11}\frac{\partial^2\phi}{\partial x^2}+\varepsilon_{22}\frac{\partial^2\phi}{\partial y^2}=e_{11}\frac{\partial^2 u}{\partial x^2}+\frac{\partial^2 v}{\partial x\partial y}(e_{26}+e_{12})+e_{26}\frac{\partial^2 u}{\partial y^2}\ . \qquad (E.1)$$

The right-hand side is assumed to be known, $f(x - V_p t, y)$ say. The solution will consist of two parts: the complementary and the particular solution. The complementary solution is found from the homogeneous differential equation:

$$\varepsilon_{11}\frac{\partial^2\phi_n}{\partial x^2}+\varepsilon_{22}\frac{\partial^2\phi_n}{\partial y^2}=0\ . \qquad (E.2)$$

Because of the assumption that the x-direction is unbounded $\phi$ in complex form will vary as $\sim e^{-j(kx-\omega t)}$ with x and t so that the homogeneous differential equation becomes:

$$\frac{\partial^2\phi_n}{\partial y^2}-\frac{\varepsilon_{11}}{\varepsilon_{22}}k^2\,\phi_n=0\ . \qquad (E.3)$$

The solution is of the form

$$\phi_n = A\,e^{-\sqrt{\frac{\varepsilon_{11}}{\varepsilon_{22}}}ky}+B\,e^{\sqrt{\frac{\varepsilon_{11}}{\varepsilon_{22}}}ky}\ . \qquad (E.4)$$

B must be 0 since $\phi$ is zero for large values of y. The complementary solution is then

$$\phi_n = K\,e^{-\frac{k}{r}y}\,e^{j(\omega t-kx)}\ . \qquad (E.5)$$

For the particular solution let either $\frac{\partial}{\partial y}\to-\alpha_1 k$ or $\frac{\partial}{\partial y}\to-\alpha_2 k$ and use the principle of superposition, solving for each mode separately:

$$-k^2\varepsilon_{11}\phi_1+\alpha_1^2\varepsilon_{22}k^2\phi_1=-e_{11}k^2u_1-j\alpha_1k^2(e_{26}+e_{12})v_1+e_{26}k^2\alpha_1^2u_1 \quad (E.6)$$

$$\phi_1 = \frac{(e_{11} - e_{26}\alpha_1^2)u_1 + j\alpha_1(e_{26} + e_{12})v_1}{\varepsilon_{11} - \alpha_1^2 \varepsilon_{22}} . \tag{E.7}$$

Similarly

$$\phi_2 = \frac{(e_{11} - e_{26}\alpha_2^2)u_2 + j\alpha_2(e_{26} + e_{12})v_2}{\varepsilon_{11} - \alpha_2^2 \varepsilon_{22}} . \tag{E.8}$$

The total solution is then

$$\phi = \phi_n + \phi_1 + \phi_2 . \tag{E.9}$$

In order to determine the coefficient K in $\phi_n$ (Eq. (E.5)) the simplifying assumption is made in [4] that $D_2 = 0$ for $y < 0$. Since it must be continuous, the following boundary condition follows from Eq. (3.35) for $y = 0$:

$$D_2 = 0 = e_{26} \left.\frac{\partial u}{\partial y}\right|_{y=0} + e_{26} \left.\frac{\partial v}{\partial x}\right|_{y=0} - \varepsilon_{22} \left.\frac{\partial \phi}{\partial y}\right|_{y=0} . \tag{E.10}$$

Applying this the result is

$$K = \sum_{i=1}^{2} \frac{e_{26}\alpha_i C_1^{(i)} + j\, e_{26} C_2^{(i)}}{\sqrt{\varepsilon_{11}\varepsilon_{22}}} - r\alpha_i \frac{(e_{11} - e_{26}\alpha_i^2) C_1^{(i)} + j\alpha_i(e_{26} + e_{12}) C_2^{(i)}}{\varepsilon_{11} - \alpha_i^2 \varepsilon_{22}} . \tag{E.11}$$

# APPENDIX F

## THE FREQUENCY RESPONSE OF A 20 ELEMENT SURFACE-WAVE TRANSDUCER ARRAY

By means of the geometric-arithmetic mean Eq. (6.16) is programmed below for the special case of $\eta = 1/2$, $K' = K = 1.85407$. The result is shown in Fig. 6.9.

```
C*****THIS PROGRAM COMPUTES THE FREQUENCY RESPONSE OF A 20 ELEMENT
C*****SURFACE WAVE TRANSDUCER ARRAY, WITH HALF THE SURFACE AREA
C*****METALIZED. THE LOAD IS A 9PF CAPACITOR,9X THE VALUE OF C-OUT
      DIMENSION V(80),OME(80)
      K=1
      I=1
      OM=.675
   10 ALF=OM*0.78539816
      B=SIN(ALF)
      A=1.
   20 A1=0.5*(A+B)
      B1=SQRT(A*B)
      A=A1
      B=B1
      C=(A-B)/2.
      IF(C-.000001)21,21,20
   21 V(I)=.01*A*SIN(40.*ALF)/COS(2.*ALF)
      V(I)=ABS(V(I))
22    OME(I)=-OM
      I=I+1
      IF(K-1)25,25,75
   25 OM=OM+0.025
      GO TO 86
   75 OM=OM+0.005
86    IF(ABS(OM-1.)-1.E-5) 40,40,30
40    V(I)=3.38885/20.
      GO TO 22
   30 IF(K-1)35,35,90
   35 IF(OM-2.)10,60,60
   60 CALL PLOT4(V,OME,I)
      K=2
      I=1
      OM=0.9
   90 IF(OM-1.1)10,10,95
   95 CALL PLOT4(V,OME,40)
      STOP
      END
```

# APPENDIX G

## CALCULATION OF THE Y-PARAMETERS FOR ONE INTERDIGITAL PERIOD

Consider Fig. 6.16a. If $V_{AB} = 0$ the two sections obviously degenerate into a transmission line. Hence $y_{11}$, $y_{12}$, $y_{21}$ and $y_{22}$ are determined. If $V_n$ and $V_{n+1}$ are set to zero the resulting I for an applied $V_{AB}$ will give $y_{33}$. In the same circuit $I_n$ will yield $y_{13}$ and $-I_{n+1}$ will determine $y_{23}$. By reciprocity $y_{31}$ and $y_{32}$ are then also known. In Fig. 6.16b the voltage $V_{AB}$ has been reflected across the ideal transformers. Because of symmetry it is possible to identify $I_x$ as one-half the input current, except for the portion through the capacitor C. Furthermore, it is seen that $I_n$ and $I_{n+1}$ are equal. Kirchhoff's voltage law in the left mesh is

$$V_{AB} = -jR_o\tan(\theta/4)\ I_N + R_oI_x/j\sin(\theta/2)\ , \tag{G.1}$$

for the center loop it is

$$2V_{AB} = 2jR_o\tan(\theta/4)\ I_N + 2R_oI_x/j\sin(\theta/2) + 2jR_o\tan(\theta/4)\ I_x\ . \tag{G.2}$$

From this $I_N$ is eliminated:

$$2V_{AB} = I_xR_o[2/j\sin(\theta/2) + j\tan(\theta/4)]\ , \tag{G.3}$$

or

$$2V_{AB} = I_xR_o\,\frac{1 - \sin^2(\theta/4)}{j\sin(\theta/4)\ \cos(\theta/4)}\ , \tag{G.4}$$

or

$$2V_{AB} = I_x/jG_o\tan(\theta/4)\ . \tag{G.5}$$

The required ratio for $y_{33}$ is

$$2I_x/V_{AB} = j4G_o\tan(\theta/4)\ , \tag{G.6}$$

hence

$$y_{33} = j\omega C + j4G_o\tan(\theta/4) \ . \tag{G.7}$$

The value obtained here for $I_x$ is now used to eliminate it from Eq. (G.1).

$$V_{AB} = -jR_o\tan(\theta/4)\ I_N + \frac{2\tan(\theta/4)}{\sin(\theta/2)} V_{AB} \ , \tag{G.8}$$

or

$$\frac{jR_oI_N}{V_{AB}} = \frac{2\tan(\theta/4)}{2\sin(\theta/4)\ \cos(\theta/4)\ \tan(\theta/4)} - \frac{1}{\tan(\theta/4)} \ , \tag{G.9}$$

or

$$\frac{I_N}{V_{AB}} = \frac{-jG_o\sin^2(\theta/4)}{\sin(\theta/4)\cos(\theta/4)} = -jG_o\tan(\theta/4) = \frac{I_{N+1}}{V_{AB}} \ , \tag{G.10}$$

hence

$$y_{13} = -y_{23} = -jG_o\tan(\theta/4) \ . \tag{G.11}$$

# APPENDIX H

## DETERMINATION OF THE RADIATION ADMITTANCE

Solution of Eq. (6.62) for the purpose of determining the radiation admittance.

The cofactor $\Delta_{33}$ is

$$\Delta_{33} = (Y_{11} + G_o)^2 - Y_{12}^2 \; . \tag{H.1}$$

The determinant is expanded in terms of the last column:

$$\Delta = Y_{33}\,\Delta_{33} + 2Y_{13}[-Y_{13}(Y_{11} + G_o) - Y_{13}Y_{12}] \; . \tag{H.2}$$

The radiation admittance is then

$$Y_a = \frac{\Delta}{\Delta_{33}} = Y_{33} - \frac{2Y_{13}^2(Y_{11} + Y_{12} + G_o)}{(Y_{11} + G_o)^2 - Y_{12}^2} \tag{H.3}$$

or

$$Y_a = j\omega C_T + j4NG_o\tan\theta/4 + \frac{2G_o\tan^2\theta/4[1/j\tan N\theta - 1/j\sin N\theta + 1]}{[1/j\tan N\theta + 1]^2 - [-1/j\sin N\theta]^2} \; . \tag{H.4}$$

The terms in [ ] are considered separately. By $a^2 - b^2 = (a+b)(a-b)$ they simplify to:

$$1/[\frac{1}{j\tan N\theta} + \frac{1}{j\sin N\theta} + 1] = \frac{j\sin(N\theta)}{\cos N\theta + j\sin N\theta + 1} \tag{H.5}$$

or

$$\frac{j\sin N\theta}{1+e^{jN\theta}} = \frac{j\sin N\theta e^{-jN\theta/2}}{2\cos(N\theta/2)} = [\frac{1}{2} - \frac{j\sin(N\theta/2)}{2\cos(N\theta/2)}]\; j\sin N\theta \; . \tag{H.6}$$

After expanding $\sin N\theta$ as $2\sin(N\theta/2)\cos(N\theta/2)$ Eq. (H.6) becomes

$$\frac{j\sin N\theta}{2} + \sin^2(N\theta/2) \; . \tag{H.7}$$

This is re-inserted into Eq. (H.4) with the desired result:

$$Y_a = 2G_o[\sin(N\theta/2)\tan(\theta/4)]^2 + j\omega C_T + j4NG_o\tan(\theta/4) + jG_o\sin(N\theta)\tan^2(\theta/4). \tag{H.8}$$

# APPENDIX I

## PROGRAM FOR THE RADIATION ADMITTANCE OF A 30 ELEMENT ARRAY

Computer program for the normalized radiation admittance of a 30 element array.

$$\omega' = \omega/\omega_o \ . \tag{I.1}$$

$$G_a Z_o(\omega_o) = \frac{\omega'}{8} [\pi/K'(\omega')]^2 [\tan(\pi\omega'/2)\sin(30\pi\omega'/2)]^2 \ . \tag{I.2}$$

$$B_a Z_o(\omega_o) = \frac{\omega'}{16} [\pi/K'(\omega')]^2 \tan(\pi\omega'/2)[60 + \tan(\pi\omega'/2)\sin(60\pi\omega'/2)] . \tag{I.3}$$

```
C*****RADIATION ADMITTANCE
C******OF A 30 ELEMENT ARRAY.
      DIMENSION G(80),OME(80)
      K=1
      I=1
      OM=.075
 10   ALF=OM*1.5707963
      BE=SIN(ALF/2.)
      A=1.
 20   A1=.5*(A+BE)
      B1=SQRT(A*BE)
      A=A1
      BE=B1
      C=(A-BE)/2.
      IF(C-.000001)21,21,20
 21   G(I)=.125*OM*(A+BE)**2*(TAN(ALF)*SIN(30.*ALF))**2
      OME(I)=.0625*OM*(A+BE)**2*TAN(ALF)*(60.+TAN(ALF)*SIN(60.*ALF))
 22   I=I+1
      IF(K-1)25,25,75
 25   OM=OM+.0125
      GO TO 86
 75   OM=OM+.0025
 86   IF(ABS(OM-1.)-1.E-5)40,40,30
 40   G(I)=323.
      OME(I)=0.0
      GO TO 22
 30   IF(K-1)35,35,90
 35   IF(OM-1.325)10,60,60
 60   CALL PLOT4(G,OME,I)
      K=2
      I=1
      OM=.9
 90   IF(OM-1.1)10,10,95
 95   CALL PLOT4(G,OME,I)
      STOP
      END
```

# REFERENCES

## REFERENCES


1. H. F. Tiersten, "Wave Propagation in an Infinite Piezoelectric Plate," J. Acoust. Soc. Am., Vol. 35, p. 234, 1963.

2. C. C. Tseng and R. M. White, "Propagation of Piezoelectric and Elastic Surface Waves on the Basal Plane of Hexagonal Piezoelectric Crystals," J. Appl. Phys., Vol. 38, p. 4274, 1967.

3. James J. Campbell and William R. Jones, "A Method for Estimating Optimal Crystal Cuts and Propagation Directions for Excitation of Piezoelectric Surface Waves," IEEE Trans. on Sonics and Ultrasonics, Vol. SU-15, No. 4, October 1968.

4. G. A. Coquin and H. F. Tiersten, "Analysis of the Excitation and Detection of Piezoelectric Surface Waves in Quartz by Means of Surface Electrodes," The Journal of the Acoustical Society of America, Vol. 41, No. 4, Part 2, 1967.

5. Warren P. Mason, Crystal Physics of Interaction Processes, Academic Press, 1966.

6. H. Deresiewicz and R. D. Mindlin, "Waves on the Surface of a Crystal," Journal of Applied Physics, Vol. 28, No. 6.

7. W. Richard Smith, H. M. Gerard, and W. R. Jones, "Analysis and Design of Dispersive Interdigital Surface-Wave Transducers," IEEE Trans. on Microwave Theory and Techniques, Vol. MTT-20, No. 7, July 1972.

8. Rabindra N. Ghose, Microwave Circuit Theory and Analysis, McGraw-Hill Book Company, 1963.

9. T. L. Szabo and A. J. Slobodnik, "The Effect of Diffraction on the Design of Acoustic Surface-Wave Devices," IEEE Trans. on Sonics and Ultrasonics, Vol. SU-20, No. 3, July 1973.

10. Smith, Gerard, Collins, Reeder, and Shaw, "Analysis of Interdigital Surface-Wave Transducers by Use of an Equivalent Circuit Model," IEEE, MTT-17, No. 11, 1969.

11. Gerard, Smith, Jones, and Harrington, "The Design and Applications of Highly Dispersive Acoustic Surface-Wave Filters," IEEE, SU-20, No. 2, April 1973.

12. D. A. Berlincourt, D. R. Curran, and H. Jaffe (W. P. Mason, Ed.), Physical Acoustics, Vol. 1A, Academic Press: New York, 1964.

13. R. H. Tancrell and M. G. Holland, "Acoustic Surface-Wave Filters," IEEE Proceedings, Vol. 59, No. 3, March 1971.

14. M. Abramowitz and I. A. Stegun, "Handbook of Mathematical Functions," AMS55, National Bureau of Standards.

15. R. F. Milsom and M. Redwood, "Interdigital Piezoelectric Rayleigh-Wave Transducer: An Improved Equivalent Circuit," Electronic Letters, Vol. 7, No. 9, 1971.

16. C. C. Tseng, "Frequency Response of an Interdigital Transducer for Excitation of Surface Elastic Waves," IEEE, ED-15, No. 8, August 1968.

17. R. M. White and F. M. Voltmer, "Direct Piezoelectric Coupling to Surface Elastic Waves," Appl. Phys. Lett., Vol. 7, No. 12, December 1965.

18. Larry A. Coldren, "Optimizing Loss-Compensated Long Delay Devices," IEEE, Vol. SU-20, No. 1, January 1973.

19. A. W. Warner, M. Onoe and G. A. Coquin, "Determination of Elastic and Piezoelectric Constants for Crystals in Class (3m)," J. Acoust. Soc. Am., Vol. 42, October 1966.